

UNDERSTANDING THE SURFACE-ATMOSPHERE INTERACTIONS ON TITAN

A Dissertation

Presented in Partial Fulfillment of the Requirements for the  
Degree of Doctorate of Philosophy

with a

Major in Physics

in the

College of Graduate Studies

University of Idaho

by

Rajani D. Dhingra

Major Professor: Jason W. Barnes, Ph.D.

Committee Members: Matthew M. Hedman, Ph.D.; Gwen Barnes, Ph.D.; Leslie L. Baker, Ph.D.

Department Chair: Ray Von Wondruska, Ph.D.

May 2019

## AUTHORIZATION TO SUBMIT DISSERTATION

This dissertation of Rajani D. Dhingra, submitted for the degree of Doctorate of Philosophy with a Major in Physics and titled “Understanding the surface-atmosphere interactions on Titan,” has been reviewed in final form. Permission, as indicated by the signatures and dates below is now granted to submit final copies for the College of Graduate Studies for approval.

Advisor: \_\_\_\_\_  
Jason W. Barnes, Ph.D. Date \_\_\_\_\_

Committee Members: \_\_\_\_\_  
Matthew M. Hedman, Ph.D. Date \_\_\_\_\_

\_\_\_\_\_  
Gwen Barnes, Ph.D. Date \_\_\_\_\_

\_\_\_\_\_  
Leslie L. Baker, Ph.D. Date \_\_\_\_\_

Department Chair: \_\_\_\_\_  
Ray Von Wondruszka, Ph.D. Date \_\_\_\_\_

## ABSTRACT

With a thick atmosphere, a methane-based hydrological cycle, stable bodies of standing fluid at its surface, and many active surface processes, Saturn's largest moon Titan is surprisingly Earth-like. Methane rain on Saturn's moon Titan makes it the only place, other than Earth, where rain interacts with the surface. Looking at Titan is like looking back in time to understand the evolution of present day Earth from early-Earth.

This thesis combines several studies related to Titan's hydrologic system, particularly the ways fluid interacts with the surface of Titan. Understanding this atmosphere—surface interaction is of great importance to understand Titan's meteorology and evolution. Following an introduction about the discovery and need to study Titan, chapter 2 addresses the possible reasons behind Ontario Lacus being the solo lake in the south pole of Titan.

In chapter 3 we discuss our novell 'wet-sidewalk' observation. Basically if ground gets wetted, and illuminated by the Sun at right geometries we get this broad specular reflection (glint) that's super-bright. That we've seen one near Titan's north pole means that it's rained there now coincident with north polar summer, and furthermore we've got a new technique for monitoring when and where rainfall occurs across Titan's surface. It is extremely difficult to detect rainfall events on Titan due to its thick atmospheric haze and very limited opportunities to view the surface (and its changes). Our wet-sidewalk observation using VIMS —Visual and Infrared Mapping Spectrometer, on the north pole of Titan is the first of its kind i.e using broad surface reflection and the delayed north polar activity. Hence this observation and the rainfall discovery on the north pole is of extreme importance to understand Titan's climate.

While the presence of a hydrological cycle might help explain how the depressions on Titan's surface are filled with liquid methane, the formation mechanisms of the depressions still remain a mystery at the end of Cassini in 2017. We address this question using a morphometric measurement methodology (EFDA—Elliptical Fourier Descriptor Analysis) to quantify the shapes of Titan's lakes in Chapter 4. We find that the major variation in the shapes of lakes on Titan are from circular to elliptical followed by longer lakes with asymmetry along their long axis and longer lakes with asymmetry along their short axis. Also, smaller lakes on Titan are more circular indicating that probably lakes are initially formed by a punch but evolve to get bigger with more complexities in their shoreline.

We then conclude the thesis by stating our future work about expanding the morphometric analyses to more lakes on Titan and finding more 'wet-side walk' like features on Titan's north pole.

## ACKNOWLEDGMENTS

The first person to thank for this thesis and work is my advisor Dr. Jason W. Barnes. He offered me the opportunity to work on Titan, trusted me and my capabilities. He gave me the freedom to work on science problems I found exciting and the exposure to know people in scientific community. He advised me not only with science but also with oratory and writing skills. Thanks Jason, for giving me the opportunity to fulfill my dream to work on Titan while pursuing my Ph.D.

I must thank all my committee members for their time and effort. I wish to thank Dr. Matthew Hedman especially for having an open door policy and spending his precious time on various aspects of my thesis and scientific education.

My daughter Oas Dhingra deserves immense acknowledgments for bearing with my patchy presence on this journey. Having her by my side kept me afloat on this path. The last two years of my Ph.D. would not have been possible if not for her. Her spark kept me ignited and going. Thanks Oas for coming into my life and being born as my daughter.

Acknowledgements to five friends of mine who helped me in the last two extremely difficult years of my Ph.D. Cheyenne Smith, Gwen Barnes, Rebecca O'Daniel, Alicia Peterson, Stacey Hurst. If not for you, I would have quit this journey of life and science. Special thanks to Rumi for letting me see light when I had none and Jamie Derrick for reminding my feisty-ness to me.

Acknowledgments to my labmates, John Ahlers, Rob Chancia and Shannon MacKenzie with whom I shared meals and long chats about YORP effects, methane clathrates and even dynamics of spit . My new labmates Steven Kreyche, Micheal Heslar and Joseph who keep the lab enviroment challenging and other colleagues in science, planetary science and Titan science for various fruitful discussions, opportunities and ideas.

Gratitude to my parents for teaching me the importance of education, my sister, Rashmi Shukla for being my confidante in my journey, my brother Abhinav Mishra for making the load lighter with his jokes, and Deepak Dhingra, my husband for motivating me, time and again. Generous thanks to my batchmates, Lokendra Khanal, Rob Chancia, Shahla Nemati, Negar Rajabi and Randy Millerson for sulking equally, fighting equally, and enjoying equally.

## DEDICATION

For Oas to believe in grit, perseverance and in the courage of dreaming...

Not a hope, Not a wish but a pulsating, stubborn, desire...

# TABLE OF CONTENTS

AUTHORIZATION TO SUBMIT DISSERTATION . . . . .	ii
ABSTRACT . . . . .	iii
ACKNOWLEDGMENTS . . . . .	iv
DEDICATION . . . . .	v
TABLE OF CONTENTS . . . . .	vi
LIST OF TABLES . . . . .	viii
LIST OF FIGURES . . . . .	ix
CHAPTER 1: INTRODUCTION . . . . .	2
MOTIVATION FOR THIS THESIS . . . . .	5
CHAPTER 2: LARGE CATCHMENT AREA RECHARGES TITAN'S ONTARIO LACUS . . . . .	8
INTRODUCTION TO THE CHAPTER . . . . .	8
INTRODUCTION . . . . .	9
CATCHMENT AREA . . . . .	12
METHOD . . . . .	12
RESULTS . . . . .	14
MASS BALANCE . . . . .	16
METHOD . . . . .	16
RESULTS . . . . .	17
STREAM PROFILE DETERMINATION . . . . .	19
METHOD . . . . .	19
RESULTS . . . . .	19
DISCUSSION . . . . .	22
CONCLUSION . . . . .	23
ACKNOWLEDGEMENTS . . . . .	23
CHAPTER 3: OBSERVATIONAL EVIDENCE FOR SUMMER RAINFALL AT TITAN'S NORTH POLE . . . . .	24
INTRODUCTION TO CHAPTER 3 . . . . .	24
INTRODUCTION . . . . .	24
OBSERVATION . . . . .	25
METHOD . . . . .	27
HYPOTHESES . . . . .	27
MODELING SURFACE ROUGHNESS . . . . .	32
RESULTS AND DISCUSSION . . . . .	32
CONCLUSION . . . . .	32
CHAPTER 4: USING ELLIPTICAL FOURIER DESCRIPTOR ANALYSIS (EFDA) TO QUANTIFY TITAN LAKE MORPHOLOGY . . . . .	37
INTRODUCTION TO CHAPTER 3 . . . . .	37
INTRODUCTION . . . . .	38

SIZE DISTRIBUTION AND ORIENTATION . . . . .	40
OBSERVATIONAL DATA . . . . .	40
METHOD AND RESULTS . . . . .	43
ELLIPTICAL FOURIER DESCRIPTOR ANALYSIS FOR OUTLINE-SHAPE QUANTIFICATION . . . . .	43
METHOD . . . . .	44
TESTING EFDA ON LAKE FORMS . . . . .	49
APPLICATION TO TITAN LAKES . . . . .	51
OBSERVATIONAL DATA AND METHOD . . . . .	51
DISCUSSION AND CONCLUSION . . . . .	53
CHAPTER 5: CONCLUSIONS . . . . .	59
REFERENCES . . . . .	61

# LIST OF TABLES

2.1	List of the parameters used in the mass balance study for Ontario Lacus. * based on Mitri et al. (2007) ** based on Schneider et al. (2012) . . . . .	18
3.1	Details of T106, T120 and T121 flybys, which cover the location of BEF over three time stamps. It helps us determine the existence of this feature over time, and we conclude that it is an ephemeral feature. The inferred specular points of the flybys are tabulated. We also show the distance of T106 and T121 specular points from the BEF. Sp. Pt. means Specular Point. The fact that the distance of inferred specular point . . . . .	28
3.2	The observation geometry of the pixels used to determine the spectra in Figure 4B. All the units are from the same cube to minimize atmospheric effects. . . . .	34

## LIST OF FIGURES

1.1	The diagram of the Cassini spacecraft. Cassini was a cooperative project of NASA, the European Space Agency and the Italian Space Agency. Image source : NASA photojournal .	3
1.2	Representative VIMS spectra of the bright and dark regions on Titan. Grey bands indicate where Titan’s surface is not seen in the VIMS data due to atmospheric absorption and scattering. DISR (Descent Imager Spectral Radiometer) was an Optical Remote Sensing Instrument for the Huygens Probe. The derived DISR spectra is shown in black for comparison. Both the spectra indicate a strong blue slope to the spectra of Titan in the observed wavelengths.(Clark et al., 2010) . . . . .	4
1.3	The image of Titan as seen from Voyager 1 in visible light and as seen from the infra-red (0.93 $\mu\text{m}$ ) (ISS) camera of Cassini. Image source : NASA photojournal . . . . .	5
1.4	Titan’s north pole in orthographic projection after the end of Cassini mission. This collage has all the flybys of Titan that cover the north pole and was made by Shannon MacKenzie. The color scheme is R:5 $\mu\text{m}$ , G: 2 $\mu\text{m}$ , B:1.3 $\mu\text{m}$ . The bright reflection is a mirror like reflection from the shores of Kraken Mare (Top left region of the image). Less brighter orange pixel shows the waves in this big sea, Kraken Mare. Reddish 5 $\mu\text{m}$ bright material are evaporites that are left behind after evaporation of the liquid. The other smaller dark dots in the lower right part of image are the smaller lakes on Titan and suitably the region is called, Lake district. The black dot near Punga Mare marks the north pole of Titan. . . . .	6
2.1	Titan’s south polar topographic map derived by Lorenz et al. (2013) in Polar stereographic projection. Ontario Lacus is located within the region marked by the black box. The black arrows indicate the other low elevation regions in the south pole that are empty. The seams in the image are the available topography information while the rest of the topography is generated by an interpolation procedure due to the absence of global topographic data. The spatial sampling is 22 km (0.5°) per pixel. . . . .	10
2.2	The spatial extent of the study area and available data coverage. A) RADAR coverage for the south polar region of Titan, B) Ontario Lacus C) The longest stream in the region, Saraswati Flumen in the vicinity of Ontario Lacus creates a deltaic deposition (Wall et al., 2010). . . .	11
2.3	A) High resolution stereo DEM acquired using the RADAR T57/T58/T65 stereo (1.4 km per pixel resolution) data. B) Flow accumulations (bright white pixels) calculated by ArcGIS’ hydrology tool on the topographic data of Ontario Lacus. The white lines indicate regions where fluid accumulates. The blue dotted line demarcates the spatial extent of Ontario Lacus.	13

- 2.4 A) Catchment area of Ontario Lacus (in polar stereographic projection) derived from hydrological analysis. The magenta extent marks combined catchment area that drains into Ontario Lacus. The black dotted line marks the region which does not drain into Ontario Lacus but its surrounding basins. The catchment regions are overlaid on the DEM of the region to provide the elevation context. B) The three major catchment regions of Ontario Lacus (see Discussion section). Solid line shows the catchment that distinctively contributes to Ontario Lacus. The faint line to its right shows the catchment that might not directly contribute to Ontario but is inferred based on regional trends. The dotted line in B) shows the catchment that does not contribute to Ontario. It drains into the Romo Planitia, close to the south pole. C) RADAR image of a section of the catchment area (boxed area in B) indicating a potential drainage divide (shown by white arrow) which might affect the total catchment area of Ontario Lacus. 14
- 2.5 A diagrammatic representation of all the hydrological parameters included in the mass balance calculations for Ontario Lacus. . . . . 17
- 2.6 The general topographic profile of a few streams around Ontario Lacus. A flat profile might indicate a mature stream with no tectonic uplift. As the profile suggests, Saraswati (in red) flumen is flatter, whereas the profile of other two fluminae, Karesos and Hubur (in blue and green respectively) are steeper – not too surprising as they originate in mountains. The abrupt changes in the profile of Karesos could be a topographical artifact because of coarse resolution topography data. However, the broad trend still suggests a steeper gradient of Karesos flumen compared to the other two fluminae. The inset shows location of these fluminae near Ontario Lacus in a RADAR map. The gentler gradient of Saraswati Flumen could also suggest that it has a much larger drainage with headwaters not covered by the limited DEM dataset. We indicate this absence of data through a question mark in the stream profile. . . . . 20
- 2.7 T56 flyby synthetic aperture RADAR (SAR) image of Saraswati Flumen that shows a putative oxbow lake (or lakebed, perhaps). A) Shows western shoreline of Ontario Lacus in RADAR data. Saraswati Flumen’s extent is shown in yellow. Saraswati Flumen is also shown in Figure 2C by yellow arrows and the context provided in 2A and 2B. B) The blue box shows a zoomed in view of Saraswati Flumen with the green arrow pointing at the putative Oxbow lake. 7C is similar to 7B but without the stream’s extent marked. . . . . 21
- 3.1 VIMS wet-sidewalk color composite (R:5 $\mu$ m, G: 2.7 $\mu$ m, B:2 $\mu$ m) of Titan’s north polar region showing the region corresponding to the BEF in the flybys A) T106, 24 October, 2014 B) T120, 07 June, 2016, and C) T121, 25 July, 2016. The yellow box in 1C shows the disappearance of the Bright Ephemeral Feature (BEF) three Titan days later (See Table 1). D) Zoomed-in view of the north polar region from the T120 flyby annotated to identify the features. E) Analog for the T120 BEF on a cloudy day after rainfall. F) Analog for the T120 BEF as mudflat in Utah’s Bonneville salt flats . . . . . 26

- 3.2 The figure is in a different orientation than Figure 1. Kraken Mare is in the bottom right as opposed to the bottom left in the previous figures. A) RADAR map of the north polar region of Titan in Polar Stereographic projection. The yellow box indicates the region corresponding to the BEF illustrating that the region is mostly solid land. The non-data regions are white. B) VIMS infrared color composite (R:5  $\mu\text{m}$ , G: 2.7  $\mu\text{m}$ , B:1.3  $\mu\text{m}$ ) representing the yellow-boxed region as in the RADAR map of the north pole. C) VIMS infrared color composite (3B) (R:5  $\mu\text{m}$ , G: 2.7  $\mu\text{m}$ , B:1.3  $\mu\text{m}$ ) overlain on the north polar map of RADAR (3A) showing the BEF and specular point. The red arrow indicates the specular reflection point (82.7°N, 78.6°W) near Xolotlan Lacus. The magenta arrows indicate the BEF we observe in T120. . . . . 29
- 3.3 A) The colored boxes correspond to the different regions in the T120 observations: dark blue (clouds), green (land), light blue (sea), red (specular reflection), magenta (BEF), and yellow (evaporites). B) The spectra corresponding to the regions in similar colors as the boxes in A. Grey solid boxes show spectral regions affected by methane absorption and thus blocked by Titan’s atmosphere. C) Shows the spectra for the location of the BEF. The slightly higher reflectance at shorter wavelengths of the T106 observation (cyan) is because of the higher emission angles. The magenta spectrum corresponds to the BEF during the T120 June 2016 flyby which is distinctly brighter than other spectra at 5 $\mu\text{m}$ . The yellow spectrum indicates reflectances for the same region three Titan days later during the T121 July 2016 flyby. . . . . 30
- 3.4 A) Modeled reflectance (I/F) variation with surface roughness for the broad specular reflection (BEF) observed during the T120 flyby. The modeled (magenta) reflectance peaks at roughness ( $\sigma$ ) values of  $\sim 14^\circ$  indicating that the BEF’s surface roughness could be of that order. B) T120 *Cassini* image cube CM1866022476 where the BEF is observed. C) Model-generated synthetic images for the T120 observation geometry with a surface roughness parameter of  $2^\circ$  reveals only the specular reflection. One thing to note is the scale in the synthetic images: as we increase the roughness or specular deviation angle — $\sigma$ —the specular reflection spreads over a larger number of pixels, each pixel receiving lesser solar flux for higher  $\sigma$  and hence the scale changes. D)  $\sigma$  of  $12^\circ$  covers the extent of BEF. E)  $\sigma$  of  $24^\circ$  distributes the entire solar flux onto the Titan hemisphere. . . . . 33
- 3.5 Orthographic wet-sidewalk color composite for the T119 (06th May, 2016) flyby. This is in same orientation as Figure 1. The T119 flyby occurred two Titan days before (BEF) T120 (07th June, 2016). The purplish hues in this color composite indicated by blue arrows show the cloud cover over the north pole. The BEF region corresponding to T120 is shown by a magenta arrow. . . . . 35
- 3.6 I/F variation with the distance of specular point. Both reflectance values (model generated (blue) and T120 actual observation (green)) show similar trends. The reflectance decreases as the distance from the specular point increases, but the model-generated reflectance values are off by a factor of  $\sim 2$ . We multiply the model (Red) by a ratio (2.3) of averaged slopes of model and data to scale the model but still notice the difference in slopes. This could be due to the reflections from wetted surfaces that have a non-zero average slope unlike our model. . . . . 35

- 4.1 shows the size distribution of the equivalent radii ( $\sqrt{(Area/\pi)}$ ) of the north polar Titan lakes. The size distribution (green) of the equivalent radii of lakes on the north pole of Titan follow a lognormal distribution (red). Terrestrially, the diameter of thermokarst lakes follow a lognormal distribution (??). The volcanic paterae on Io (?) also follow lognormal distribution. . . . . 41
- 4.2 A) RADAR (false colored) image of Titan's north polar (north western part) lakes in blue. We don't show the RADAR north polar map because the right quadrant of the north pole between the longitudes of 220° and 330°W harbors the bigger seas. B) Rose diagram indicating the orientation of the Titan lakes (angle between the line joining the antipodal pair of a lake and the north pole). The orientation of lakes show a NE-SW (NorthEast-SouthWest) or (45°W - 225°W) direction in B. The colors in this plot are just the bar colors for viewing ease. . . . . 42
- 4.3 A) (modified from Wikipedia) shows the methodology of Elliptical Fourier Analysis. Leaf outline is shown in blue. The red ellipse over the blue leaf outline is the first harmonic. The (fifth and) tenth harmonic regenerates the sinuosities of leaf's edge and shape. B) RADAR image of Myvatn Lacus (78 °N, 135 °W) (peculiarly shaped). Figure C) shows that by 20th harmonic the extremely complicated shape of even Myvatn Lacus can be explained quantitatively by the Elliptical Fourier Analysis . . . . . 47
- 4.4 A) shows the synthetic lake shapes we use for analysis. The kidney bean lake shape is in red, pointy lake shape is in blue, and sharp lake shape is in green. B) Principal component plot with the geomorphological shapes. The shaded grey shapes in the morphological space are the shape variations along the principal component axes. PC1 explains 90 % of the variation in shape while PC2 explains ~ 10 % of the variation in shape. The red dots indicate the four kidney beans with different rotation angles (90°,180°,270°,360°). The ellipse around the red points represents the 95% confidence interval. Similarly the blue and green dots indicate the pointy lakes and sharp lakes with the ellipses representing the 95% confidence interval. . . . . 48
- 4.5 A) shows the Earth lakes we use for analysis. The lake shapes blue in color are classified as volcanic lakes. Similarly the lake shapes in red are classified as tectonic lakes. Since the shapes of these two kinds of lakes are discretely different we chose these two lake types to see if they separate in the principal component space. The shaded colors indicate the group that the lakes belong to according to our k-means cluster analysis. B) Principal component plot with the end member shapes. PC1 explains 84.2 % of the variation in shape while PC2 explains ~ 5.55 % of the variation in shape. We can see that principal component 1 explains the variation of lake shapes from circular to elliptical (fat to fit). Principal component 2 explains the curvature in the shape. The red dots indicate the distribution of the tectonic lakes. As expected they clump more toward the skinny or elliptical side of shape variation in the principal component space. Similarly the blue dots represent the terrestrial volcanic lakes (more circular in shape). These cluster toward the circular end of the principal component plot. The ellipse represent the 95% confidence interval for both the populations. . . . . 50

- 4.6 Top panel represents the lake shapes with their respective names on the north pole of Titan. The numbers in the brackets indicate the group (using our k-means cluster analysis) that the lake belongs to. Bottom left panel indicates the first two principal component's plot for Titan lakes (from the top panel). We randomly chose five standard lakes (Feia Lacus, Oneida Lacus, Rukwa Lacus, Sparrow Lacus, Vanern Lacus) that we digitized everyday before starting digitization of other lakes. PC1 shows the shape variation from circular to elliptical and explains 30.4% of variation in the shapes of Titan lakes considered in this study. PC2 shows the shape variation from pointy extensions to a curvature in the pointy extensions and explains 15.6% of the variation in data. The ellipse shows the 95% confidence interval so that there is a 95% probability that the Titan lakes lie within the ellipse. Bottom right panel shows the four groups of lakes that we derived from the k-means analysis on the principal component plot. . . . . 52
- 4.7 Phylogram for the heirarchical clustering of Titan north polar lakes. Letas Lacus exists by itself like in the principal component analysis. Same lakes re-outlined to determine the error are all together in same clusters. Other clusters of lakes when compared with their shapes can be seen clustering well in similar shapes. The heirarchical cluster helps us group similar shapes together thereby indicating similar formation mechanisms. . . . . 54
- 4.8 Top panel shows the elbow method for the determination of number of clusters in the k-means clustering analysis. Bottom panel shows the four clusters of lake shapes. . . . . 55
- 4.9 Geographic location of the four clusters of lake shapes (derived from k-means clustering) on the north pole of Titan. The base images are ISS and RADAR north polar image of Titan. The colors are **Group 1**: round, e.g :Yessey Lacus), **Group 2**: (long with asymmetries along their long axis, e.g :Rukwa Lacus), **Group 3**: (long with asymmetries along their short axis, e.g :Vanern Lacus), and **Group 4**:long lakes, e.g :Oneida Lacus . . . . . 56

Exploring Xanadu through my eyes,  
I see the faint star Sun is in the sky  
Sailing up and down in my rover-boat,  
In the methane river on Titan —my home  
Strange but true  
Clouds of Methane, rain here  
Life here is something new!  
Transferring energy from the great red spot,  
I melted rocket full of ice on Enceladus,  
To be transported to us.  
Then got a call from the International Savior Station (ISS)  
My picnic was over,  
We left back to our home,  
Me, My Spacecraft n Rover

My home Titan is special in its own ways as this is the energy, power and industrial hub for human genre. While the young Titanians go to Mars for education, some educators arrive from Moon too. As I pack my bag for tomorrow's class, I get reminded of my class on observations from Radio Astronomy laboratory on Moon. The atmosphere less moon, offers the best observations of celestial sphere. I would like to observe Earth in Radio waves for my class tomorrow!

*I wrote this poem and article back in 2008 when I had an immense desire to study Titan.*

## CHAPTER 1: INTRODUCTION

Human curiosity has driven mankind's exploration to far and beyond the solar system. This need for quenching our curiosity is reflected in the question motivating this thesis. How did Saturn's moon Titan with a hydrocarbon based hydrological cycle, a thick atmosphere, and stable bodies of surface liquids, end up being a world like Earth yet more esoteric? Finding a piece to this giant puzzle is the impetus behind this thesis.

Saturn's largest moon, Titan has attracted planetary scientists and astronomers alike ever since its discovery by Christiaan Huygens in 1655 (Huygens, 1999). It is at a distance of 1.2 million km from Saturn and takes 15.9 Earth days to complete an orbit. As Titan follows Saturn orbiting the Sun, a Titanian year is approximately 30 Earth years. At a distance almost 10 times as far from the Sun as Earth (about 1.4 billion km) Titan is cold and dark. Despite the frosty temperatures and 1/100th of the sunlight received on Earth, Titan's surface temperature and pressure conditions make it a fascinating place to study. The pressure-temperature conditions (1.4 atm, 90-94K) (Fulchignoni et al., 2005) are close to the triple point of hydrocarbons (e.g methane's triple point is  $\sim 92\text{K}$ ). Hence, hydrocarbons play the same role on Titan as water plays on the Earth.

Titan is the only moon in our solar system with a thick atmosphere. It hosts standing bodies of stable liquids and a hydrocarbon-based hydrological cycle that circulates from the atmosphere to the surface, and back to the atmosphere. Titan is deemed a world of intriguing mysteries, since its discovery. The mystery deepened with the discovery of the dense atmosphere by Jose Comas i Sola in 1907 (Comas Sola, 1908) due to limb darkening, (Limb Darkening is an optical effect where the center of the object looks brighter than the limbs) comparing it to similar observations of Neptune disk. The existence of Titan's atmosphere was confirmed by Gerard Kuiper (Kuiper, 1944) but led to more questions about the sustained presence of methane. The photolysis of methane by ultraviolet solar photons and cosmic rays destroys methane into higher order hydrocarbons. The continued presence of methane in Titan's atmosphere suggests an active process replenishing what could have been lost over the age of solar system.

About 73 years elapsed between the first speculative guesses by Comas Sola that Titan possessed a thick atmosphere to the actual detection of molecular compounds by the Voyager flyby of the Saturn system in 1980. These remarkable discoveries were just the beginning of unveiling the esoteric planetary body Titan is.

Pioneer11 was the first spacecraft to flyby Titan and confirm that Titan has an atmosphere. Inspired by Pioneer 11's result, Voyager 1's course was modified for a close-up flyby of Titan. Voyager 1 helped decipher Titan's atmospheric chemistry, scale height, and surface pressure and temperature (Hanel et al., 1981; Lindal et al., 1983), among other things. These results were exciting because the pressure temperature conditions on Titan place methane near its triple point. Thus, methane acts like water acts on Earth, with solid, liquid, and gaseous phases co-existing in Titan's environment.

However, the visible cameras onboard Voyager were unable to penetrate Titan's thick atmosphere so while methane rain was expected on Titan's surface, we couldn't decipher the distribution of these fluids. Motivated by the Voyager 1 and 2 results, a joint endeavor of NASA, ESA (the European Space Agency) and the Italian space agency (ASI), *Cassini* was conceived. The *Cassini* mission was composed of an orbiter and a probe (Huygens). The probe, built by ESA, parachuted to the surface of Titan, in

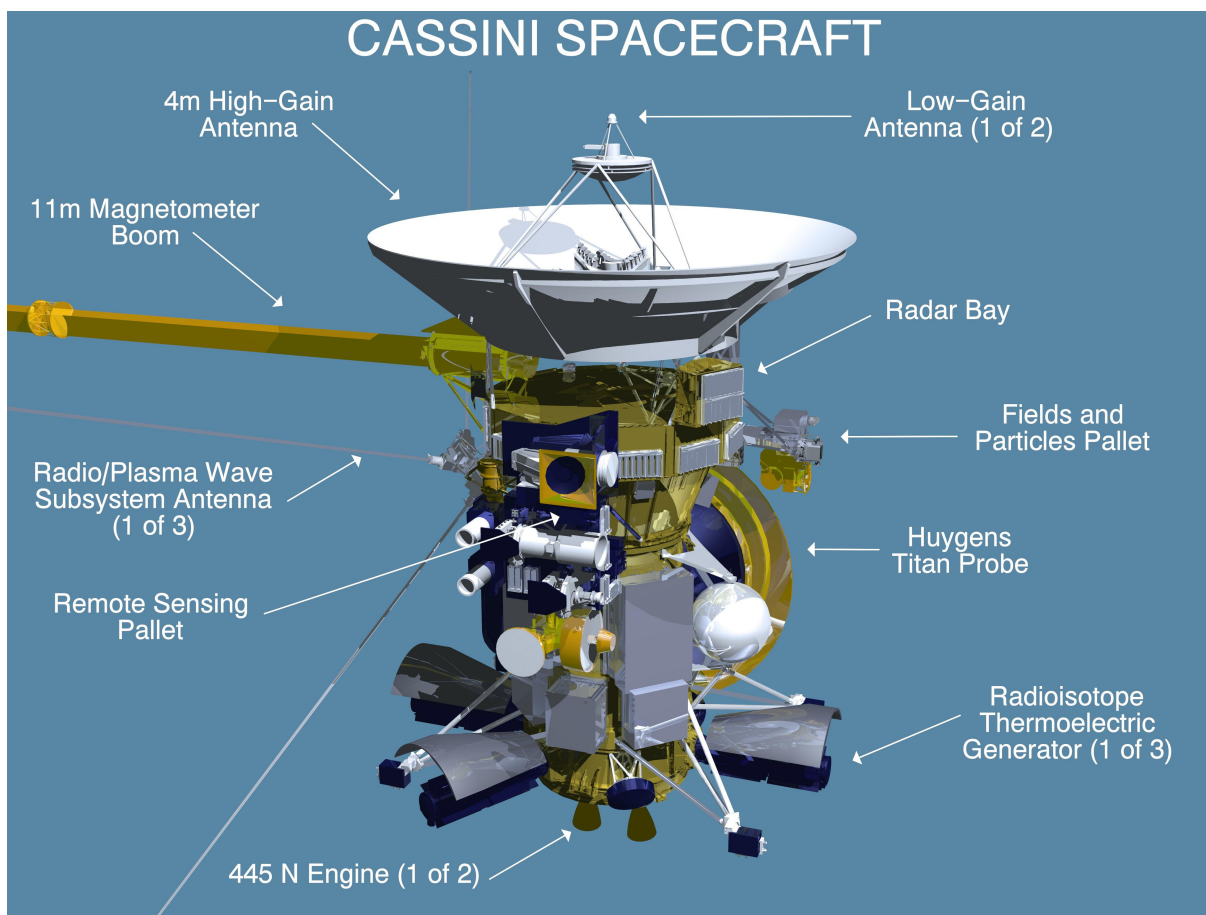


Figure 1.1: The diagram of the Cassini spacecraft. Cassini was a cooperative project of NASA, the European Space Agency and the Italian Space Agency. Image source : NASA photojournal

January 2005 —the most distant landing to date in our solar system. Huygens then returned exemplary information about the atmospheric haze through its two and a half hour descent. However, the image that startled scientists and public alike was the first image of Titan's surface of rounded cobbles of ice on a flood-plain damp with liquid methane.

The *Cassini* orbiter had 12 instruments for remote sensing observations. The Ku-band RADAR operating at  $\sim 2.2$  cm was capable of obtaining images of the surface at a scale of 300 meters. The VIMS (Visual and Infrared Mapping Spectrometer) instrument could look through the atmosphere at Titan's surface in infra-red wavelengths and so could the ISS (Imaging Science Subsystem) camera. Pertinent to my thesis, I will emphasize the VIMS (Visual and Infrared Mapping Spectrometer) instrument. I also use ISS (Imaging Science Subsystem) and the RADAR instrument's data for my research to create a comprehensive understanding across different wavelengths.

In Titan's atmosphere, at short (blue) wavelengths, light is strongly absorbed by the reddish haze particles. At longer wavelengths, light is scattered by the haze, although the column optical depth is still high. In the near-infrared region, the haze becomes more transparent since the haze particles are smaller than the redder wavelengths. Where the methane absorption is weak, clear regions or atmospheric

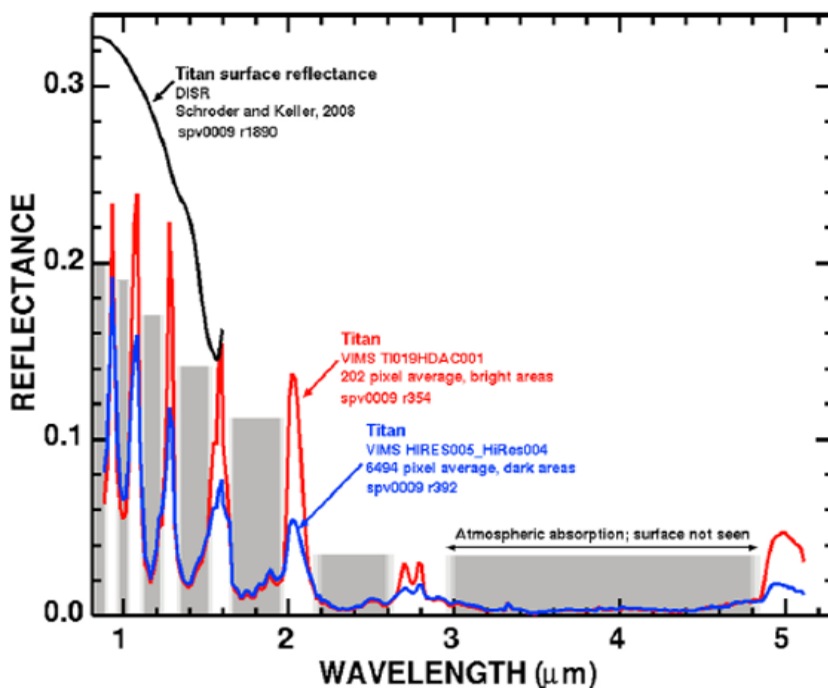


Figure 1.2: Representative VIMS spectra of the bright and dark regions on Titan. Grey bands indicate where Titan’s surface is not seen in the VIMS data due to atmospheric absorption and scattering. DISR (Descent Imager Spectral Radiometer) was an Optical Remote Sensing Instrument for the Huygens Probe. The derived DISR spectra is shown in black for comparison. Both the spectra indicate a strong blue slope to the spectra of Titan in the observed wavelengths. (Clark et al., 2010)

‘windows’, situated near 0.83, 0.94, 1.07, 1.28, 1.6, 2.0, 2.9 and 4.8  $\mu\text{m}$  enable access to the surface and characterization of its properties.

VIMS consists of two camera instruments, a ‘pushbroom’ mapping spectrometer that studies visible light (VIMS-VIS) and a ‘whiskbroom’ mapping spectrometer for infrared light (VIMS-IR). VIMS ‘image cubes’ contain information in 352 different wavelengths of light from ultraviolet to the mid-infrared. The visible channel produces hyperspectral images spanning the spectral range 0.3-1.05  $\mu\text{m}$  over 96 spectral bands. The infrared channel covers the wavelength range 0.85-5.1  $\mu\text{m}$  over 256 spectral bands (Brown et al., 2004). This is much higher spectral resolution than the Imaging Science Subsystem ISS, but the spatial resolution of VIMS is approximately 100 times lower than the resolution of ISS.

The *Cassini* ISS and the VIMS cameras first peered through Titan’s atmosphere and provided the intriguing views of Titan’s surface. Titan’s surface is morphologically sculpted by a rich variety of aeolian, pluvial, fluvial, lacustrine, tectonic, endogenic, and exogenic processes. Both Titan and Earth have wind, rain, evaporation, erosion, and standing bodies of liquid. Titan, however, is very early-earth like. Exploring Titan would enable to understand various aspects of early Earth evolution, including probably the origin of life. To understand the evolution of the chemistry on Earth to pre-biotic chemistry and to biology, we must go to a natural laboratory in a different world where a primitive environment is preserved and pristine chemistry is still at work.

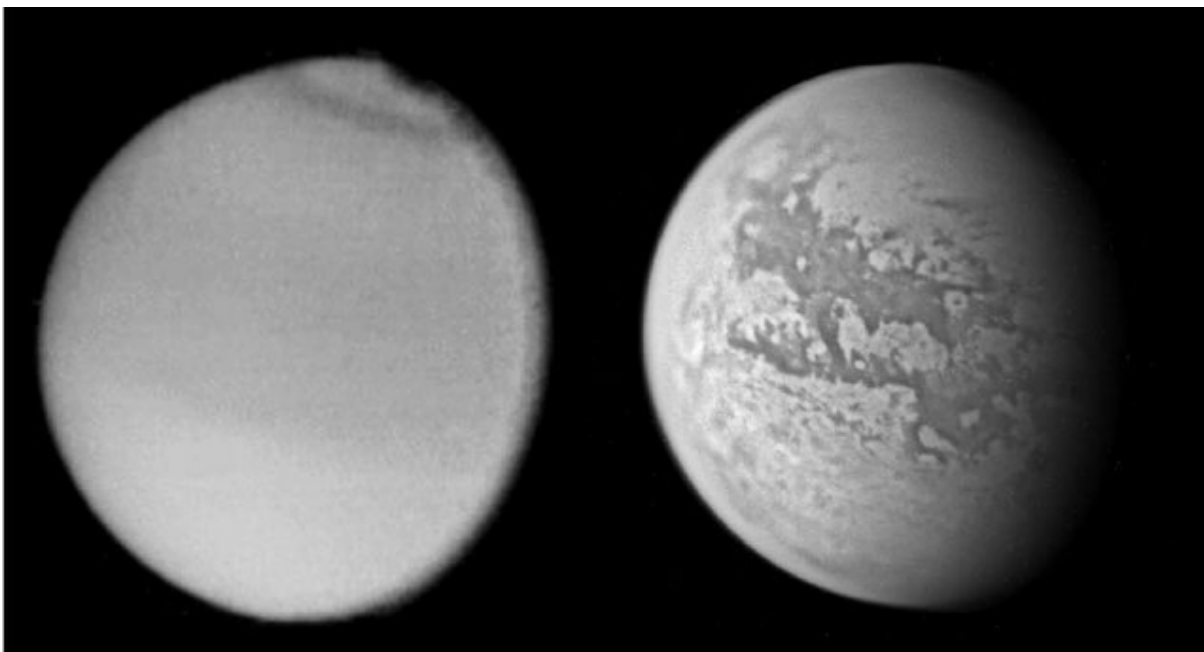


Figure 1.3: The image of Titan as seen from Voyager 1 in visible light and as seen from the infra-red ( $0.93 \mu\text{m}$ ) (ISS) camera of Cassini. Image source : NASA photojournal

## 1.1 MOTIVATION FOR THIS THESIS

The main goal of my thesis is to shed light on the nature of the ‘hydrological cycle’ on Titan. To answer questions like : How have the atmosphere and surface of Titan evolved over its history? and How do the atmosphere and surface interact through the hydrological cycle?

Most of the Titan’s fluids are located poleward, more in the north than south. This dichotomy is well documented and has been debated for long. For my first project (Chapter 2 ), I addressed the science question of what could be the reason that Titan’s otherwise dry south pole has one large filled lake —Ontario Lacus. I used geomorphology and mass balance equations to approximate the input fluid amount in Ontario Lacus with respect to available topography information (Lorenz et al., 2013). I found that Ontario Lacus has a huge catchment area, larger than any on Earth’s lakes, extending till the southern-mid latitudes of Titan. To put this in perspective, Ontario Lacus is about the size of Lake Michigan. Yet, Lake Michigan has a catchment area one and a half orders of magnitude smaller than Ontario Lacus (Dhingra et al., 2018). 5.5% of Titan’s surface area ( $8.3 \times 10^7 \text{ km}^2$ , assuming Titan is a sphere) is covered by Ontario Lacus’ catchment area. We think this is substantial planetary coverage for a lake as big as Lake Michigan, whose catchment area covers only 0.02% of Earth’s surface. This study shows that the physical movement of fluids on Titan, including the changes in fluid level, flow, and dynamic processes (like formation of catchment areas) are extremely similar to that of Earth’s.

The products of photolysis products in the atmosphere fall down on Titan’s surface, contributing to its organic inventory. Methane also rains out of the atmosphere. My second project was a study of this aspect of the hydrological cycle —rainfall (Chapter 3). In one of the Titan flybys, we used the VIMS

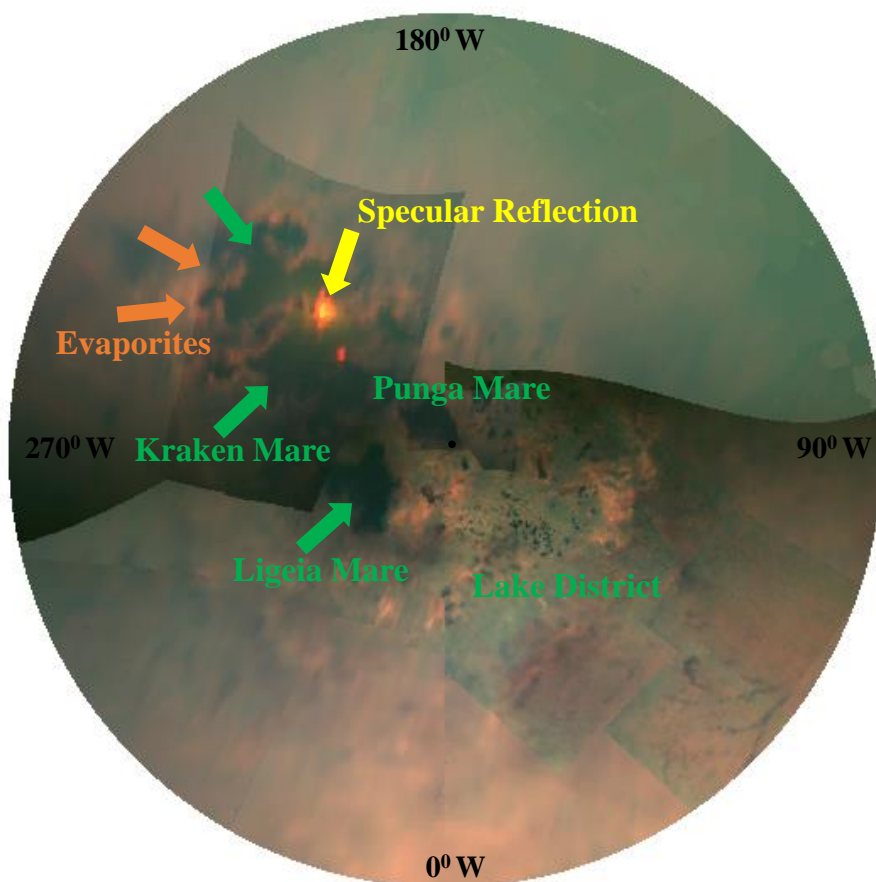


Figure 1.4: Titan's north pole in orthographic projection after the end of Cassini mission. This collage has all the flybys of Titan that cover the north pole and was made by Shannon MacKenzie. The color scheme is R:5 $\mu$ m, G: 2 $\mu$ m, B:1.3 $\mu$ m. The bright reflection is a mirror like reflection from the shores of Kraken Mare (Top left region of the image). Less brighter orange pixel shows the waves in this big sea, Kraken Mare. Reddish 5 $\mu$ m bright material are evaporites that are left behind after evaporation of the liquid. The other smaller dark dots in the lower right part of image are the smaller lakes on Titan and suitably the region is called, Lake district. The black dot near Punga Mare marks the north pole of Titan.

(Visual and Mapping Spectrometer) data to observe a brightly reflecting region that was not observed in the subsequent flyby, two Titan days later. We interpret this ephemeral feature based on our analysis and spectra as a recently rain-wetted region. Basically, after a rainfall event we can see a solid surface reflecting sunlight as a wet-sidewalk effect. The intensity of brightness depends on the viewing geometry. Our detection of this on Titan indicates that we have spotted rainfall on Titan and have devised a new way to discover more rainfall features. This result was important because any signs of precipitation on the north pole were missing as per the suggestions of the GCM (General Circulation Model). Our observation helped nail this change in season which will help in long term climate change determination on Titan.

Meanwhile, I realized that while we know something about the composition of the fluids and other active hydrologic processes on Titan, we have insufficient information about the formation mechanism of the depressions that harbor the fluids. I used a new methodology called EFDA (Elliptic Fourier Descriptor Analysis) that has been used in biology and paleontology to quantify shapes. There were issues using this method in planetary landforms because of the absence of a synchronous point. I adapted the methodology to work for Titan's lakes and found that Titan's lakes can be grouped into four classes indicating four probable lake formation mechanisms or stages of formation of Titan's lakes. The main take-away of this study is that I can use this methodology to study landforms across planets/satellites and quantify their shapes to provide constraints on formation mechanisms.

The presence of organics and water ice bedrock make Titan susceptible to water-based and organic-based life-forms. Titan may represent a habitable environment in which an exotic form of life could have evolved. For these and other reasons, Titan remains a high priority target for future spacecraft missions. Currently proposed mission designs for studying Titan include drone —such as the New Frontiers mission proposal currently undergoing Phase A review Dragonfly.

## CHAPTER 2: LARGE CATCHMENT AREA RECHARGES TITAN'S ONTARIO LACUS

“Large catchment area recharges Titan’s Ontario Lacus” *Icarus*, vol. 299, 2018, 331-338

Originally published in

Dhingra R. D., Barnes J. W., Yanites B. J. and Kirk R. L. (1 January, 2018), Large catchment area recharges Titan’s Ontario Lacus, *Icarus*, 299, 331-338, [DOI.org/10.1016/j.icarus.2017.08.009](https://doi.org/10.1016/j.icarus.2017.08.009)

### 2.1 INTRODUCTION TO THE CHAPTER

In my first semester in the fall of 2014, I took a course taught by Dr. Brian J. Yanites titled, ‘Principles of Geomorphology’, in the Dept. of Geology. We had to do a project at the end of the course. My advisor Dr. Barnes advised me to look at the south pole of Titan. The dichotomy of distribution of liquids between the north and south pole is clearly evident and he advised me to look around Ontario Lacus, the only south polar lake.

This motivated me to ask the question of why is Ontario Lacus the only filled lake in Titan’s south pole. My geomorphic analyses using topography data from *Cassini* helped me formulate an answer to this outlying question on Titan. We found that Ontario Lacus has an extensive catchment area that extends to the southern mid-latitudes. The extended catchment area along with the VIMS based cloud observations at 40°S pointed that if the observed clouds are precipitative and rain out then all the fluid will drain to Ontario Lacus. I published these results in the journal *Icarus* that is widely read in Titan research.

We seek to address the question of what processes are at work to fill Ontario Lacus while other, deeper south polar basins remain empty. Our hydrological analysis indicates that Ontario Lacus has a catchment area spanning 5.5% of Titan’s surface and a large catchment area to lake surface area ratio. This large catchment area translates into large volumes of liquid making their way to Ontario Lacus after rainfall. The areal extent of the catchment extends to at least southern mid-latitudes (40°S). Mass conservation calculations indicate that runoff alone might completely fill Ontario Lacus within less than half a Titan year (1 Titan year = 29.5 Earth years) assuming no infiltration. *Cassini* Visual and Infrared Mapping Spectrometer (VIMS) observations of clouds over the southern mid and high-latitudes are consistent with precipitation feeding Ontario’s large catchment area. This far-flung rain may be keeping Ontario Lacus filled, making it a liquid hydrocarbon oasis in the relatively dry south polar region.

## 2.2 INTRODUCTION

With a thick atmosphere, a methane-based hydrological cycle, stable bodies of standing fluid at its surface, and many active surface processes, Saturn’s largest moon Titan is surprisingly Earth-like. The pressure-temperature conditions (1.4 atm, 90-94K) (Fulchignoni et al., 2005) are close to the triple point of hydrocarbons (e.g methane’s triple point is  $\sim 92\text{K}$ ). Hence, hydrocarbons play the same role on Titan as water plays on the Earth. The movement of fluid on the surface has created fluvial networks and valleys (Porco et al., 2005; Elachi et al., 2006; Barnes et al., 2007; Jaumann et al., 2008) which have been extensively observed and studied (Perron et al., 2006; Burr et al., 2013) by the *Cassini* mission. Titan’s surface conditions therefore make it the only known extra-terrestrial planetary body to currently have an active surface hydrology governed by an Earth-like hydrological cycle.

As a result of this cycle, Titan has lakes and seas of hydrocarbons at its poles (Stofan et al., 2007). However, the exact composition of the liquid for any given lake is not well known. Thermodynamic models estimate lake composition using *in situ* observations from the *Huygens* probe (e.g Cordier et al. (2009)). This model led to the conclusion that the lakes consist mostly of ethane, with lesser amounts of methane (10%) and propane (7%) along with other hydrocarbons. The discovery of ethane in Ontario Lacus based on VIMS observations (Brown et al., 2008) is consistent with the model predicted composition of lakes.

However, recent observations reveal that one composition model does not fit all liquid bodies. Bathymetry studies (Mastrogiuseppe et al., 2014; Le Gall et al., 2016) and lab based experiments (Mitchell et al., 2015) indicate that the northern sea Ligeia Mare has a composition of nearly pure methane. Lorenz (2014) suggests that composition varies across Titan’s seas due to the differing solute abundance because of latitude dependent precipitation and evaporation. MacKenzie and Barnes (2016) also find that the evaporite configuration of different lakes varies thereby indicating potentially different bulk composition of the lakes. These findings reinforce Lorenz’s idea of latitude based precipitation and evaporation (or some similar latitudinal influenced mechanism) leading to diverse composition of the hydrocarbon lakes and seas. In spite of these developments, the precise bulk composition of these lakes still remains indeterminate.

The mechanism driving spatial distribution of the lakes on Titan’s surface is also not well understood. While many lakes dot the north polar region of Titan (Stofan et al., 2007; Sotin et al., 2012) it is perplexing to see an almost barren south polar region. The south polar region is devoid of liquid except four small lakes and one large lake, Ontario Lacus. Ontario Lacus was the first fluid body observed by *Cassini* mission using the Imaging Science Subsystem (ISS) instrument (Turtle et al., 2009). Several studies have been carried out to interpret its composition (Brown et al., 2008), smoothness (Wye et al., 2009; Cornet et al., 2012b), and its bathymetry (Hayes et al., 2010).

Ontario Lacus measures 235 km x 75 km (Wall et al., 2010) with surface area of  $\sim 16,200 \text{ km}^2$ . The other four small lakes (Wood et al., 2013) in the south polar region are Crveno Lacus ( $\sim 32 \text{ km} \times 24 \text{ km}$ ), Shoji Lacus ( $\sim 6 \text{ km} \times 6 \text{ km}$ ), Tsomgo Lacus ( $\sim 53 \text{ km} \times 15 \text{ km}$ ), and Kayangan Lacus ( $\sim 9.5 \text{ km} \times 9.5 \text{ km}$ ). Some large basins near the south pole of Titan exist at lower elevations than Ontario Lacus, but remain empty currently. Figure 3.4 shows Hagal, Rossak, and Romo basins, along with Ontario Lacus’ basin.

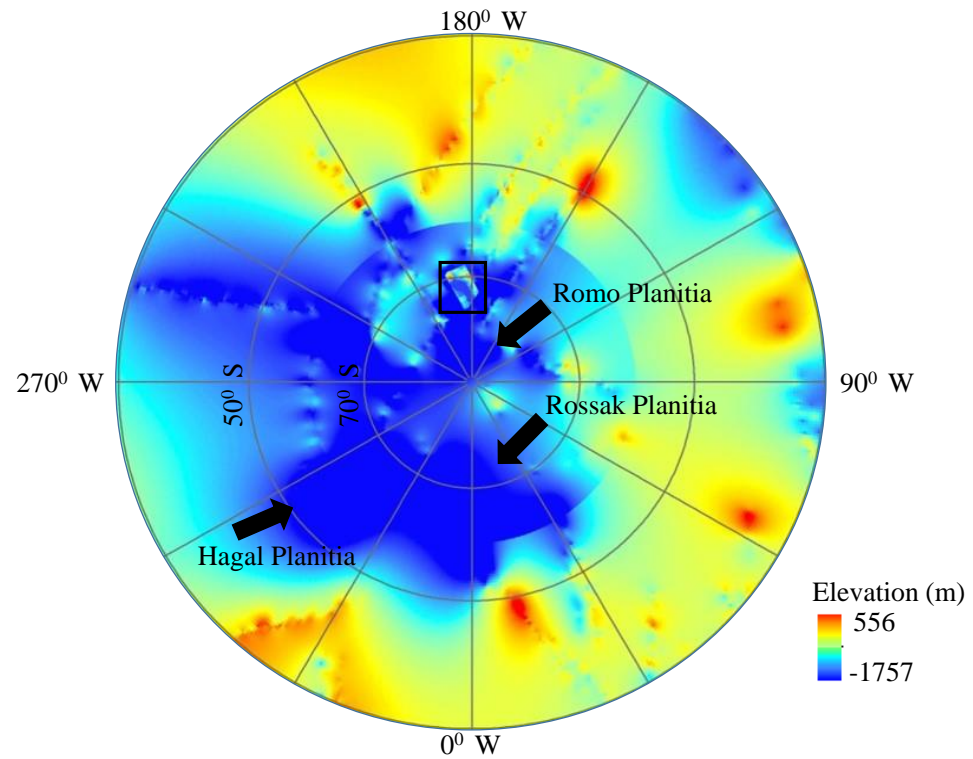


Figure 2.1: Titan's south polar topographic map derived by Lorenz et al. (2013) in Polar stereographic projection. Ontario Lacus is located within the region marked by the black box. The black arrows indicate the other low elevation regions in the south pole that are empty. The seams in the image are the available topography information while the rest of the topography is generated by an interpolation procedure due to the absence of global topographic data. The spatial sampling is 22 km ( $0.5^\circ$ ) per pixel.

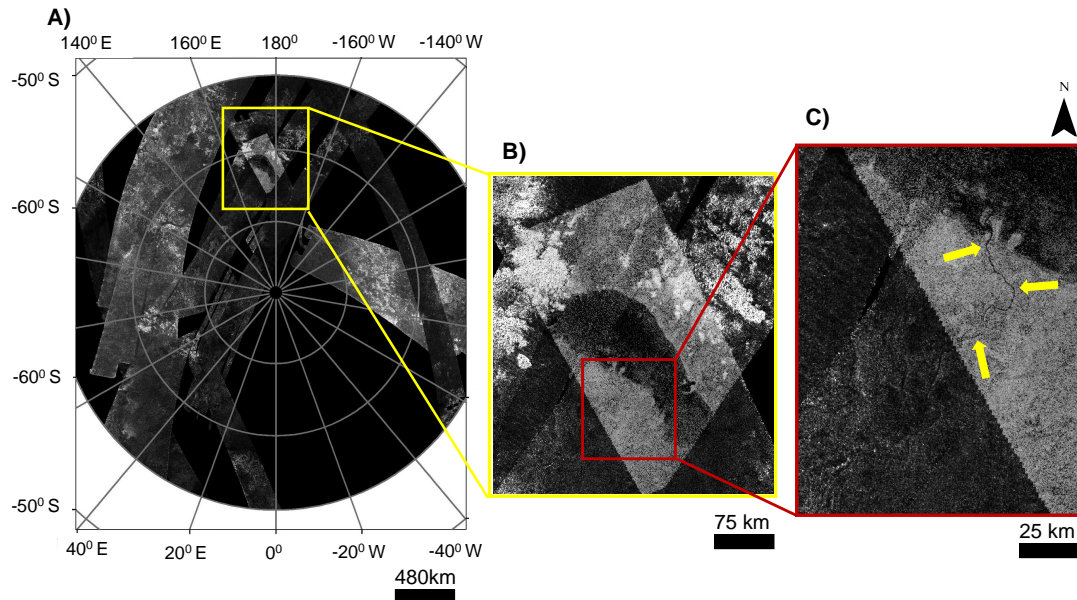


Figure 2.2: The spatial extent of the study area and available data coverage. A) RADAR coverage for the south polar region of Titan, B) Ontario Lacus C) The longest stream in the region, Saraswati Flumen in the vicinity of Ontario Lacus creates a deltaic deposition (Wall et al., 2010).

Ontario Lacus is readily recognizable in the south polar region by its shape which resembles a right human footprint (Figure 2). The morphology of Ontario Lacus tells a story of active processes. Mountains surround the northern end of Ontario Lacus and rise to heights of  $\sim 400$  m. The lake's western shore hosts a delta-like morphological feature (Wall et al., 2010) at the end of Saraswati Flumen, a very long channel (300 km) distinctly observable in the RADAR data and as shown in Figure 2B and 2C by arrows. A bay exists along the eastern shoreline which has likely been modified by fluvial processes (Wall et al., 2010). The southeast corner of Ontario Lacus shows a bathtub ring of evaporite (Barnes et al., 2009; Cornet et al., 2012a; MacKenzie et al., 2014). These processes collectively indicate that Ontario Lacus likely represents a dynamic hydrological system. Earlier studies (Cornet et al., 2012a; Hayes et al., 2010) suggested that Ontario Lacus lies in a shallow depression but more recent bathymetric studies by the radar detection of a lake-bottom reflection indicate that the depth could be as much as  $\sim 90$  m in some places, with an average depth of  $\sim 50$  m (Mastrogioseppe et al., 2016).

Aharonson et al. (2009) proposed that the asymmetry in the liquid distribution between the north and south pole may be due to the long term climate variations caused by the eccentricity of Saturn's orbit around the Sun. This scenario has been further explored using General Circulation Models (GCM) (Lora and Mitchell, 2015). Although plausible, the lack of pervasive evaporite deposits at the south polar region (MacKenzie et al., 2014) does not align with these hypotheses. In either scenario, it is difficult to explain why Ontario Lacus, neither the lowest point of the south pole nor the largest basin, remains filled in an otherwise dry region. In this work, we address this question via a detailed hydrological analysis of Ontario Lacus using topographic and synthetic aperture RADAR datasets. The major objectives of this

study are to identify and characterize the major drainage features around Ontario Lacus, and determine whether surface hydrology of the region around Ontario Lacus can shed light on why it is currently filled.

We discuss our three main analyses in the following sections. Section 2 discusses the analysis for catchment area using RADAR derived high resolution topography as well as low spatial resolution global topography (based on extrapolated data). In section 3, we evaluate the feasibility and conditions for the fluid availability at Ontario Lacus using a simple mass balance model utilizing current estimates of precipitation, evaporation and infiltration. Section 4 illustrates our stream profile analysis around Ontario Lacus aimed at understanding the hydrological evolution of the region which is followed by discussion and conclusions in section 5.

## 2.3 CATCHMENT AREA

Catchment area refers to the area from which rainfall flows into a river, or lake. It forms an important parameter to understand the surface hydrology of a region.

### 2.3.1 METHOD

We analyze the topography of the region around Ontario Lacus using ArcGIS to determine the extent of its catchment area. Sparse coverage of high resolution topographic data is an obstacle for our present day understanding of Titan. The extent of the available stereo-derived topography (1.4 km per pixel) data of our study area is indicated by a black outline in Figure 1. These data provide the local scenario for the determination of the catchment area of Ontario Lacus. Details of the topographic mapping are discussed in Section 4.1.

To fill in the gaps of topography, Lorenz et al. (2013) interpolated a global topography map for Titan using SARTopo and altimetry data (Stiles et al., 2009). To test the validity of this approach Lorenz et al. (2013) downsampled the Earth’s topography data with the geographical distribution where Titan data are available and carried out a spline interpolation. The topography map generated all the major topographical features on the Earth except the Tibetan plateau. This indicates that Lorenz et al. (2013) interpolation technique captures the overall trend in topography.

The global topography map has a resolution of  $\sim 22$  km per pixel, fifteen times coarser than the available high resolution stereo topography in the immediate vicinity of Ontario Lacus. Despite this difference, the interpolated map is useful as it provides the regional context necessary for estimating the catchment area contributing to Ontario Lacus. We re-interpolate these data using the Topo to Raster tool available in ArcGIS 10.1 (ESRI) to generate correct surfaces (Tarboton, 1997). The resulting topography map is used to determine the catchment area of Ontario Lacus as follows:

1. We first remove depression artifacts or pixel-scale lows from the digital elevation model. These “sinks” are localized surfaces of internal drainage that do not drain anywhere and thus cause the algorithm to go into an infinite loop.
2. The algorithm then generates a flow direction raster where each cell drains or flows in a particular direction depending on the elevation of the surrounding terrain.

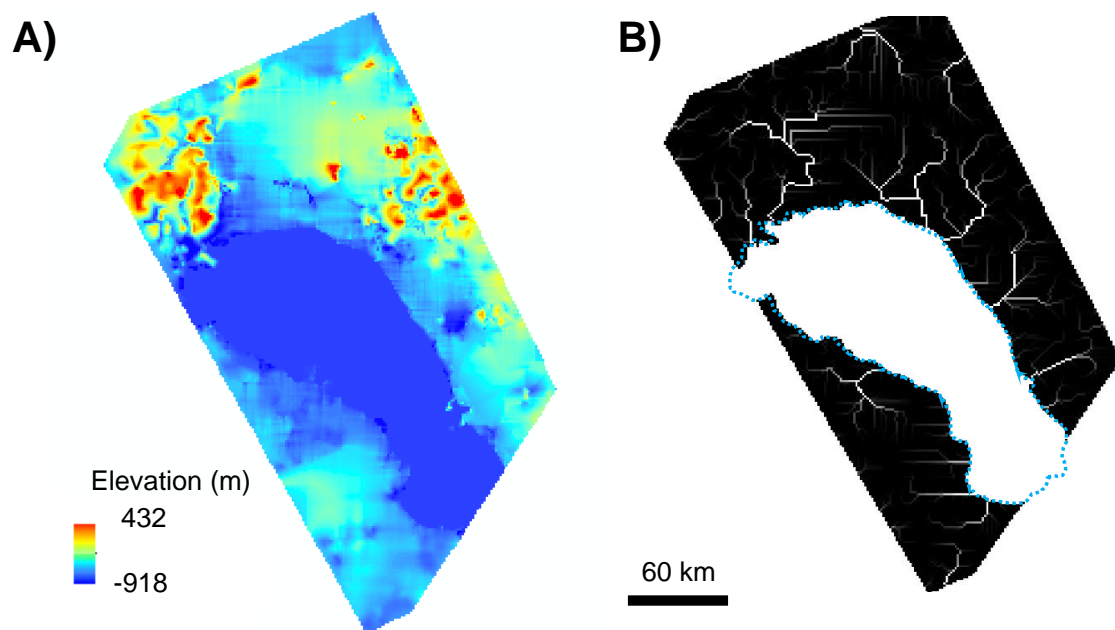


Figure 2.3: A) High resolution stereo DEM acquired using the RADAR T57/T58/T65 stereo (1.4 km per pixel resolution) data. B) Flow accumulations (bright white pixels) calculated by ArcGIS' hydrology tool on the topographic data of Ontario Lacus. The white lines indicate regions where fluid accumulates. The blue dotted line demarcates the spatial extent of Ontario Lacus.

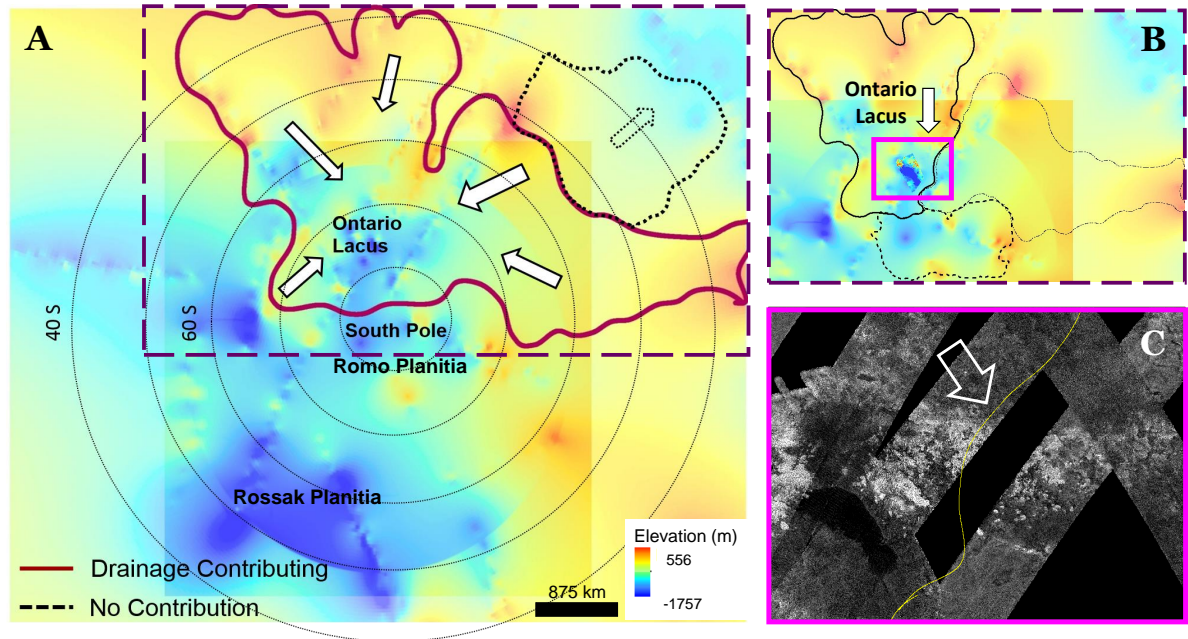


Figure 2.4: A) Catchment area of Ontario Lacus (in polar stereographic projection) derived from hydrological analysis. The magenta extent marks combined catchment area that drains into Ontario Lacus. The black dotted line marks the region which does not drain into Ontario Lacus but its surrounding basins. The catchment regions are overlaid on the DEM of the region to provide the elevation context. B) The three major catchment regions of Ontario Lacus (see Discussion section). Solid line shows the catchment that distinctively contributes to Ontario Lacus. The faint line to its right shows the catchment that might not directly contribute to Ontario but is inferred based on regional trends. The dotted line in B) shows the catchment that does not contribute to Ontario. It drains into the Romo Planitia, close to the south pole. C) RADAR image of a section of the catchment area (boxed area in B) indicating a potential drainage divide (shown by white arrow) which might affect the total catchment area of Ontario Lacus.

3. From the flow direction raster, we generate a drainage network map based on local flow accumulations.
4. We then place bucket points at the edge of an accumulation or at major confluences. Specifying a bucket point indicates the outlet of the catchment area into the lake or stream for calculating the total flux into the body.

We validate our results obtained from the global interpolated data by performing the above analysis on the high resolution but limited coverage topographic data around Ontario Lacus. Despite a fifteen times difference in resolution, the results from the high and low resolution topography data are consistent.

### 2.3.2 RESULTS

The total catchment area of Ontario Lacus is shown in Figure 2.4 and corresponds to an area of  $\sim 4.6 \times 10^6 \text{ km}^2$ . The catchment is made up of two sub-catchment regions as shown in Figure 4B: western

sub-catchment (bound by thick line), and eastern sub-catchment (bound by thin line). The one towards the south (bound by dashed line) drains away from Ontario Lacus and is not included. Based on the available topography data, the western and eastern sub-catchments drain into Ontario Lacus and so we have used the combined area of these two regions as the catchment of Ontario for our calculations. The RADAR images of the eastern sub-catchment indicate potentially high elevation regions (bright terrain in RADAR data) which might affect the contribution of this sub-catchment to Ontario. However, incomplete RADAR coverage over the eastern sub-catchment prevents a definitive determination of the drainage divide. While the catchment area estimates should be considered with some caution, broad scale topography of the region shows draining towards Ontario Lacus. Any small changes to the contribution will not drastically change our final interpretation.

To put this in perspective, Ontario Lacus is about the size of Lake Michigan. Yet, Lake Michigan has a catchment area of  $\sim 0.11 \times 10^6$  km<sup>2</sup>, one and a half orders of magnitude smaller than Ontario Lacus. 5.5% of Titan's surface area ( $8.3 \times 10^7$  km<sup>2</sup>, assuming Titan is a sphere) is covered by Ontario Lacus' catchment area. We think this is substantial planetary coverage for a lake as big as Lake Michigan, whose catchment area covers only 0.02% of Earth's surface. Another Earth analog could be Lake Eyre in Australia, which sits in an endorheic basin (a drainage basin that doesn't drain into the ocean), like Ontario's, and covers 1/6th of the Australian continent. Lake Eyre has one of the biggest catchments of all the lakes on Earth, which at  $\sim 1.2 \times 10^6$  km<sup>2</sup> is still just one quarter the size of Ontario's catchment. The evaporation rate and precipitation rate around Lake Eyre region are 0.2 m/Earth year and 0.25 m/Earth year. For comparison, the evaporation and precipitation rate we use for Ontario Lacus are listed in Table 1.

The ratio of catchment area to surface area for a lake is a measure of inflow into the system. From our data this ratio for Ontario Lacus is 83 while it is 118 for Lake Eyre. Therefore in hydrological context, Ontario Lacus might be similar to Lake Eyre, although more arid. Despite being mostly dry, Lake Eyre basin still gets filled by periodic floods and groundwater recharge with varying amounts of fluid. Even a slight rainfall converts Lake Eyre into a semi-arid region. A similar increase in precipitation might result in filling of the paleo-basins on the south pole over geological time scales, however such an increase has not been observed during *Cassini's* lifetime.

We are unable to contrast the catchment area of Ontario Lacus with other deeper basins on the south pole due to poor altimetry coverage available in those regions. The interpolated global topography map is primarily derived from RADAR altimetry and SARTopo. Stiles et al. (2009) derived a technique for estimating topography using the overlap between each of the five radar beams that make up a SAR image, which he named SARTopo. Since Ontario Lacus has been well covered by RADAR strips we were able to extend our analysis to the surrounding regions. We were not able to derive any meaningful watersheds for the other basins using the global topography map. For the bigger seas on the north pole of Titan Lorenz et al. (2013) roughly estimated the catchment areas as thrice the surface areas of the seas.

A future mission to obtain global topography with a resolution of  $\sim 50$  km would be required to do this task completely. It is perplexing that the other, deeper basins are closer to the pole and still remain dry which is in contrast to the latitude based precipitation suggested by GCM models like that of Schneider et al. (2012). However, it is intriguing to note that the largest sea at Titan's North Pole is

also farthest from the pole.

## 2.4 MASS BALANCE

Our results from section 2, namely the large catchment area for Ontario Lacus, motivate us to use mass balance calculations to try to understand the movement of fluids in the drainage system of Ontario Lacus. We do this by assuming conservation of mass flux and calculating the mass balance in/out of the system. The parameters of this model comprise of precipitation, evaporation, runoff and infiltration as shown in Figure 5. The model helps us approximate how each parameter contributes in the fluid movement.

### 2.4.1 METHOD

We model incoming fluid accumulation and outgoing losses to determine whether a lake might be filled or empty.

$$\text{Change in the lake volume} = \text{Input} - \text{Loss} \pm \text{Sources or Sinks} \quad (2.1)$$

Input derives from the precipitation over the catchment area (calculated in Section 2.2). Loss occurs due to evaporation from the lake's surface. The difference between precipitation and infiltration (i.e the runoff) would eventually feed the lake. Ontario's surface area as determined using ArcGIS is  $\sim 16,200$  km<sup>2</sup>. The depth of the lake has 90 m as an upper limit and 50 m as an average. We express this balance in the form of an equation:

$$\frac{\delta(HA_l)}{\delta t} = PA_c - EA_l \quad (2.2)$$

where  $H$  represents the depth of the lake,  $A_l$ , the surface area of the lake,  $P$ , the precipitation over the catchment area  $A_c$ , and  $E$  is the evaporation from the lake.

We assume that the lake is in a steady-state, i.e there is no change in the liquid level. We acknowledge that, since evaporites have been identified along the shoreline of Ontario Lacus (Barnes et al., 2009; Cornet et al., 2012a; MacKenzie et al., 2014), the lake level has definitely changed over geologic time. Furthermore, Hayes et al. (2010) and Turtle et al. (2011c) indicate that the lake level may have changed in *Cassini's* lifetime. Cornet et al. (2012b), however, suggests no change in Ontario Lacus' extent between 2005 and 2010. We proceed with the steady state assumption since the lack of gross variations places an upper limit on  $\frac{\delta(HA_l)}{\delta t}$ .

In the absence of knowledge of the porosity of Titan's surface (Hayes et al., 2008), we assume it to be impervious and as such our estimates are a maximum for runoff. Hence evaporation is the only process by which the system is losing liquid. The left hand side of equation 2 disappears under our steady-state assumption, reducing our model to:

$$PA_c = EA_l \quad (2.3)$$

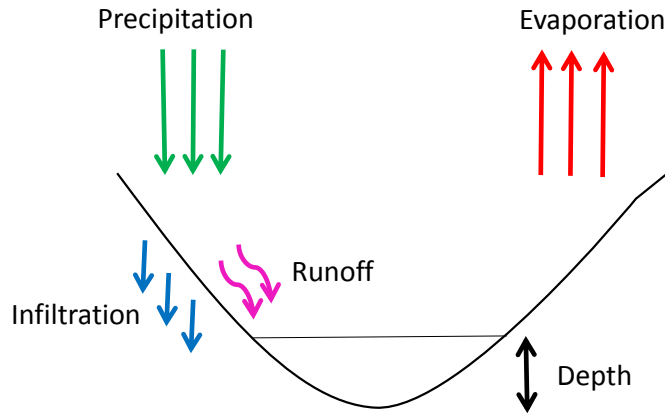


Figure 2.5: A diagrammatic representation of all the hydrological parameters included in the mass balance calculations for Ontario Lacus.

Thus, the factors that determine whether Ontario Lacus remains filled according to this mass balance calculation are the contributing catchment area, lake's surface area, precipitation and evaporation rates.

#### 2.4.2 RESULTS

Precipitation into a catchment area determines the fluid input. We find the volume of the fluid input to Ontario Lacus as  $\sim 5,440 \text{ km}^3/\text{Titan year}$  based on precipitation rates from Mitri et al. (2007) and  $\sim 18,442 \text{ km}^3/\text{Titan year}$  based on precipitation rates from Schneider et al. (2012). While Mitri et al. (2007) uses a bulk aerodynamic model to get the precipitation and evaporation rate, the rates calculated by Schneider et al. (2012) uses simulations with a three-dimensional atmospheric model coupled to a dynamic surface reservoir of methane. Since the catchment area of Ontario Lacus is large ( $\sim 4 \text{ million km}^2$ ), it plays a major role in quantifying the fluid input. However, there are no firm estimates on either the evaporation or precipitation rates on the surface of Titan. So, we proceed further by utilizing the values from the literature to evaluate whether any of the lower or upper bounds scenarios (low precipitation, low evaporation and high precipitation, high evaporation) are consistent with our observational inferences assuming that rates of evaporation/precipitation are valid.

Comparing the estimated rate of fluid input volume ( $\sim 5,440 \text{ km}^3/\text{Titan year}$ ) with the volume of Ontario Lacus ( $\sim 1,462 \text{ km}^3$  as an upper limit corresponding to depth of  $0.09 \text{ km}$ ) suggests that the lake would be filled in less than half a Titan year (1 Titan year =  $\sim 29.5$  Earth years) provided precipitation happens at the same rate that we use in our previous calculation of fluid input to Ontario Lacus and

the lake starts empty. With the depth of the lake at an average of 0.05 km even less volume is needed. Therefore, when we use the average depth, precipitation floods the lake in one Titan year. Table 1 lists the parameter values that we use and the results that we get using the mass balance calculations.

Evaporation from the lake's surface accounts for the fluid loss from Ontario Lacus. Mitri et al. (2007) determines the evaporation rate as 11m/Earth year (324 m/Titan year) for wind speeds of 1m/sec. Since these wind speeds seem high for Titan surface conditions (Lorenz, 2014), we take the baseline value of 1m/Earth year or 30m/Titan year as the evaporation rate. We also use another value for evaporation rate, 23 m/Titan year (Lorenz, 2014), as an alternative lower value. The volume lost from Ontario's system amounts to be 1660 km<sup>3</sup>/Titan year or 1306 km<sup>3</sup>/Titan year depending on the evaporation rate we choose.

Thus, using the available evaporation and precipitation rates for Titan, the evaporation from Ontario Lacus' surface area would be smaller than the precipitation (over the catchment area) in our mass balance calculation. It follows that the input fluid volume to Ontario Lacus is larger than the fluid loss from the system by evaporation alone. These results complement our results of a sizeable catchment area (in section 2) contributing fluid to Ontario Lacus. However, this consistency between observed inference and theoretical estimates should be treated with caution in view of the uncertainties associated with evaporation and precipitation rates. We certainly need more robust measures of these parameters from future missions to Titan.

Table 2.1: List of the parameters used in the mass balance study for Ontario Lacus. \* based on Mitri et al. (2007) \*\* based on Schneider et al. (2012)

	Semi Minor Axis	75 km
	Semi Major Axis	235 km
Ontario	Area	16,200 km <sup>2</sup>
	Maximum Depth	0.09 km
	Maximum Volume	1,462 km <sup>3</sup>
Result from 2.1	Total Catchment Area	4,600,000 km <sup>2</sup>
Input for eqn 3	Precipitation Rate 1*	1.2 m/Titan year
	Precipitation Rate 2**	4 m/Titan year
	Evaporation Rate 1*	30 m/Titan year
	Evaporation Rate 2**	23.6 m/Titan year
Results from 2.2	Runoff 1*	5,440 km <sup>3</sup> /Titan year
	Runoff 2**	18,400 km <sup>3</sup> /Titan year
	Evaporative Loss 1*	1,660 km <sup>3</sup> /Titan year
	Evaporative Loss 2**	1,300 km <sup>3</sup> /Titan year

## 2.5 STREAM PROFILE DETERMINATION

We extract elevation profiles of some of the prominent streams in the area to compare their maturity levels or tectonic upliftments (Cartwright et al., 2011; Burr et al., 2013) around the region. A flatter stream profile generally indicates a matured stream that has worked its way over the bedrock by erosion and flow over a long time (Davis, 1899) assuming no tectonic uplift to rejuvenate the stream. In contrast, a stream profile with many knickpoints might indicate a tectonically active region (Wobus et al., 2006). Thus, observing the stream profile gives us insights into the hydrological evolution of the region.

### 2.5.1 METHOD

The high resolution digital elevation models (DEMs) on Titan are generated by stereoanalysis of overlapping SAR (Synthetic Aperture RADAR) swaths and are controlled to agree with altimetry and SARTopo data in absolute elevation (Elachi et al., 2004; Kirk and Howington-Kraus, 2008).

The DEM for this analysis was generated in two parts from the SAR image swaths taken on flybys T57 and T58 each combined with the swath from T65. Incidence angles in the stereo overlap vary from  $38.5^\circ$  to  $45.3^\circ$  (North to South) for T57,  $25.7^\circ$  to  $34.5^\circ$  (North to South) for T58, and  $22.3^\circ$  to  $33.0^\circ$  (West to East) for T65 flyby. Given that the pairs have almost perpendicular look directions, and using a matching precision of 1.4 pixel (250 m), the expected vertical precision EP (Leberl et al., 1992) ranges from 85 to 120 m, or an average around 100 m but with the south end (T58) generally being a little bit better. The DEM was produced in BAE System’s SOCET SET stereo software package (Miller and Walker, 1993, 1995), using a rigorous sensor model for the RADAR SAR images.

Because of the difficulty of matching noisy radar images, the DEM was made by interactive measurement of a large number of ground points that were connected into a triangulated surface and then interpolated. The precision and accuracy of the altimetry are much better than the stereo precision, so the absolute heights in the DEM are only good to the  $\sim 100$  m level set by the stereo.

Using these DEMs we first map Karesos Flumen, Hubur Flumen, and Saraswati Flumen in the vicinity of Ontario Lacus. Then we extract the stream elevation profile from the high resolution topography data. A MATLAB-based algorithm convolves the accumulated flow at a given location with its elevation and flow direction to generate the profiles as shown in Figure 6.

### 2.5.2 RESULTS

The extracted stream profiles indicate that Karesos and Hubur Fluminae, which fall from the high northern mountains near Ontario Lacus have steep gradients. The elevation at the head of these streams extends as high as 400 meters. The abrupt changes in the profile of fluminae are topographical artifacts because of coarse resolution topography data. In contrast, the western stream, Saraswati Flumen (the one associated with the deltaic deposition), has a much gentler gradient which suggests either a more developed fluvial system than the rugged mountains in the north or that the substrate beneath Saraswati is more erodible, consistent with its geological setting relative to the mountainous rivers. Alternatively, our observation of the gentler gradient could be due to a much larger drainage for Saraswati Flumen,

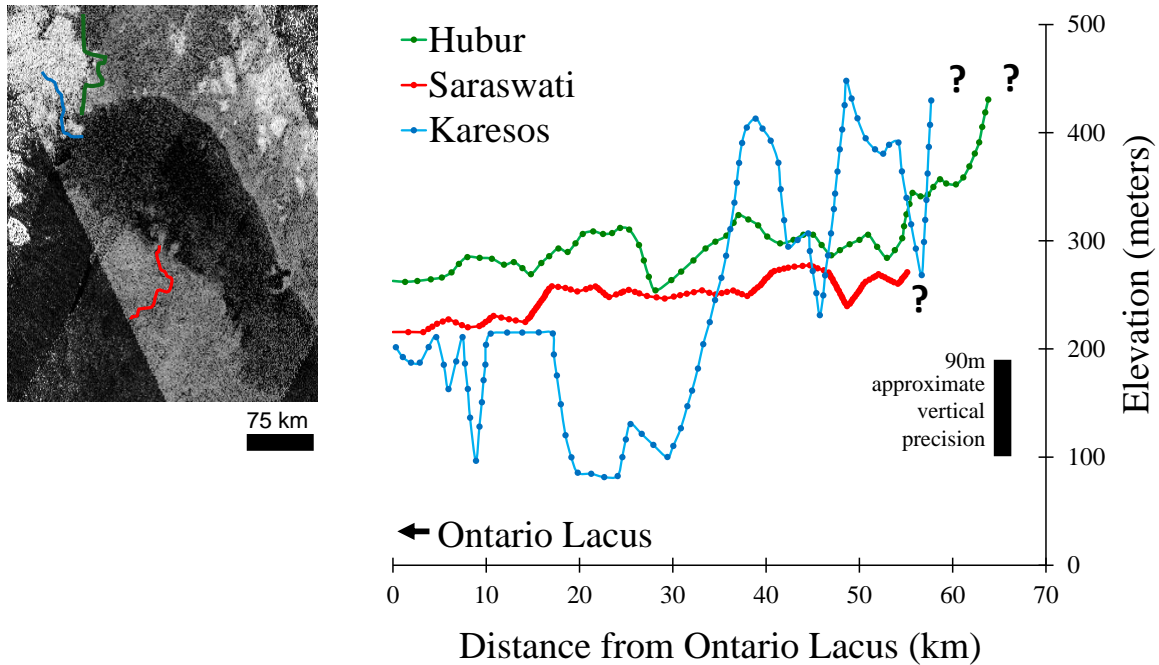


Figure 2.6: The general topographic profile of a few streams around Ontario Lacus. A flat profile might indicate a mature stream with no tectonic uplift. As the profile suggests, Saraswati (in red) flumen is flatter, whereas the profile of other two fluminae, Karesos and Hubur (in blue and green respectively) are steeper – not too surprising as they originate in mountains. The abrupt changes in the profile of Karesos could be a topographical artifact because of coarse resolution topography data. However, the broad trend still suggests a steeper gradient of Karesos flumen compared to the other two fluminae. The inset shows location of these fluminae near Ontario Lacus in a RADAR map. The gentler gradient of Saraswati Flumen could also suggest that it has a much larger drainage with headwaters not covered by the limited DEM dataset. We indicate this absence of data through a question mark in the stream profile.

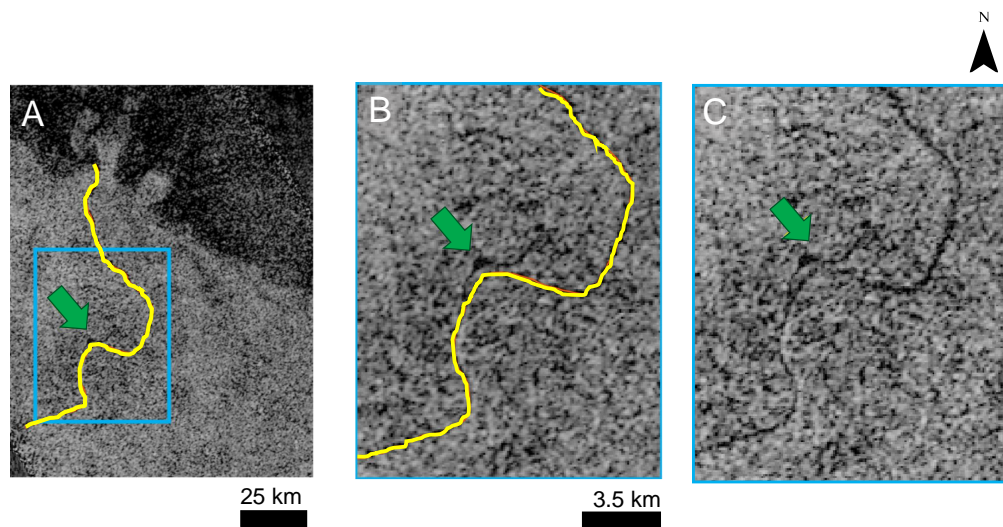


Figure 2.7: T56 flyby synthetic aperture RADAR (SAR) image of Saraswati Flumen that shows a putative oxbow lake (or lakebed, perhaps). A) Shows western shoreline of Ontario Lacus in RADAR data. Saraswati Flumen's extent is shown in yellow. Saraswati Flumen is also shown in Figure 2C by yellow arrows and the context provided in 2A and 2B. B) The blue box shows a zoomed in view of Saraswati Flumen with the green arrow pointing at the putative Oxbow lake. 7C is similar to 7B but without the stream's extent marked.

with its headwaters invisible because they are unavailable in the SAR imagery. Since we carry out this analysis only on the high resolution DEM we are restricted by the available data. Hubur, like Saraswati, is a longer river, and thus the steeper part of the stream profile might not be available in our data for the mapping.

We also report the occurrence of a putative oxbow lake along the path of Saraswati flumen in the RADAR data (see Figure 7). Such features on Earth are associated with low gradient, sediment rich river systems. When a meandering river straightens its course the bend in the river is cut off from the flow, creating an isolated lake. Oxbow lakes are more frequently found in the course of alluvial rivers on Earth. The observation of a putative oxbow lake supports the idea that the western channel, Saraswati Flumen, might be an alluvial channel that experienced fluctuations in its discharge in the past. However, high resolution imagery data of the region is required to validate this observation.

In order to see the evolution of hydrological processes in Titan-like conditions we investigate how Hack’s Law evolves on Titan’s streams. Hack’s Law (Willemin, 2000) relates the flow length of a stream to its contributing drainage area. If “L” is the length of the longest stream and “A”, the catchment area of the basin, then Hack’s Law may be written as  $A = C L^h$  where C is an empirical constant. The exponent “h” is 1.65 to 1.7 for most terrestrial rivers.

We determine Hack’s Law for Saraswati Flumen, the longest channel in our study area by using the catchment area, A and stream length, L for every point along the river to derive h. Using a power law fit the exponent “h” is found to be 1.6. These observations might be an early indication that there could be some similarity in hydrological processes on Titan and Earth. However Hack’s Law is empirical and adding more data points to it is necessary for a more accurate exponent value.

## 2.6 DISCUSSION

Our study highlights that the large catchment area of Ontario Lacus may be the main factor for keeping Ontario filled, while nearby deeper basins in Ontario’s vicinity remain dry. The catchment area extends to at least the southern mid-latitudes (40°S) based on our analysis. *Cassini* VIMS has observed clouds at southern mid-latitudes (~40°S) (Brown et al., 2009; Rodriguez et al., 2011) in the previous flybys. Various climate models also predict the formation of clouds over these latitudes (Rannou et al., 2006; Mitchell, 2012). The presence of certain types of clouds implies precipitation in those regions. If these clouds do bring rain then our analysis suggests that a large fraction of this rain, drains into Ontario Lacus. As a consequence, the large catchment might keep Ontario Lacus filled.

The eastern sub-catchment, bound by the thin line amounts to ~2 million km<sup>2</sup>. Although the incomplete RADAR coverage of the eastern sub-catchment suggests some discontinuities between this catchment and Ontario Lacus, the lack of any topographic minima in the immediate vicinity gives us confidence that this sub-catchment ultimately drains towards Ontario Lacus. It should be noted, however, that even the western sub-catchment by itself represents a substantial catchment area for Ontario Lacus and therefore would still support our large catchment area hypothesis for the filled nature of this lake. The eastern sub-catchment amounts to be ~2 million km<sup>2</sup>. If we consider that the eastern sub-catchment does not contribute to the fluid input of Ontario Lacus we are still left with the western sub-catchment of another 2

million km<sup>2</sup>. When multiplied by the precipitation rate (1.2 m/Titan year) the volume contribution from the western sub-catchment amounts to be 2400 km<sup>3</sup>/ Titan year. This volume still exceeds the present volume of Ontario Lacus (1,462 km<sup>3</sup>). The estimated values however should be treated with caution in view of the associated uncertainties.

Our mass balance model implies that the fluid input to the lake exceeds the estimated fluid loss from the lake. This, in conjunction with the huge catchment area contributing fluid is in line with our observation of currently filled Ontario Lacus at the south pole of Titan. The large catchment area of Ontario Lacus compared to the surface area of the lake would likely dwarf the fluid loss due to evaporation. We, therefore expect that even small amount of precipitation, but spread over the large catchment area of Ontario Lacus, will have the potential to keep this lake filled.

However, we acknowledge that the evaporation rate depends on the composition of the lake. If the composition of the lake is purely methane brought in by fresh rain (Turtle et al., 2011a), then it will evaporate faster because methane’s vapor pressure is 3 orders of magnitude higher than ethane’s. Thus, there is a probability that Ontario Lacus is highly enriched in ethane and hence ceases to evaporate any further. Since the loss tangent (or opacity) of liquid ethane is greater than that of methane (Mitchell et al., 2015), the preceding hypothesis indicates that RADAR wouldn’t be able to see the depths of Ontario Lacus if it were only liquid ethane which is not the case (Mastrogiuseppe et al., 2016). Ontario Lacus probably is a mixture of ethane and methane.

Our analysis also suggests that even though Ontario Lacus is not at the lowest elevation on the south pole, it still is in a regional minimum.

## 2.7 CONCLUSION

The main challenge in our study is the coarse cell size of topographical data. However, useful information can still be extracted from the available data. Better topographic coverage of the region at higher spatial resolution would significantly strengthen such analyses in the future. A hydrological model defining fluid flow combined with General Circulation Models (GCMs) to constrain the weather will likely add greater details to this study.

## 2.8 ACKNOWLEDGEMENTS

The authors acknowledge support from the NASA/ESA *Cassini* Project. JWB acknowledges support from NASA *Cassini* Data Analysis and Participating Scientists (CDAPS) grant NNX15AI77G. RD acknowledges the support from Lynn Carlson at Brown University for guidance regarding handling the coarse resolution topography data. RD is grateful to Deepak Dhingra, Shannon MacKenzie, Johnathon Ahlers, Dr. Nimmo, and both the anonymous reviewers for manuscript suggestions, and would also like to thank the *Cassini* team for all the years of profound work.

## CHAPTER 3: OBSERVATIONAL EVIDENCE FOR SUMMER RAINFALL AT TITAN’S NORTH POLE

“Observational evidence for summer rainfall at Titan’s north pole” *Geophysical Research Letter*, 46, 2019, pp. 1205-1212

Originally published in

Dhingra R. D., Barnes J. W, Robert H. Brown, B J. Buratti, C. Sotin, P. D. Nicholson, K. H. Baines, R. N. Clark, J. M. Soderblom, Ralph Jaumann, Sebastien Rodriguez, Stephane Le Mouelic, Elizabeth P. Turtle, Jason Perry, Valeria Cottini, and Don Jennings, Observational evidence for summer rainfall at Titan’s north pole, *Geophysical Research Letter*,

### 3.1 INTRODUCTION TO CHAPTER 3

When I joined the lab in 2014, the T104th flyby data was coming down. This flyby looks like a chapter book introduction to known processes on Titan’s north pole. Few years later we were down to T120 series of data coming down. In my previous attendance to the Titan Surface Meetings, I heard researchers talk about the absence of clouds on Titan’s north pole despite the arrival of Summer. In the recent VIMS observations we had started observing more clouds. My next chapter is about a wet sidewalk event that we observed in the T120 flyby. A wet-sidewalk event —is the bright reflection of a wetted solid surface at right geometries, right after a fresh rainfall event. This indicates that we had observed fresh rainfall on Titan’s north pole. Not only that, we had also devised a new method to search for rainfall events on distant bodies. We published this research in *Geophysical Research Letters*.

Methane rain on Saturn’s moon Titan makes it the only place, other than Earth, where rain interacts with the surface in modern times. When and where that rain wets the surface changes seasonally in ways that remain poorly understood. Here, we report the discovery of a bright ephemeral feature covering an area of 120,000 km<sup>2</sup> near Titan’s north pole in observations from *Cassini’s* near-infrared instrument, VIMS on June 7, 2016. Based on the overall brightness, spectral characteristics, and geologic context, we attribute this new feature to specular reflections from a rain-wetted solid surface like those off of a sunlit wet sidewalk. The reported observation is the first documented rainfall event at Titan’s north pole and heralds the arrival of the northern summer (through climatic evidence), which has been delayed relative to model predictions. This detection helps constrain Titan’s seasonal change and shows that the “wet-sidewalk effect” can be used to identify other rain events.

### 3.2 INTRODUCTION

A major objective of the *Cassini* Solstice Mission was to search for evidence of seasonal changes on Titan (Tokano et al., 2006; Ádámkóvics et al., 2007) —both atmospheric (clouds) and surficial (rainfall) —that were expected to occur as Titan moved toward the northern summer solstice in 2017. *Cassini*

arrived in the Saturn system during southern summer (2004) and observed clouds and rainfall at the south pole (Porco et al., 2005; Turtle et al., 2009), consistent with General Circulation Models (GCMs) (Tokano and Lorenz, 2006; Schneider et al., 2012). However, as northern summer approached, the increase in cloud activity in the northern hemisphere that was predicted by such models was not observed. In particular, models predicted an increase in the cloud, storm, and rain activity by 2016. Instead, only small, isolated patches of clouds over the north pole began appearing in 2014 (T104 and later flybys).

While both *Cassini* and Earth-based telescopes (Schaller et al., 2006; Roe et al., 2002) have observed clouds on Titan, rain has only been inferred through observed surface changes that require high resolution views. Although four instruments on *Cassini* were able to observe Titan’s surface: the RADAR (Elachi et al., 2004), Imaging Science Subsystem (ISS) (Porco et al., 2004), Visual and Infrared Mapping Spectrometer (VIMS) (Brown et al., 2004), and Composite Infrared Spectrometer (CIRS) (Coustenis et al., 2007), only the VIMS and ISS instruments operate at short enough wavelengths to observe surficial veneers like rainfall.

The ISS instrument observed Titan’s surface through the CB3 filter at  $0.93 \mu\text{m}$ , and detected surface darkening associated with rainfall events at southern high latitudes near the beginning of the mission (southern summer) (Turtle et al., 2009) and later at equatorial latitudes close to the spring equinox (Turtle et al., 2011b). Subsequent to each of these events, VIMS observed surface brightening over months to years after the presumed rainfall (Barnes et al., 2013). In neither case could VIMS detect the initial darkening of the surface (likely due to timing and flyby geometries). CIRS in the past has detected seasonal changes in surface temperature variations (Cottini et al., 2012).

### 3.3 OBSERVATION

Herein, we report the discovery of an extensive ephemeral feature (Figure 3.1) near Titan’s north pole that was observed by *Cassini* VIMS during the T120 (June 07, 2016) flyby and which had disappeared by the next flyby, T121 (July 25, 2016, with similar observation geometry); 3 Titan days (48 Earth days) later. The ephemeral feature is distinct due to its brightness, especially at longer wavelengths ( $5 \mu\text{m}$ ) and covers an area of  $\sim 120,000 \text{ km}^2$  (spreading across 12 VIMS pixels; bigger than any of the Great Lakes on Earth). The spatial sampling of these pixels is on average  $\sim 130 \text{ km}$  in the north-south direction and  $\sim 50 \text{ km}$  in the east-west direction. In addition to the spectral data from VIMS, we use data from the RADAR, ISS, and CIRS instruments to constrain the origin and nature of this anomalously bright, ephemeral feature that we henceforth call the “Bright Ephemeral Feature” (BEF). The ISS and VIMS data provide spectral information, RADAR data provide geologic context, while the CIRS data provide insight into the regional temperatures.

The previous flyby, T119 (06 May, 2016), occurred 2 Titan days before the T120 flyby, and showed cloud cover over the north pole in VIMS data (see SOM for an image of T119). Prior to this, the region had most recently been observed by VIMS during the T106 flyby  $\sim$  two years earlier (24 Oct, 2014), and the BEF was not observed (Figure 1A) (See SOM for observation geometries). The ephemeral nature of the feature suggests that the BEF was formed by some transient, short-lived process at the north polar region of Titan, which distinctly brightened the region during T120 flyby. Later, the region resumed its

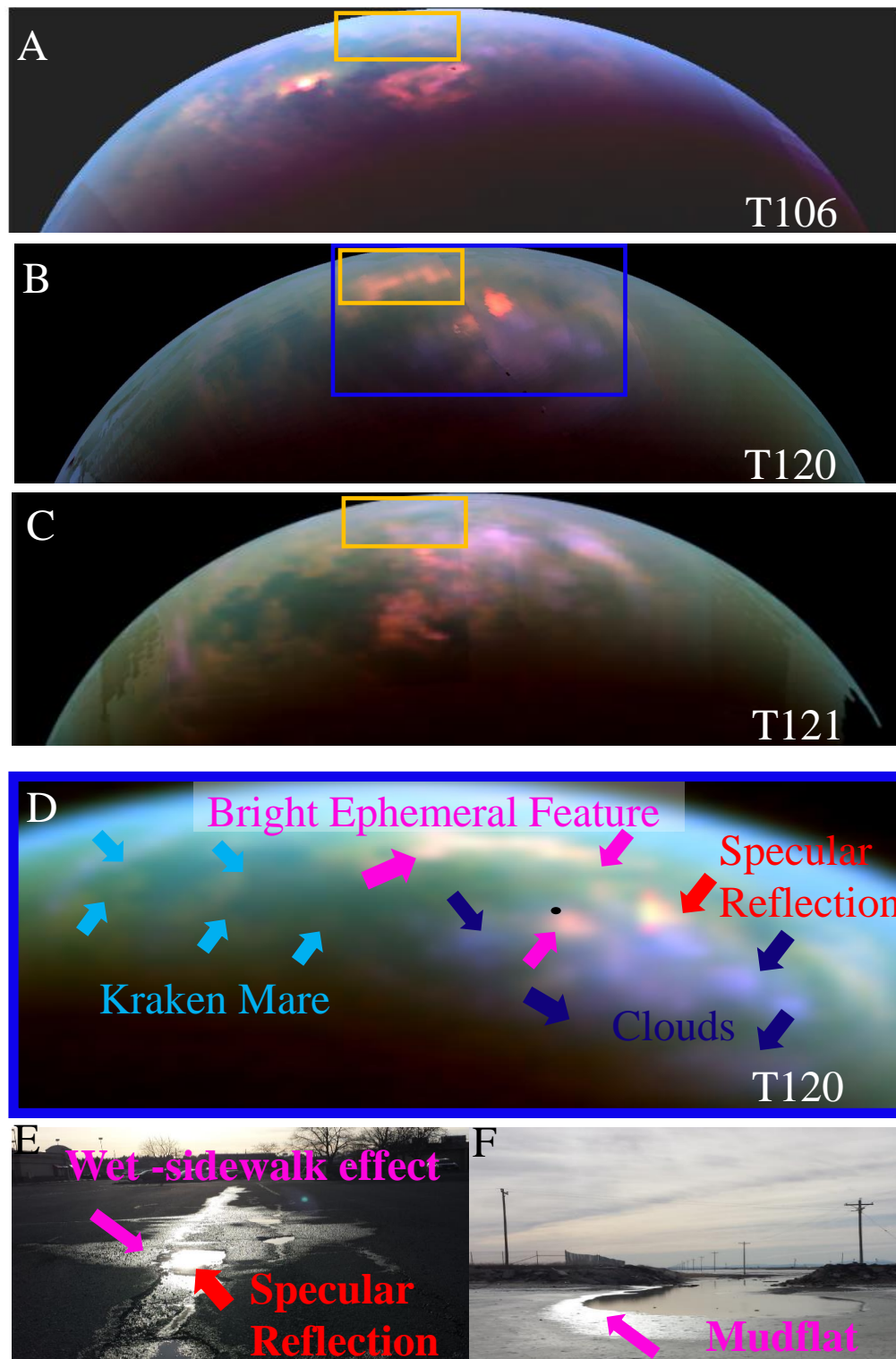


Figure 3.1: VIMS wet-sidewalk color composite (R:5 $\mu$ m, G: 2.7 $\mu$ m, B:2 $\mu$ m) of Titan's north polar region showing the region corresponding to the BEF in the flybys A) T106, 24 October, 2014 B) T120, 07 June, 2016, and C) T121, 25 July, 2016. The yellow box in 1C shows the disappearance of the Bright Ephemeral Feature (BEF) three Titan days later (See Table 1). D) Zoomed-in view of the north polar region from the T120 flyby annotated to identify the features. E) Analog for the T120 BEF on a cloudy day after rainfall. F) Analog for the T120 BEF as mudflat in Utah's Bonneville salt flats

usual spectral characteristics by the next flyby, T121 (Figure 1C). We propose that the BEF represents a broad specular reflection from a wetted surface brought about by rainfall.

### 3.4 METHOD

To study how quickly the Bright Ephemeral Feature (BEF) changed, we compared the region corresponding to the BEF in the T120 flyby with the next flyby, T121, and the prior flyby in which the region was visible, T106. Table 1 shows the observation geometries of the VIMS data cubes used. To rule out the possibility that we did not observe the BEF in T106 and T121 due to unfavorable geometry, we list the distance of the T120 BEF from the specular point in each flyby in Table 1. The distance of BEF from the inferred specular point for T106 and T121 (847 km and 470 km) is marginally different from T120's (632 km). Given the small change in the distance between the BEF and T106, T121 specular points, we would have observed the feature if BEF was present on T106 and T121 flybys. This indicates that we do not see the feature in T106 and T121 flyby due to its ephemerality rather than observation geometry.

We create a VIMS color composite of the observation and overlay it on the RADAR map of the north pole of Titan to infer the geographic location of the BEF in Figure 2. We then create spectra of different spectroscopic units and compare their brightnesses in Figure 3.

When we compare the spectra of different units from the T120 observation in Figure 3B, namely, BEF, specular, clouds, evaporite, and land, we use spectra from the same cube to minimize the atmospheric effects due to observation geometry (See SOM).

The areas where we see the BEF in VIMS are observed at high phase and emission angles by ISS (at  $0.93\mu\text{m}$ ) which makes it difficult for ISS to detect any darkening or brightening associated with the region. CIRS observations of the region, before and during/after the rainfall event, do not provide clear indications of a temperature drop due to any rainfall-derived cooling of the region.

### 3.5 HYPOTHESES

Several mechanisms could potentially produce the reported spectral signature in VIMS data: clouds, fog, evaporites, direct specular reflections (i.e., reflections off large smooth surfaces), and broad specular reflections. In the following text, we consider the merits of each of these possibilities and demonstrate how all but the broad specular reflections can be ruled out.

The T120 flyby contains extensive clouds in addition to the BEF that serve as the basis for our spectral comparison. Although VIMS observes from 0.3 to  $5.1\mu\text{m}$  in 352 spectral channels, Titan's surface is only visible through the atmosphere in seven narrow spectral windows, at 0.92, 1.06, 1.26, 1.57, 2.0, 2.7 and  $5\mu\text{m}$  (Brown et al., 2004). VIMS data are expressed in terms of surface reflectance as I/F (where I is the observed radiance and  $\pi F$  is the incident solar irradiance). The surface and clouds on Titan show distinct spectral responses (Rodriguez et al., 2006, 2009). We incorporate these spectral response characteristics into a color composite (RGB=  $5\mu\text{m}$ ,  $2\mu\text{m}$ , and  $2.7\mu\text{m}$ ) (Barnes et al., 2007; Sotin et al., 2012) to facilitate the identification of various spectral units in the observation. Though also bright at  $5\mu\text{m}$ , clouds are brighter at  $2.7\mu\text{m}$  (McCord et al., 2006; Rodriguez et al., 2011; Griffith et al., 2009) owing to their high altitude. The wings of the  $2\mu\text{m}$  band of clouds also indicate altitude. As a result, the color

<b>Flyby Info</b>	<b>Cube No</b>	<b>Pixel Sampling</b> (pixel/degree)	<b>Phase</b> ( $^{\circ}$ )	<b>Incidence</b> ( $^{\circ}$ )	<b>Emission</b> ( $^{\circ}$ )	<b>Inferred Sp. Pt.</b>	<b>Dist. from BEF</b> (km)
T106, 24 Oct. 2014	CM1792831393	2.2	120	50	73	71 $^{\circ}$ N, 65 $^{\circ}$ W	847
T120, 07 June 2016	CM1844022476	2.08	116	52	65	82 $^{\circ}$ N, 78 $^{\circ}$ W	632
T121, 25 July 2016	CM1848148220	3.1	113	65	55	83 $^{\circ}$ N, 6 $^{\circ}$ W	470

Table 3.1: Details of T106, T120 and T121 flybys, which cover the location of BEF over three time stamps. It helps us determine the existence of this feature over time, and we conclude that it is an ephemeral feature. The inferred specular points of the flybys are tabulated. We also show the distance of T106 and T121 specular points from the BEF. Sp. Pt. means Specular Point. The fact that the distance of inferred specular point

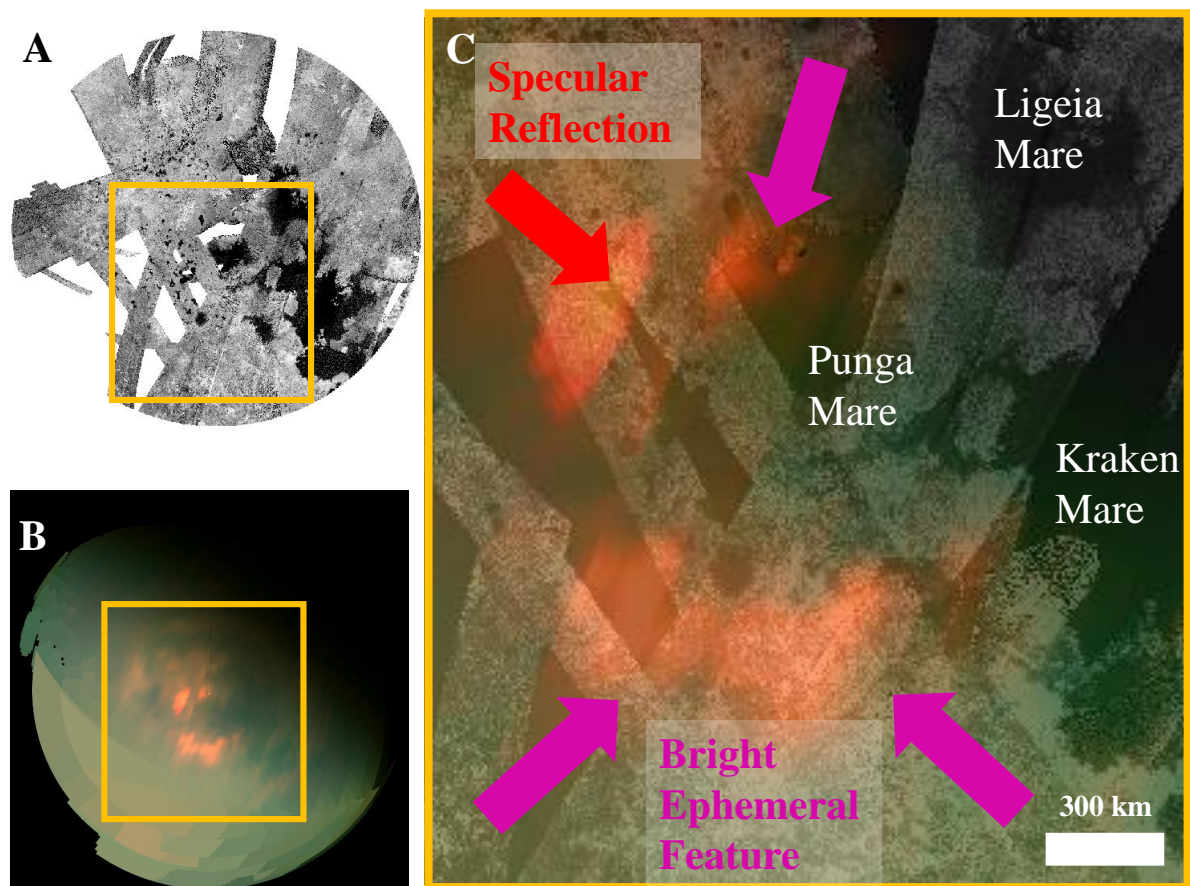


Figure 3.2: The figure is in a different orientation than Figure 1. Kraken Mare is in the bottom right as opposed to the bottom left in the previous figures. A) RADAR map of the north polar region of Titan in Polar Stereographic projection. The yellow box indicates the region corresponding to the BEF illustrating that the region is mostly solid land. The non-data regions are white. B) VIMS infrared color composite (R:5  $\mu\text{m}$ , G: 2.7  $\mu\text{m}$ , B:1.3  $\mu\text{m}$ ) representing the yellow-boxed region as in the RADAR map of the north pole. C) VIMS infrared color composite (3B) (R:5  $\mu\text{m}$ , G: 2.7  $\mu\text{m}$ , B:1.3  $\mu\text{m}$ ) overlain on the north polar map of RADAR (3A) showing the BEF and specular point. The red arrow indicates the specular reflection point (82.7°N, 78.6°W) near Xolotlan Lacus. The magenta arrows indicate the BEF we observe in T120.

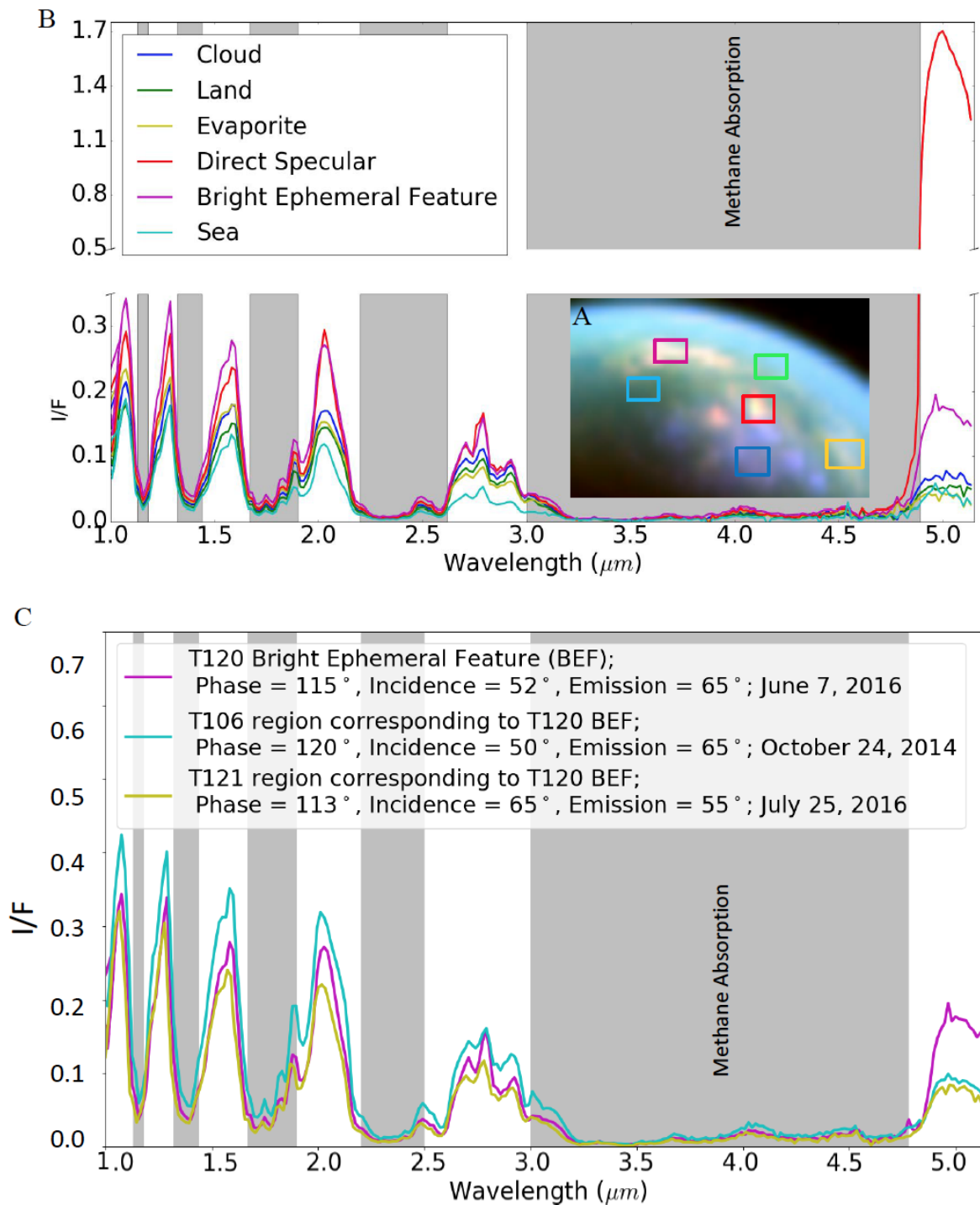


Figure 3.3: A) The colored boxes correspond to the different regions in the T120 observations: dark blue (clouds), green (land), light blue (sea), red (specular reflection), magenta (BEF), and yellow (evaporites). B) The spectra corresponding to the regions in similar colors as the boxes in A. Grey solid boxes show spectral regions affected by methane absorption and thus blocked by Titan's atmosphere. C) Shows the spectra for the location of the BEF. The slightly higher reflectance at shorter wavelengths of the T106 observation (cyan) is because of the higher emission angles. The magenta spectrum corresponds to the BEF during the T120 June 2016 flyby which is distinctly brighter than other spectra at  $5\mu\text{m}$ . The yellow spectrum indicates reflectances for the same region three Titan days later during the T121 July 2016 flyby.

composite effectively distinguishes clouds (purple in Figure 1D) from BEF (orange in Figure 1D).

Low-lying clouds or fog (Brown et al., 2009), however, cannot be entirely ruled out simply based on spectral comparison of the BEF with typical high-altitude clouds. Near-surface fog is difficult to distinguish from bright surface features in spectra without a reliable atmospheric radiative transfer correction. However, both the bright and red ( $5\mu\text{m}$ ) spectrum of the BEF (in Titan’s atmospheric windows) and the fact that the BEF does not extend over nearby large lakes (where one might expect the humidity to be higher) argues against the possibility of a low-lying fog. Even if the latter case is true, the occurrence of a fog layer necessitates a wet (humid) source underneath. Thus, the wetting of land surface by rain is strongly supported, especially considering the large areal spread of the BEF.

Evaporites, direct specular reflections, and broad specular reflections are all surface phenomena. While broad specular reflections from a liquid surface can occur if the surface is roughened by waves (Barnes et al., 2014) or nitrogen bubbles (Hofgartner et al., 2014a; Malaska et al., 2017), a broad specular return from a solid surface requires smoothing of the surface at length scales comparable to the wavelength of light, as would occur if the surface were wet (like a wet-sidewalk after rainfall). RADAR and ISS data observations (Figure 2) show that the BEF occurs over a solid land surface, bordering known lakes in some places: the north- western edge of the BEF coincides with Lagoda Lacus (equivalent radius of  $\sim 54$  km). However, waves on Lagoda Lacus would be discrete, smaller than the lake area, and cannot cause the bright pixels. The BEF is  $\sim 3$  orders of magnitude larger than the lake.

A commonly observed unit, particularly in the north, are  $5\mu\text{m}$  bright deposits observed to abut many filled and empty lakes that are believed to be evaporitic material, comprising deposits left behind when lakes evaporate (Figure 3B) (Barnes et al., 2011; MacKenzie et al., 2014). Two lines of logic, however, strongly disfavor evaporite deposits for the BEF. The first is the spatial extent. Evaporites typically only border the edges of lake —the deposit observed along the southern end of Ladoga Lacus spans an area of  $300\text{ km}^2$  (as observed during the T76 flyby, May 08, 2011) compared to the BEF, spanning an area of  $\sim 120,000\text{ km}^2$ . Second, and most importantly, no evaporites have been observed to form and then disappear within a window of only a few Titan days, as was observed for the BEF (Fig. 1A, B, C).

Direct specular reflections, which we define as the reflection of light off a surface that is smooth at scales both comparable to the wavelength of light and to the projected image of the Sun on the surface (Stephan et al., 2010; Soderblom et al., 2012), depend on viewing-geometry and result in an unusually high I/F. In the T120 flyby we observe the direct specular reflection from the Sun (I/F of  $\sim 2$  in the  $5\mu\text{m}$  spectral window) from the surface of Xolotlan Lacus at  $82.7^\circ\text{N}$ ,  $78.6^\circ\text{W}$ .

We observe the direct specular reflection of the Sun (I/F of  $\sim 2$  in the  $5\mu\text{m}$  spectral window) in the T120 flyby, at  $82.7^\circ\text{N}$ ,  $78.6^\circ\text{W}$  from the surface of the lake, Xolotlan Lacus (Figure 2C),  $\sim 632$  km away from the BEF. As a sidenote, the specular point seems close to the BEF or wet side walk in the Earth analog (Figure 1E). This is due to the smaller angular distance between the specular point and the BEF as compared to T120 observation.

Even though the BEF does not occur at the specular point, it does show spectral similarities to direct specular reflections on Titan. We compare the spectrum of the BEF with those of sea, clouds, land, evaporites, and the direct specular reflection (Figure 3 A, B), all taken from the same flyby (T120) to minimize atmospheric effects (See Method for observation geometry). The direct specular reflection is the

brightest “feature” at  $5\mu\text{m}$  in the observation. The next brightest feature at  $5\mu\text{m}$  (by 50%) is the BEF. A rough surface cannot, on its own, reflect specularly. However, surface wetting coats the irregular surfaces of the rough region resulting in a smoother surface than what is underneath. The spectral brightness and observation geometry immediately indicate that the BEF is a broad specular reflection due to smoothing of a surface that was otherwise dry.

### 3.6 MODELING SURFACE ROUGHNESS

In order to test our hypothesis, we model the BEF’s surface roughness to characterize specular reflections from a macroscopically rough surface (Figure 4). We use a numerical planetary specular model (Barnes et al., 2014) with Gaussian-distributed slopes and azimuthal symmetry, for the same observation geometry as the T120 observation (Figure 4B).

For small roughnesses with RMS slopes of  $\sigma \sim 2^\circ$  (Figure 4C), only the direct specular reflection at the specular point appears. As we increase the roughness parameter — $\sigma$ —the specular reflection spreads over a larger number of pixels, each pixel receiving lesser solar flux, resulting in a fuzzier reflection distributed over a broader region. Over an area equivalent to the BEF, the model-determined  $\sigma$  values indicate that the required slopes to get signals comparable to our observation are  $\sim 12 - 14^\circ$  (Figure 4D). This is twice the  $\sigma$  value of the inferred waves in Punga Mare (liquid surface), which were determined using the same model, to be  $\sim 6^\circ$ . Figure 4E shows that, at higher slopes, ( $\sim 24^\circ$ ) the reflections become independent of the roughness parameter and show the entire solar flux ( $I/F_{max}$ , see Method) distributed over Titan’s hemisphere.

### 3.7 RESULTS AND DISCUSSION

Based on our detailed analysis of the *Cassini* data coupled with roughness modeling and testing the feasibility of various possibilities, we propose that the BEF represents a broad specular reflection from a rough, wetted surface —presumably brought about by rainfall (T120 flyby, June 07, 2016), 2 Titan days after the observed cloud coverage (T119 flyby, May 06, 2016). A rough land surface could be smoothed by a recent surface wetting due to a summer-rainfall event. Earth analogs of wetted sidewalks (Figure 1E) and a mudflat (Clark et al., 2010) in Utah’s Bonneville Salt Flats (Figure 1F) broadly fit the BEF profile. The RADAR data show the area to be rough, variegated, and non-uniform (at scales of  $\sim 2$  cm). A wet-sidewalk region is wet on a solid but rough substrate that at the right geometries produces broad specular reflections. These help us conclude that the BEF would have properties similar to a wet sidewalk that arises from a recently wetted, solid and rough surface on the north pole of Titan.

### 3.8 CONCLUSION

The reduced and delayed cloud and storm activity at Titan’s north pole as opposed to the model predicted activity suggests that our current understanding of Titan’s changing seasons is incomplete. Our reported observations represent the first documented rainfall event on the north pole of Titan. We discover this rainfall based on a novel technique “wet-sidewalk effect” (broad specular reflections from a

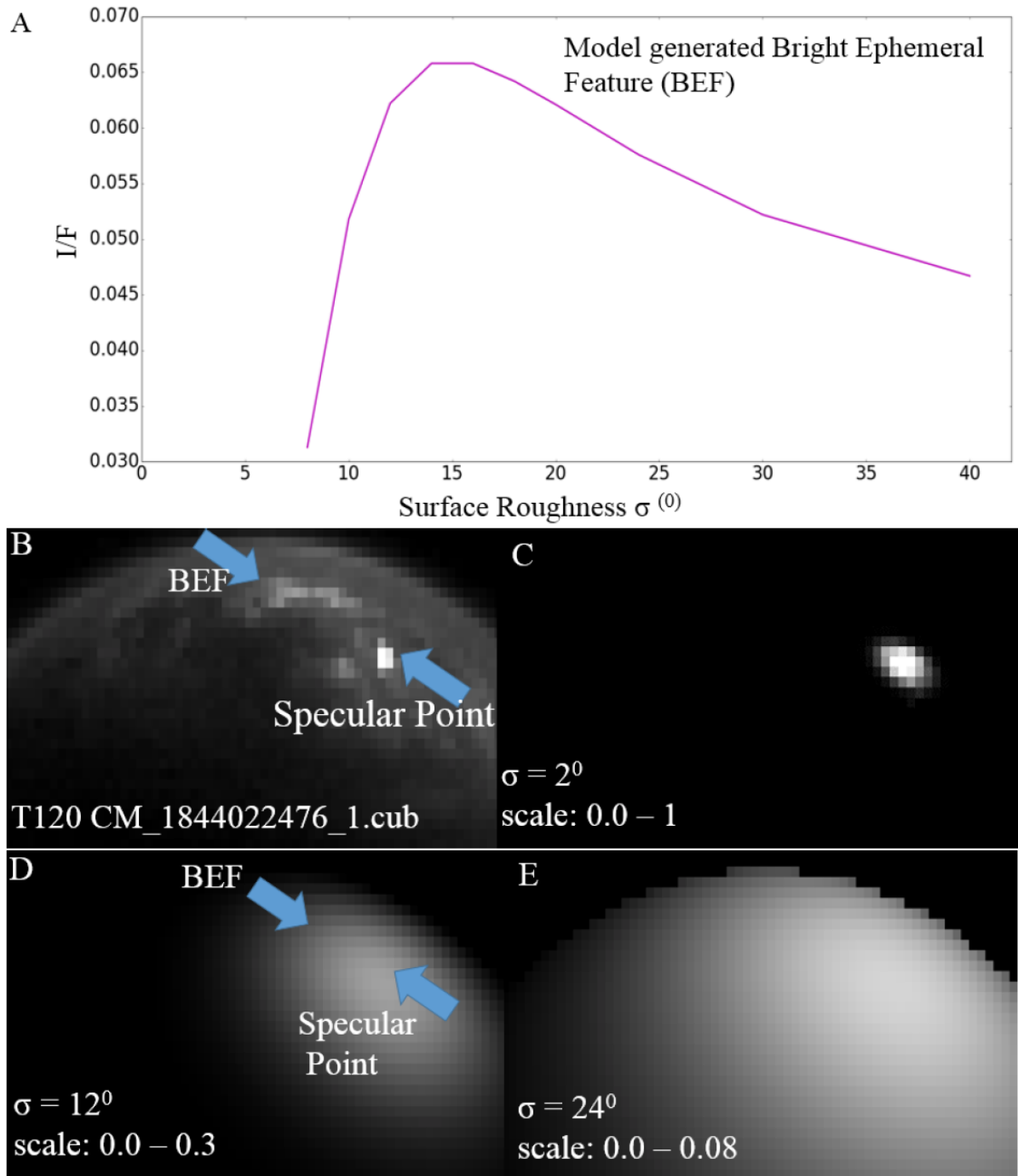


Figure 3.4: A) Modeled reflectance ( $I/F$ ) variation with surface roughness for the broad specular reflection (BEF) observed during the T120 flyby. The modeled (magenta) reflectance peaks at roughness ( $\sigma$ ) values of  $\sim 14^{\circ}$  indicating that the BEF's surface roughness could be of that order. B) T120 *Cassini* image cube CM1866022476 where the BEF is observed. C) Model-generated synthetic images for the T120 observation geometry with a surface roughness parameter of  $2^{\circ}$  reveals only the specular reflection. One thing to note is the scale in the synthetic images: as we increase the roughness or specular deviation angle — $\sigma$ —the specular reflection spreads over a larger number of pixels, each pixel receiving lesser solar flux for higher  $\sigma$  and hence the scale changes. D)  $\sigma$  of  $12^{\circ}$  covers the extent of BEF. E)  $\sigma$  of  $24^{\circ}$  distributes the entire solar flux onto the Titan hemisphere.

<b>Spectral Unit</b>	<b>Phase (°)</b>	<b>Incidence (°)</b>	<b>Emission (°)</b>
BEF	116	46	72
Sea	116	67	53
Specular	116	58	58
Clouds	116	63	54
Evaporite	116	63	69
Land	116	54	61

Table 3.2: The observation geometry of the pixels used to determine the spectra in Figure 4B. All the units are from the same cube to minimize atmospheric effects.

smoothened, original rough surface). Identifying the location and timing of the rainfall offers important data points for Titan GCMs, helping constrain why the northern summer cloud activity is delayed relative to predictions —especially because the north pole hosts most of Titan’s lakes and seas. Apart from helping us understand Titan’s weather and long term climate, a broad specular reflection observation like this helps us derive the roughness of the solid surfaces on Titan. Surface roughness of a region holds clues to its geologic evolution, nature of surface interactions and even has implications for landing site evaluations for future missions to Titan.

## ACKNOWLEDGMENTS

The authors acknowledge support from the NASA/ESA Cassini Project. RD, JWB, CS and JS acknowledge support from NASA Cassini Data Analysis and Participating Scientists (CDAPS) grant NNX15AI77G. RD is grateful to Shannon MacKenzie, Deepak Dhingra, Johnathon Ahlers, Robert Chancia, Matthew Hedman and Subrata Chakraborty for manuscript suggestions, and would also like to thank the Cassini team for all the years of profound work. The VIMS data are available at the PDS imaging node (<https://pds-imaging.jpl.nasa.gov/volumes/vims.html>). The RADAR data was obtained from (<http://pds-imaging.jpl.nasa.gov/volumes/radar.html>). Thanks to Dr. Jani Radebaugh and the other reviewer for their constructive comments and helpful suggestions on an earlier version of the manuscript.

## SUPPORTING INFORMATION FOR “OBSERVATIONAL EVIDENCE FOR SUMMER RAINFALL AT TITAN’S NORTH POLE”

We show in Figure S1 the cloud cover in the T119 flyby that occurred two Titan days before our discovery flyby, T120. The cloud cover is not necessarily above the BEF yet covers a large region over the north pole. Assuming these are precipitating clouds, they could move in two Titan days around the north pole and could be the source of precipitation. At the right geometries the precipitation can be detected as a broad specular reflection like that in T120.

In Table 2, we tabulate the observation geometry for each spectra in Figure 3B.

In our modeling of the surface roughness of the BEF, we find that the modeled reflectance (I/F) is

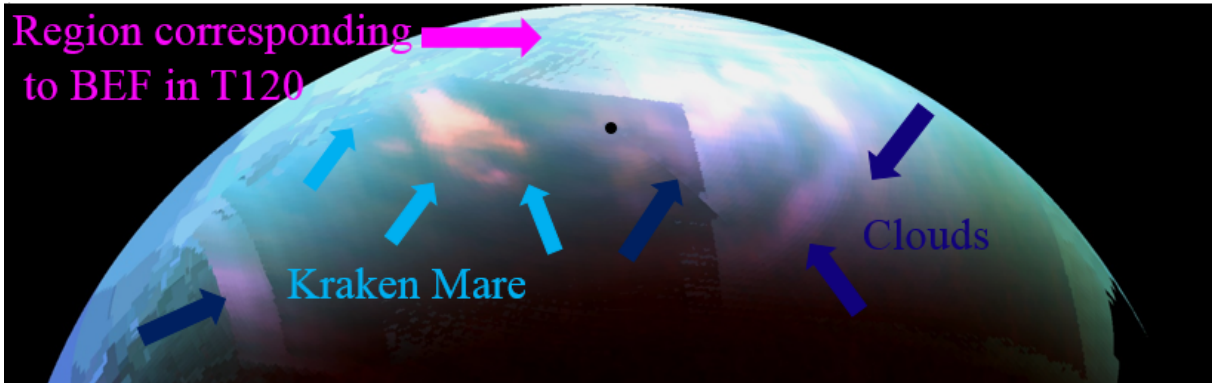


Figure 3.5: Orthographic wet-sidewalk color composite for the T119 (06th May, 2016) flyby. This is in same orientation as Figure 1. The T119 flyby occurred two Titan days before (BEF) T120 (07th June, 2016). The purplish hues in this color composite indicated by blue arrows show the cloud cover over the north pole. The BEF region corresponding to T120 is shown by a magenta arrow.

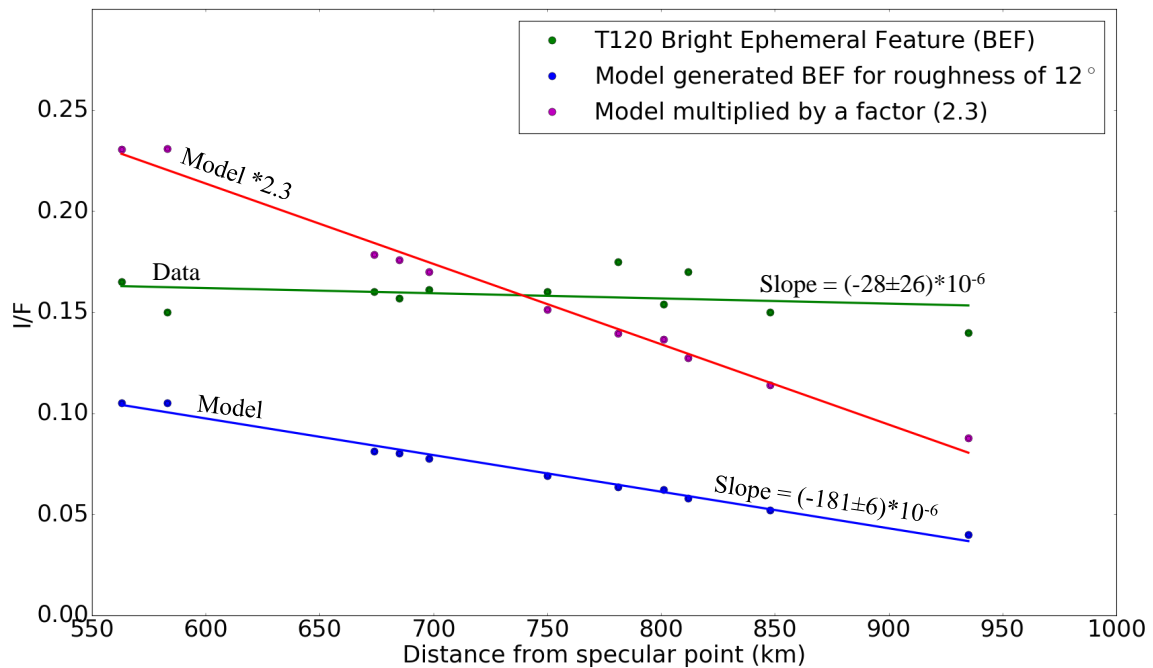


Figure 3.6: I/F variation with the distance of specular point. Both reflectance values (model generated (blue) and T120 actual observation (green)) show similar trends. The reflectance decreases as the distance from the specular point increases, but the model-generated reflectance values are off by a factor of  $\sim 2$ . We multiply the model (Red) by a ratio (2.3) of averaged slopes of model and data to scale the model but still notice the difference in slopes. This could be due to the reflections from wetted surfaces that have a non-zero average slope unlike our model.

lower than the observed reflectance by a factor of  $\sim 2$ . The modeled and observed reflectances also have different slopes as shown in Figure S2. This difference in slope and the intensity variation as we move away from the specular point indicate that there is a disagreement between the model and the observations. This could happen for many reasons, including contribution from Titan's forward scattering hazes or that the wetted surfaces have a non-zero average slope unlike our model (Figure S2).

We presently do not know the length scales over which the model-determined surface roughness of  $\sim 12\text{-}14^\circ$  occur. However, we do have observational and theoretical constraints that allow us to derive those length scales. Surface tension is the theoretical parameter that restricts the spread of liquid methane over an icy bedrock (17 dyne/cm; water's surface tension is 70 dyne/cm). That liquid methane has a lower surface tension than water indicates it spreads readily. RADAR data provide an observational constraint, suggesting the topography of the region to be rough and variegated at scales of  $\sim 2$  cm. To infer the topography of the BEF region under these constraints, we assume different grain size dimensions, namely gravel (2 - 64 mm), cobble (64 - 256 mm), and boulder (200 - 630 mm) as length scales and calculate the corresponding vertical relief. If the primary source of our measured  $\sim 12\text{-}14^\circ$  surface roughness were gravel, then under the surface roughness conditions, the vertical relief would range from sub-mm to a couple of millimeters ( $\sim 0.7$  - 21 mm). If cobbles instead cause the observed roughness, then the peak to trough surface heights are  $\sim 21$  - 85 mm. The range ( $\sim 8.5$  cm) for the values of cobbles is larger than the observational constraint from the RADAR data. We therefore infer that the geomorphology of the region corresponding to the BEF could be a mix of gravels and small cobbles of vertical relief ranging from sub-mms to a couple of centimeters.

# CHAPTER 4: USING ELLIPTICAL FOURIER DESCRIPTOR ANALYSIS (EFDA) TO QUANTIFY TITAN LAKE MORPHOLOGY

“Using Elliptical Fourier Descriptor Analysis (EFDA) to quantify Titan lake morphology”  
*Astrophysical Journal, Submitted*

Rajani D. Dhingra, Jason W. Barnes, Matthew M. Hedman, and Jani Radebaugh

## 4.1 INTRODUCTION TO CHAPTER 3

I participated in the 3MT (3 Minute Thesis) competition held at the University of Idaho in my sixth semester after I was done with my preliminary examination. Sarah Jacobs, the winner of 3MT presented her research on morphometry where she was comparing the staple and stigma length of a particular species of flower. She used a methodology called Elliptical Fourier Descriptor Analysis (EFDA).

The Titan researchers had continuously been discussing the formation mechanism of lakes on Titan. I had heard them hypothesize various scenarios backed up by many discussions. I got the idea to use shape based analysis to understand formation mechanisms of lakes on Titan. My preliminary research suggested that this method has not been used in planetary science till then.

After a lot of hiccups and trial and errors I made this methodology work for Titan’s lakes. I have received the reviews on this manuscript and will work on them after my thesis is submitted.

We quantitatively constrain possible lake formation mechanisms on Titan using the morphometry of lakes. We map the lakes on Titan’s north pole and find that the equivalent radii of 224 lakes follow a relatively narrow lognormal distribution like Earth’s thermokarst lakes and Io’s volcanic paterae, indicating a limited number of formation processes. Then, we quantify the shapes of lakes using Elliptical Fourier Descriptor Analysis. The Fourier analysis decomposes the shape of a lake into multiple Fourier series, and the corresponding coefficients represent a fingerprint of the lake shape. After testing the methodology on synthetic lakes and two kinds of terrestrial lakes, we analyze 67 Titan lake shapes on the north pole of Titan. We find that the majority of shape variation in Titan’s lakes is from circular to elliptical followed by lakes with significant asymmetries along their short axis and long axis. We also find that a few lakes on Titan like Myvatn, Xolotlan, Sotonera, Viedma, Muggel, and Neagh Lacus have very distinctive shapes. Letas Lacus is an extreme outlier amongst the shapes of Titan lakes with an intruding island. This demonstration shows the promise of the Elliptical Fourier Descriptor approach for testing hypotheses for Titan lake formation. Our statistical analysis divides the Titan north polar lakes into four clean shape-based groups hereby indicating either four formation mechanisms or four stages of formation of Titan’s lakes. Uneven subsequent modification of the lakes, could be another reason for the differences which might be a result of different ages.

## 4.2 INTRODUCTION

Titan is the only moon in our solar system with a thick atmosphere (Sagan and Dermott, 1982; Lunine et al., 1983; Squyres et al., 1984; Niemann et al., 2005; Baines et al., 2005; Griffith, 2009) and stable bodies of surface liquids owing to the methane-based hydrological cycle (Tomasko et al., 2005; Elachi et al., 2005, 2006; Porco et al., 2005). Most of the liquids on Titan are located poleward of about 70°N in the form of three large seas (Kraken Mare, Ligeia Mare and Punga Mare) and a couple of hundred circular or irregularly rimmed or unrimmed lakes. While the presence of a hydrological cycle might help explain how the depressions are filled with liquid methane, the formation mechanisms of the depressions still remain a mystery.

Post-*Cassini*, we have gathered some understanding of the liquids on Titan via the lake and sea compositions, depths, formation mechanism hypotheses, sediments left behind after evaporation, and the geographic asymmetry in their distribution (Barnes et al., 2007; Lorenz et al., 2008; Burr et al., 2009; Wall et al., 2010; Hofgartner et al., 2014b; MacKenzie et al., 2014; Mastrogiuseppe et al., 2014; Lora and Mitchell, 2015; Mitchell et al., 2015; MacKenzie and Barnes, 2016; Mastrogiuseppe et al., 2016; Dhingra et al., 2018; ?). ? carried out the first geomorphological mapping of Titan’s poles and suggests the present-day landscape may be an erosional remnant that is being lowered in elevation through time. ? used Titan’s most complete topographic map generated by ? and conclude that, similar to Earth, Titan’s largest seas and lakes have a common equipotential surface probably connected through an aquifer or subsurface hydrocarbon reservoirs.

The leading models that explain the formation of these depressions are impact cratering (Stofan et al., 2007), volcanism (?), karstic processes (?Mitchell et al., 2014), and sublimation or dissolution of a volatile substrate (??). However, no single lake formation mechanism fully addresses the challenge of explaining the variedly differing lake shapes on Titan.

? and Lopes et al. (2007) attribute volcanic calderas and cryovolcanism as probable lake formation mechanisms due to the circular shape of several north polar lakes. However, many irregularly shaped lakes at Titan’s north pole do not reflect the caldera hypothesis. While liquid-filled calderas are common on the Earth, no interior model for Titan has yet explained the latitudinal dependence and poleward location of caldera-producing volcanic processes. Impact craters similarly do not address the preferential density of impacts on the pole.

? put forward karst dissolution as a possible explanation for the irregularly shaped depressions. On Earth, karstic lakes are formed due to the dissolution of carbonates by water. Growing evidences suggest that an organic sedimentary bedrock could also likely undergo karstic dissolution. On Titan, water ice—the bedrock—is not readily soluble in liquid methane or ethane. In addition, if we consider that the limnological time scales on Titan are longer than on Earth and the constant solid hydrocarbon particle rain from the atmosphere is the solute, the topography and depth of these lakes still do not compare with that of terrestrial karst lakes that are shallower than the Titan lakes (?Mastrogiuseppe et al., 2014). The sharp rims around some of the Titan lakes seem constructional in morphology and hence imply a constructional mechanism of lake formation.

? suggest that the dissolution processes would be 30 times slower on Titan than on Earth due to

the seasonality of precipitation (Turtle et al., 2011b, 2009; Dhingra et al., 2019), and estimate the time scales of the development of the lacustrine depressions as few as tens of millions of years at polar latitudes higher than 70°N and S.

While karst lakes result from the dissolution of a soluble rock in a solvent, thermokarst lakes result from the thawing of permafrost regions in terrestrial Arctics (Alaska, Canada). CH<sub>4</sub> and C<sub>2</sub>H<sub>6</sub> permafrost are unlikely to occur on Titan’s surface due to freezing point depression from N<sub>2</sub> dissolution (?). Although, ? does claim ‘goo-permafrost’ and ‘goo glaciers’ could occur and be composed of a thick layer (~100 m) of acetylene or ethylene. This ‘goo-permafrost’ requires mean Titan-annual temperatures below the freezing point to extend a continuum between glacier and permafrost terrains, like on Earth, suggesting collapse karst or thermokarst as a potential lake formation mechanism on Titan.

? proposes a new explanation for the orientation, shape and speed of growth of terrestrial oriented thaw lakes. The lakes’ unusual characteristics could result from seasonal slumping of the banks when the permafrost thaws abruptly. The lakes grow when rapid warming melts a lake’s frozen bank, then the soggy soil loses its strength and slides into the water. Such lakes are found in the permafrost zone in Alaska, northern Canada and northern Russia.

Sharp Edged Depression (SEDs) —lakes with raised rims of heights ~100 m —present the most baffling case in the already puzzling challenge of lake formation mechanisms. ? and ? discuss the complexity of fitting any formation mechanism to the SEDs. The favored hypothesis for the formation of lakes to explain the SEDs are sublimation or dissolution of a volatile substrate (karst-like mechanism on Earth) however, this does not necessarily explain the formation of rims.

An underlying assumption that we make on Earth and extra-terrestrial bodies when we observe features is that ‘form follows process’. Qualitative differences in form can be identified using observations. For example; Simple craters on the Moon have bowl-shaped depressions and have diameters of less than ~15 kms. Complex craters have more complicated forms, diameters larger than ~15 kms, shallow, relatively flat floors, central uplifts, and slump blocks and terraces on the inner wall of the crater rim (?). Relatively complex forms like the Ionian paterae or the Titanian lakes are difficult to qualitatively differentiate using mere visual information.

Quantifying shapes as multivariate descriptors to extract the information stored in the shape of a structure is commonly used in evolutionary biology and paleontology (??). However, such methods of boundary morphometrics have yet to be applied to the analysis of forms in planetary studies. Using modern methods of multivariate statistics we can quantitatively classify geologic morphology and compare form among other variables. As the limnological studies of terrestrial lakes indicate, similar lake shapes might indicate similar formation mechanisms. In this work we use outline-based shape analysis or morphometry —the measurement of morphological characteristics of a geologic feature —to quantify the lake shapes and provide constraints on lake commonalities on Titan.

There have been a few previous studies quantifying the outline shapes and morphometry of Titanian lakes. Sharma and Byrne (2009) carried out an in depth study comparing 114 terrestrial lakes with 190 Titan lakes using fractal analysis. None of the terrestrial lake formation mechanisms conformed to Titan lake outlines by fractal analysis, according to their study. However, collapse karst or thermokarst lakes —lakes formed by subsumption of the frozen ice —were excluded from the Sharma and Byrne (2009)

analysis. An important limitation of fractal analysis is the empirically determined fractal dimension that depends on the image resolution.

Another study led by ? carried out shoreline analysis of Titan lakes and compared them with terrestrial lakes using ruler methodology. Their comparison of Titan lakes with Minnesotan, Siberian and African-rift valley lakes suggested that Titanian lakes are most similar to Siberian and Minnesotan lakes. The Siberian lake packets used for the analysis are formed by a thermokarst mechanism and the Minnesotan lakes by glacial recession. We found that the previous outline-based studies either excluded or partially included karst, thermokarst or a combination of both as the possible processes in action on Titan for forming the lakes.

In this manuscript, we aim to constrain the lake formation mechanisms on Titan using morphometrics. We explore two different types of morphometric analysis in this manuscript, a more classical size and orientation analysis (Section 2) and a novel shape analysis using Elliptical Fourier Descriptor Analysis (EFDA) method (Section 3).

We then apply the Elliptical Fourier Descriptor Analysis (EFDA) method on lakes in section 3.2. Subsections 3.2.1 and 3.2.2 discuss the methodology on synthetic lakes and a suite of Earth lakes to validate our technique. We finally apply the Elliptical Fourier Descriptor Analysis (EFDA) method on Titan lakes in section 3.3. Subsections 3.3.1 and 3.3.2 discuss the observational data used for Titan lakes and the results obtained. Finally, we discuss our observations and results concluding the manuscript in section 4.

## 4.3 SIZE DISTRIBUTION AND ORIENTATION

? analyze the spatial regularity of the morphological structures associated with terrestrial thermokarst lakes. They find that on Earth, the diameters of thermokarst lakes follow a lognormal distribution, under the assumptions that the lakes form over small intervals of time, and the spread in the sizes of lakes is small. We reviewed the literature for other planetary processes that follow lognormal distribution and find that the size distribution of Ionian paterae that have volcanic origin (?) also follow a lognormal distribution as well as solar system calderas (?). Intrigued by these distributions, the non-inclusion of thermokarst lakes in previous analysis, and the above-mentioned mathematical morphological studies carried out on terrestrial thermokarst lakes, we were motivated to determine the size distributions for Titan's lakes.

Oriented lakes are lakes that demonstrate a preferred long axis orientation. The orientation could result from substrate topography and structural controls like development along joints or folds.

Subsection 2.1 and 2.2 discuss the observational data, methodology, and results the analysis of the size distribution and orientation of the lakes.

### 4.3.1 OBSERVATIONAL DATA

We use RADAR (Elachi et al., 2005), VIMS (Brown et al., 2004), and ISS (Porco et al., 2004) data derived from multiple *Cassini* flybys to generate a comprehensive north polar map. We map the north polar lakes in ArcGIS using all the three datasets to cover the entire area. We use ArcGIS to retrieve

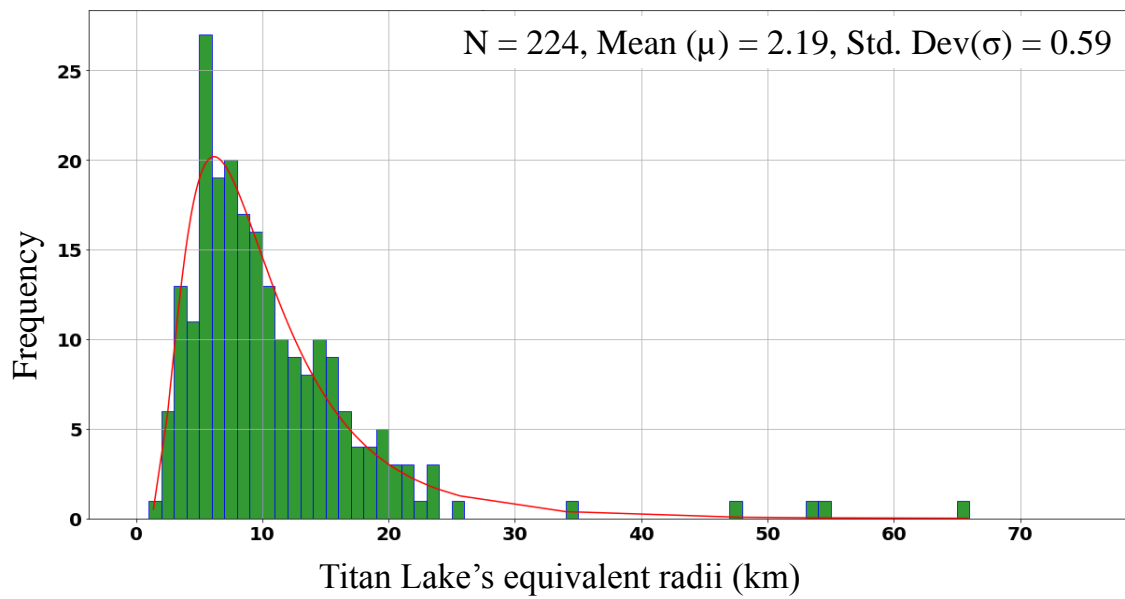


Figure 4.1: shows the size distribution of the equivalent radii ( $\sqrt{(Area/\pi)}$ ) of the north polar Titan lakes. The size distribution (green) of the equivalent radii of lakes on the north pole of Titan follow a lognormal distribution (red). Terrestrially, the diameter of thermokarst lakes follow a lognormal distribution (??). The volcanic paterae on Io (?) also follow lognormal distribution.

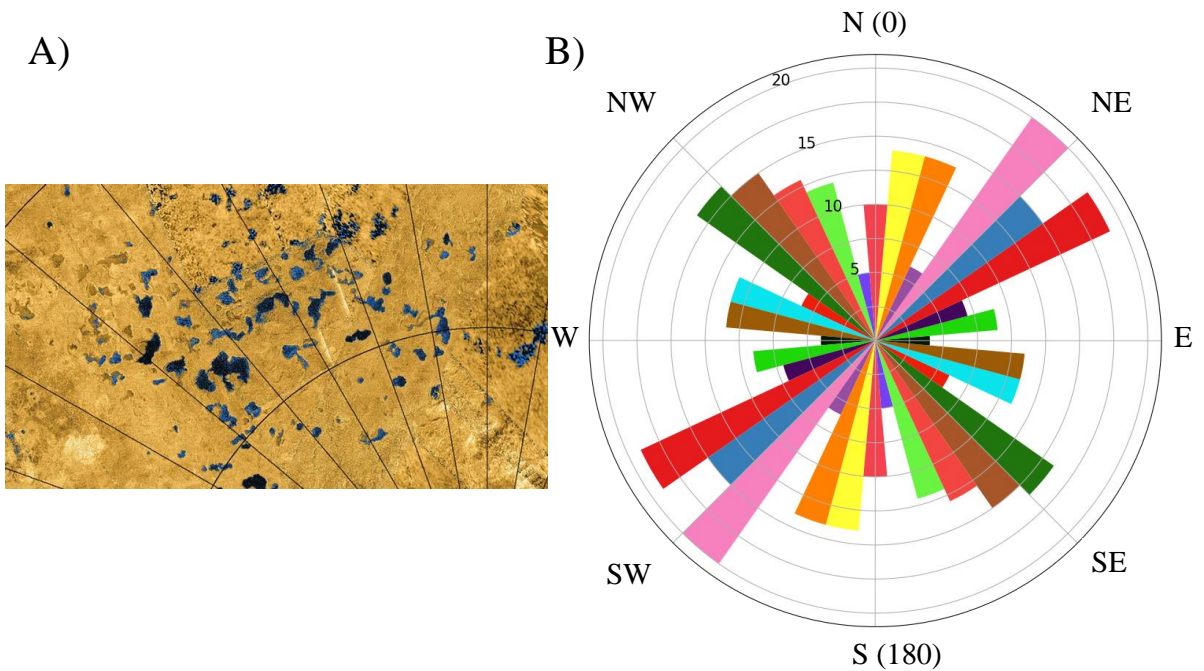


Figure 4.2: A) RADAR (false colored) image of Titan's north polar (north western part) lakes in blue. We don't show the RADAR north polar map because the right quadrant of the north pole between the longitudes of  $220^{\circ}$  and  $330^{\circ}$ W harbors the bigger seas. B) Rose diagram indicating the orientation of the Titan lakes (angle between the line joining the antipodal pair of a lake and the north pole). The orientation of lakes show a NE-SW (NorthEast-SouthWest) or ( $45^{\circ}$ W -  $225^{\circ}$ W) direction in B. The colors in this plot are just the bar colors for viewing ease.

morphometric information from the geographically projected digitized lake outlines of the 224 Titanian lakes that we analyze for size and orientation on the north pole.

### 4.3.2 METHOD AND RESULTS

We trace the lakes on the north pole of Titan using varied datasets (RADAR, VIMS and ISS), allowing for an accurate calculation of lake areas and resulting effective radii ( $\sqrt{(Area/\pi)}$ ). This measurement reveals the high degree of sinuosity and irregularity in Titan lakes' outlines. We then plot the equivalent radii of the lakes in a histogram, fit it with lognormal distribution, and statistically test the fit.

As mentioned before, terrestrial thermokarst lake diameters and caldera follow a lognormal distribution. The lognormality motivated us to plot the equivalent radii of Titan's lakes in a histogram and fit it with a lognormal distribution ( $N = 224$ , Mean = 2.19, Std. Dev = 0.59) using the Anderson Darling test. Figure 1 shows the distribution of equivalent radii of 224 Titanian lakes mapped using the different datasets (ISS, VIMS and RADAR). We do a statistical fit (red line in Figure 1) to this distribution and validate the lognormal fit of the distribution. The Anderson Darling test statistic for this fit is 0.34 which is less than the critical value (0.64) at a significance level of 10. Thus the distribution follows a lognormal distribution indicating a good fit to the distribution of Titan lake's equivalent radii.

Previously Hayes et al. (2008) divided Titan lakes into dark (filled), bright(empty) and granular(mid-way) lakes and also found that all three lake areas were distributed lognormally. To contrast the Titan lake distribution with terrestrial lakes, ? find that Earth's lake areas are power-law distributed —many small lakes, but few large lakes—for lakes  $\geq 8.75 \text{ km}^2$ .

Figure 2 A shows the RADAR image of lakes on the north pole of Titan and adjacently (B) shows lake orientation in a polar histogram. We define the orientation angle as the angle between the line joining the antipodal points for the longest axis of the lake and the north pole. We use this morphometric measurement and plot it in a rose diagram to verify if the north polar lakes demonstrate any preferred orientation. We can see that while the north polar lakes do not necessarily have a preferred orientation visually (in A) and in the plot (in B) there is a slight increase in the frequency of orientation in the north-east/south-west directions. The mountain ridge belts, the oriented valleys in Xanadu, and more crucially, at the north pole, and the really straight river valleys emptying into Ligeia Mare are few of the evidences of the tectonic processes on Titan (Cook-Hallett et al., 2015). Our rose diagram and the slight increase in the frequency of orientation in the north-east/south-west directions is further evidence of tectonism at the north pole. The tectonic lake formation mechanisms that do have a preferred long axis orientation seem to be slightly plausible in this scenario.

## 4.4 ELLIPTICAL FOURIER DESCRIPTOR ANALYSIS FOR OUTLINE-SHAPE QUANTIFICATION

Fourier-based approaches are powerful tools to extract the geometry information from the outline shapes. They work on the basis of Fourier series —decomposing a complex periodic function in terms of simple trigonometric functions like sine and cosine. The simple trigonometric functions have frequencies

that are integer multiples or harmonics of one another. Lower order harmonics help explain the coarse features in the outline while higher order harmonics are required to explain the fine scale sinuosities in the outline. The lake outlines are periodic functions in the sense that if we start traversing a closed outline we will cross a reference point repeatedly periodically, thus making a closed outline a periodic function (?). Hence we use a Fourier series based approach to quantify the geometry of the closed outlines of Titan lakes (Figure 3A).

The Elliptical Fourier Descriptor Analysis (EFDA) has many advantages over the other Fourier based approaches and tends to be a reliable method to quantify shapes because of the following reasons.

- Equally spaced points are not required.
- Any shape can be accurately represented, even ones that fold back in on themselves.
- The outline can be quantified without having a need for a synchronous point (twig on a leaf or the thumb on a hand for comparing leaves' or hands' outlines) on every shape.
- The fourier coefficients can be made independent of outline position and normalized for size and rotation.

Subsection 3.1 describes in detail the methodolgy for Elliptical Fourier Descriptor Analysis (EFDA) and its advantages as a method to quantify and compare the outlines of lake shapes.

#### 4.4.1 METHOD

Elliptical Fourier Descriptor Analysis (??) is a method that fits the 'x' and 'y' coordinates of an outline separately. Morphometric analyses need 'x', 'y' coordinates sampled on each outline as an input. So our first step is to extract the 'x', and 'y' coordinates of the lake outlines. We use the tpsUtil (?) software to convert our images (.jpgs/.pngs) to .tps files that can be handled by the tpsDig software for placing landmarks on the outline. In order to reduce inconsistencies we follow the same set of rules for digitization of every lake.

- Last point overlaps the first point making every outline a closed loop.
- All points are laid clockwise.
- To decrease the angularity in digitization and obliterate the need for higher frequency (harmonics) to fit in the outline, we heavily oversample the edge position.
- For Titan lakes : RADAR's darkest pixels are only considered in the lake outline unless other datasets (ISS, VIMS) show differently.
- For Titan lakes : If there is a granular shelf-like region in the RADAR data, it is not included in the lake outline.
- For Titan lakes : Lakes like Myvatn Lacus, Abaya Lacus, and Ranoch Lacus with prominent extensions are all considered one lake.

We then use the ‘x’ and ‘y’ coordinates generated by tpsDig into a R based package called MOMOCS (MOdern MOrphometriCS) (?). The coordinate information is used to regenerate the outline shape. This code determines a series of harmonic coefficients  $A_n$ ,  $B_n$ ,  $C_n$  and  $D_n$  with which these positions can be

$$x_n = \sum_{n=1}^N A_n \cos(nt) + B_n \sin(nt)$$

$$y_n = \sum_{n=1}^N C_n \cos(nt) + D_n \sin(nt)$$

where, n = harmonic amplitude

N = maximum no of harmonic amplitudes used in the construction

t = evaluation angle (varies from 0 to  $2\pi$ )

Higher order harmonics (larger n) better reproduce the fine details in the shape, but also have less power associated with them and very minutely improve the shape of a feature. We estimate the number of harmonics required to best fit the shape (after examining the spectrum of harmonic Fourier power). In this analysis we selected the number of harmonics to be used, so that their cumulative power gathers  $\sim 90 - 95\%$  of the total cumulative power, thereby representing the shape of the lake by  $\sim 90 - 95\%$ .

Once the right number of harmonics is determined, we perform the elliptic fourier analysis. We obtain four coefficients per harmonic, two for ‘x’ and two for ‘y’. A matrix is obtained with

$$[\text{Number of Outlines}] * [4 \text{ coefficients}] = [\text{Number of Harmonics}]$$

(4.1)

Figure 3 explains the big picture Elliptical Fourier Descriptor Analysis (EFDA) methodology in panel A as a general concept. The first harmonic is shown as a red ellipse while the tenth harmonic can be seen fitting the sinuosities of the leaf and hence its outline shape. In panel B, we show the EFDA methodology working for one of the most peculiarly shaped lakes, Myvatn Lacus near Titan’s north pole. Myvatn Lacus can be coarsely regenerated by the 9th harmonic and is faithfully matched by the 20th harmonic. We then extract the fourier coefficient for each harmonic for every shape and normalize the coefficients for the lake shape’s size and rotation that affect the results.

While the above harmonics clearly describe the shape of any given lake, their values also depend on the overall size and orientation of the lake. Hence, in order to compare the shapes of different lakes, the harmonic coefficients need to be properly normalized to remove their dependence on these parameters. The standard procedure for normalizing the coefficients to remove dependence on size and orientation is given in ? and uses the n=1 harmonics. However, this procedure assumes there is a synchronous point for the profiles, which is not the case for Titan’s lakes.

When we apply the methodology to lakes, however, a rotation issue arises. With the standard methods the same lake shape can be reoriented two different ways that differ by 180 degrees in rotation, which get misinterpreted as two very different shapes if the lake has a prominent feature on one side (see Figure 4A)

To understand this issue of rotation we referred back to the original methodology manuscript (?).

The Fourier coefficients  $A_n$ ,  $B_n$ ,  $C_n$ , and  $D_n$  of the fourier approximation to a closed contour are used as the classification of the contour. Since the fourier coefficients vary according to the starting point of a trace of the contour and the spatial rotation, magnitude and translation of the contour, self-consistent normalization procedures based only on the intrinsic shape properties of the contour are important. The rotating phasors provide normalization modes easily when the locus of the first harmonic phasor is elliptic, yielding two related classifications corresponding to the positions at either end of the major axis of the ellipse.

The contour classification associated with one semi-major axis obtained through starting point and spatial angle rotations of  $\theta_1$  and  $\psi_1$  radians respectively, (where  $\theta_1 = 2\pi\lambda_1/T$  and  $\lambda_1$  is the displacement of the starting point) is different from the contour classification of other semi-major axis obtained by a further rotation of both the starting-point and spatial angles through  $\pi$  radians. For both the contour classification, the odd harmonics remain the same for all  $n$  but the even harmonics change sign.

We took this into account by first identifying the harmonic coefficient that had the maximum loading. We find that the  $C_2$  coefficient has the maximum loading in most cases. For the outlines with negative  $C_2$  coefficient, we multiply the even harmonics of the corresponding outlines by -1 to take the rotation discrepancy into account.

After we make the changes in our algorithm to take care of the rotation we find that similar lake shapes/outlines irrespective of however they are rotated group together as shown in Section 3.2.

The Fourier coefficients can be used to carry out statistical multivariate analysis. In this manuscript we do principal component analysis, heirarchical clustering analysis, and k-means clustering on the Fourier coefficients and these three methods are explained below.

Principal Components Analysis (PCA) is the simplest of the multivariate analyses. The observations are orthogonally transformed in such a way that the first principal component accounts for much of the variability in the data (?). Each succeeding component has the highest variance possible under the constraint that it is orthogonal to the preceding components. It can be used to collapse the data to fewer dimensions that explain the variance in the data.

We use heirarchical clustering as another statistical method to see what lake shapes cluster together, how they stand with respect to the principal component analysis, and human visual semantics. Heirarchical clustering is a statistical methodology that groups similar data into clusters using heirarchy. The metric for deciding the similarity between two lake shapes in order to be clustered together or measure the dissimilaity between two clusters is usually the distance between vectors of fourier coefficients (?). The result is a group of clusters with objects in one cluster being similar to each other and each cluster being uniquely distinct.

The k-means clustering mechanism is another statistical methodology to group the dataset into a user-defined number (k) of clusters. The data cluster into k numbers of clusters even if the k is not the right number of clusters for the data. In order to address this issue, we use the elbow method to determine the optimal number of clusters (??). The elbow method runs k-means clustering on the dataset for a range of values of k (say, k from 1 to 10), and for each value of k calculates the sum of squared errors. If the plot of the sum of squared errors for each value of k resembles an arm, then the ‘elbow’ of the arm is the value of ‘k’ that suits the dataset the best. As we increase the number of k, the sum of squared

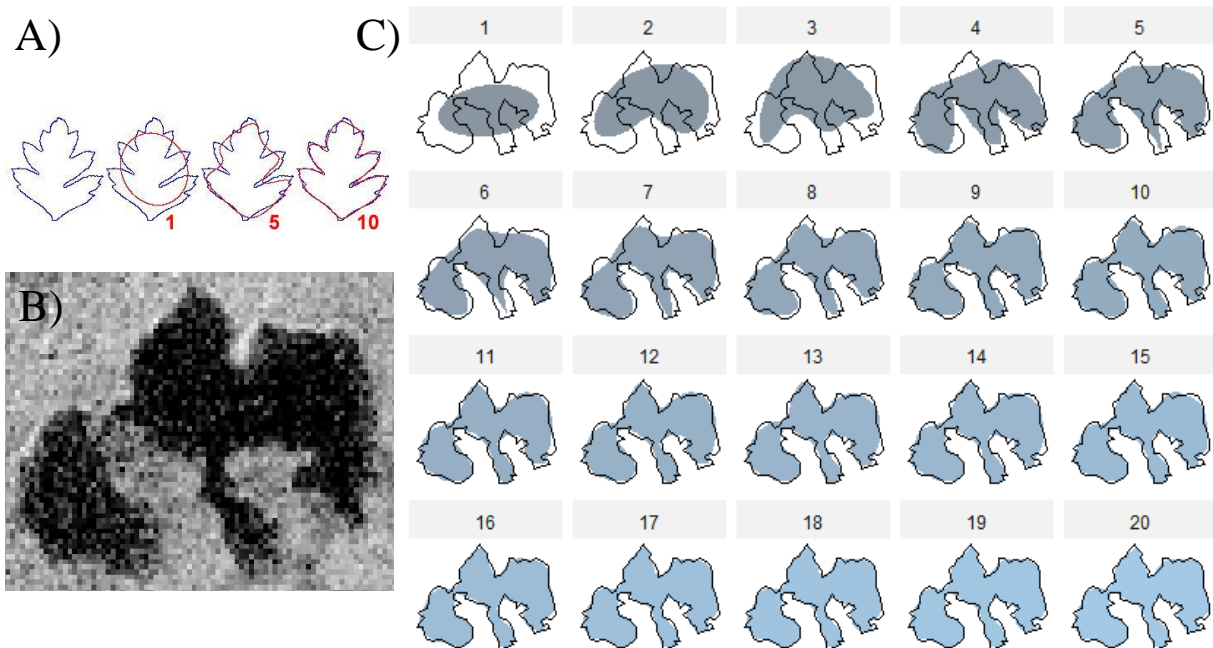


Figure 4.3: A) (modified from Wikipedia) shows the methodology of Elliptical Fourier Analysis. Leaf outline is shown in blue. The red ellipse over the blue leaf outline is the first harmonic. The (fifth and) tenth harmonic regenerates the sinuosities of leaf's edge and shape. B) RADAR image of Myvatn Lacus (78 °N, 135 °W) (peculiarly shaped). Figure C) shows that by 20th harmonic the extremely complicated shape of even Myvatn Lacus can be explained quantitatively by the Elliptical Fourier Analysis

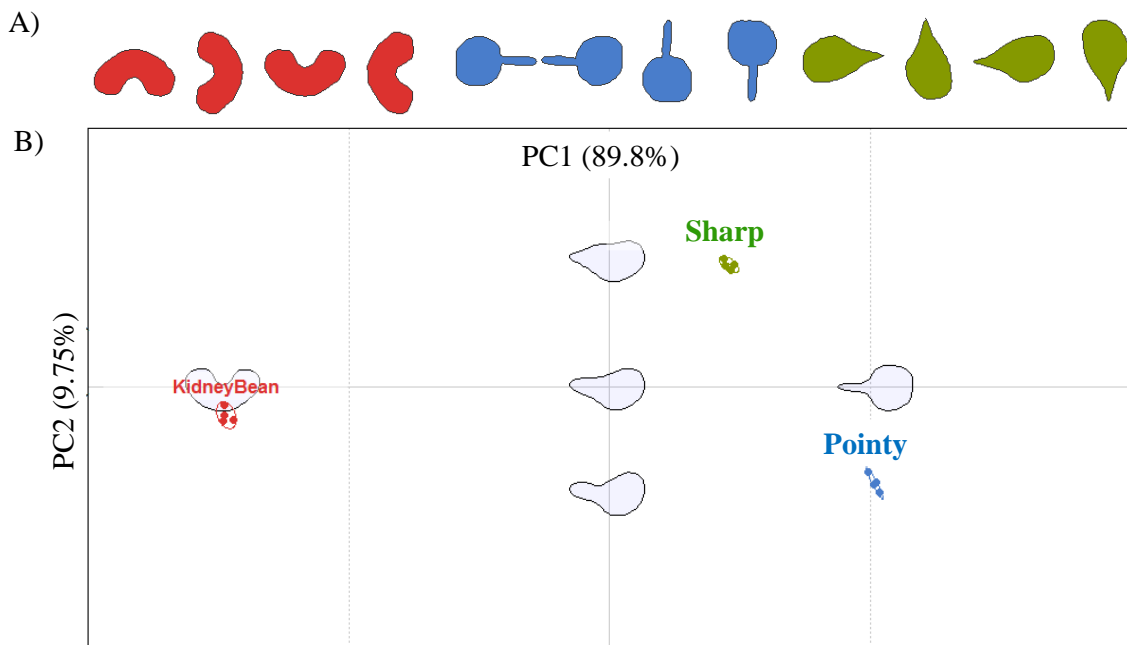


Figure 4.4: A) shows the synthetic lake shapes we use for analysis. The kidney bean lake shape is in red, pointy lake shape is in blue, and sharp lake shape is in green. B) Principal component plot with the geomorphological shapes. The shaded grey shapes in the morphological space are the shape variations along the principal component axes. PC1 explains 90 % of the variation in shape while PC2 explains  $\sim 10$  % of the variation in shape. The red dots indicate the four kidney beans with different rotation angles ( $90^\circ, 180^\circ, 270^\circ, 360^\circ$ ). The ellipse around the red points represents the 95% confidence interval. Similarly the blue and green dots indicate the pointy lakes and sharp lakes with the ellipses representing the 95% confidence interval.

errors approaches zero because each data point in the dataset gets its own cluster and hence there is no error between the datapoint and center of cluster. We want a small value of ‘k’ that still has a low sum of squared errors and the ‘elbow’ approximately represents the point where increasing ‘k’ has less returns (?).

#### 4.4.2 TESTING EFDA ON LAKE FORMS

Conventional morphometric approaches have been applied to symmetric lunar craterforms (?) to study the circularity and axial ratio of craters. However, the use of morphometrics to asymmetric, complex, and irregular natural forms have been scarcely used in planetary research. We apply the fourier based approach to Titan’s lakes to assess if distinctions in their morphology can be classified using shape information alone. An additional complexity in lake shape analysis is the absence of a synchronous point. However, the strength of fourier analysis lies in the methodology that it can be applied to practically any kind of outline that the myriad shapes of Titan lakes exemplify the best.

##### 4.4.2.1 Synthetic Lakes

We dummy run our analysis methodology on synthetic lakes. Figure 4 shows the three different shapes we use in our methodology testing (Kidney Bean(red), Sharp(green), and Pointy(blue)). We observe that in the morphological space in Figure 4, all similar lakes group together irrespective of the rotation. Similar synthetic lake outlines also clump together in three clean clusters (Kidney Bean, Pointy, and Sharp) in our Hierarchical clustering and k-means cluster analysis. With that proof of technique and validation of our new normalization scheme we progress into performing the analysis on some real lakes.

##### 4.4.2.2 Earth Lakes

Next, we carry out the analysis on terrestrial lakes. We pick two distinct types of terrestrial lakes to see if our methodology can separate their shapes and hence provide insight into their formation mechanism. We use two types of lakes whose origins as volcanic or tectonic are already known before our analysis. We select them specifically knowing their formation mechanism so that we could test the formation mechanism against their shapes. The volcanic lakes are fairly circular in shape while the tectonic lakes are fairly elongated in shape. Although volcanic lakes can be separated from tectonic lakes intuitively (visually), we intend to test how our analysis works on separating them. We use the lakes as entabulated in the book ?. The EFDA methodology can quantitatively separate the two types of shapes indicating two plausibly distinct formation mechanisms.

Figure 5, panel A shows the terrestrial lakes on which we chose to run EFDA. Panel B shows their location in the principal component plot. We can clearly separate volcanic lakes from tectonic lakes in the morphological space. However, lakes like Lake Tahoe, which is tectonic in origin yet more circular than the other tectonic lakes can be seen in the circular space in the principal component plot.

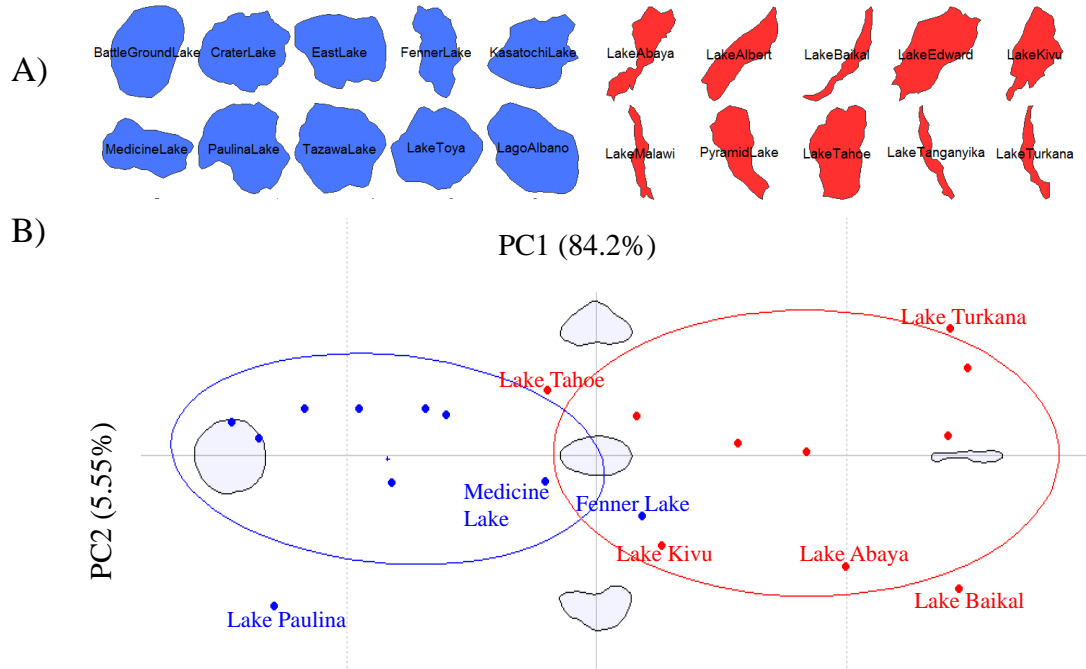


Figure 4.5: A) shows the Earth lakes we use for analysis. The lake shapes blue in color are classified as volcanic lakes. Similarly the lake shapes in red are classified as tectonic lakes. Since the shapes of these two kinds of lakes are discretely different we chose these two lake types to see if they separate in the principal component space. The shaded colors indicate the group that the lakes belong to according to our k-means cluster analysis. B) Principal component plot with the end member shapes. PC1 explains 84.2 % of the variation in shape while PC2 explains  $\sim 5.55\%$  of the variation in shape. We can see that principal component 1 explains the variation of lake shapes from circular to elliptical (fat to fit). Principal component 2 explains the curvature in the shape. The red dots indicate the distribution of the tectonic lakes. As expected they clump more toward the skinny or elliptical side of shape variation in the principal component space. Similarly the blue dots represent the terrestrial volcanic lakes (more circular in shape). These cluster toward the circular end of the principal component plot. The ellipse represent the 95% confidence interval for both the populations.

## 4.5 APPLICATION TO TITAN LAKES

We use the methodology described in section 3.2.2 to quantify the outlines of the 67 IAU named north polar lakes of Titan. We exclude the larger seas present on the north pole because the connections between them complicate the identification of discrete lakes. The Figure 7 top panel shows the outlines of the 67 lakes from the north pole of Titan that we use for our analysis. We omitted lakes that have diameters less than 2 km.

### 4.5.1 OBSERVATIONAL DATA AND METHOD

For the shape analysis we only consider the IAU named 67 lakes on the north pole of Titan. In order to determine the errors on the outline determinations, we randomly chose five lakes (Feia Lacus, Oneida Lacus, Rukwa Lacus, Sparrow Lacus, and Vanern Lacus) that we digitize before starting digitization of other lakes. The outlines of these lake and their distribution in the morphometric space indicates the human error of outlining the lakes. The lakes on which we carry out the shape analysis are shown in Figure 6. We digitize the 67 lakes for shape analysis in the software, ‘tpsDig’. The lake outlines with their ‘x’ and ‘y’ coordinates in text files are then used in a R package called MOMOCS (MODern MORphometriCS) for the Elliptical Fourier Descriptor Analysis as explained in the section 3.1.

#### 4.5.1.1 Results

Once we have the outlines of the lakes and the fourier coefficients extracted, we statistically analyse the fourier coefficients in order to decipher if there is any pattern in the lakes’ fourier coefficients. The left principal component plot in Figure 4.6 shows the variation of principal component 1 w.r.t 2 in morphological space. The first principal component varies from a  $\sim$  circular to elliptical shape and explains  $\sim$  30% of the variation in the shapes. This indicates that the majority of lake shapes on Titan’s north pole vary from circular to elliptical. The circular end member is best represented by Mweru Lacus and Quilotoa Lacus. Hlawga Lacus and Roca Lacus have the maximum ellipticity and represent the elliptical end member on the PC1 axis.

The second principal component explains  $\sim$ 15% of the variation in the lake shapes. Positive PC2 corresponds to lakes with strong asymmetries along their short axis, while those with strong negative values of PC2 have strong asymmetries along their long axis. While Muggel Lacus represents the asymmetric lake end member on negative PC2, Xolotlan Lacus represents the end member for the (asymmetric) lake with a curvature on the positive PC2.

The outliers —Myvatn Lacus, Rwegura Lacus, Sotonera Lacus, Muggel Lacus, and Feia Lacus explain that those lake shapes are peculiarly odd and rare on Titan’s surface. The PC3 represents an increasing strong kidney-bean like shape. Indeed, lakes with strong negative values of PC3 (Sotonera Lacus, Neagh Lacus) often have broad peninsulas jutting into them. We have not included Letas Lacus in this analysis. Letas Lacus has an atypical island that gives it an appearance of a two lobed lake, which is prominently different from all the other lakes on Titan’s north pole.

Figure 8 shows the results of the heirarchical clustering of lake shapes based on the on euclidean

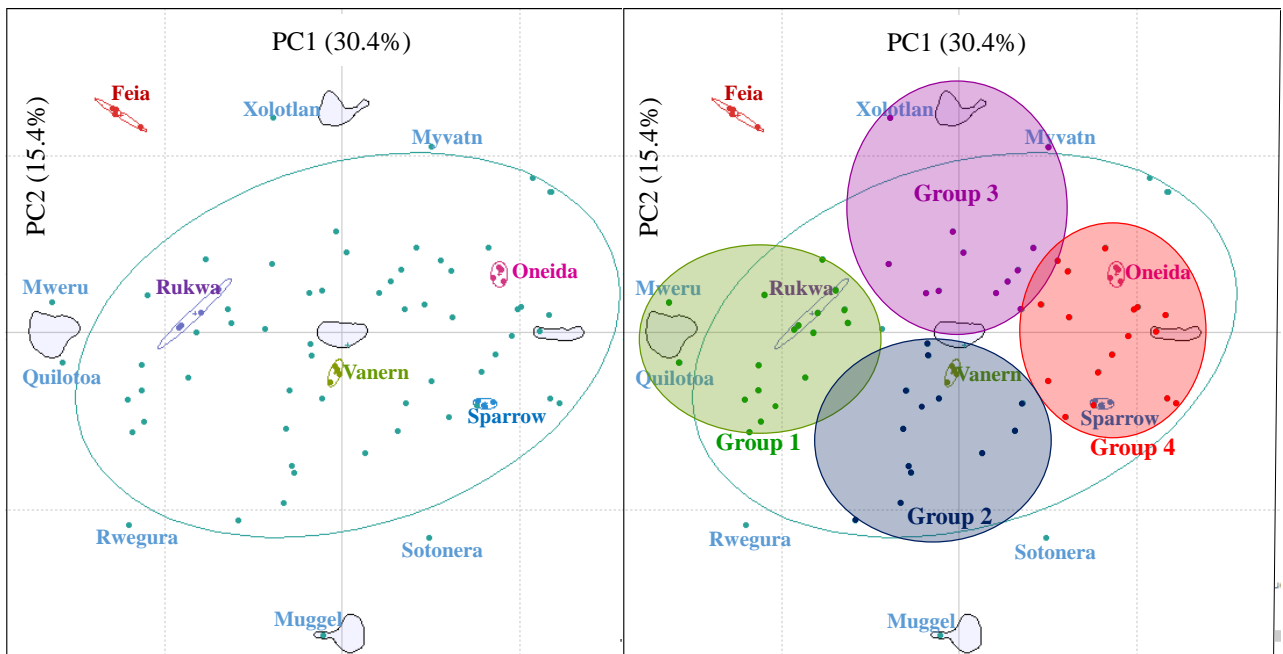
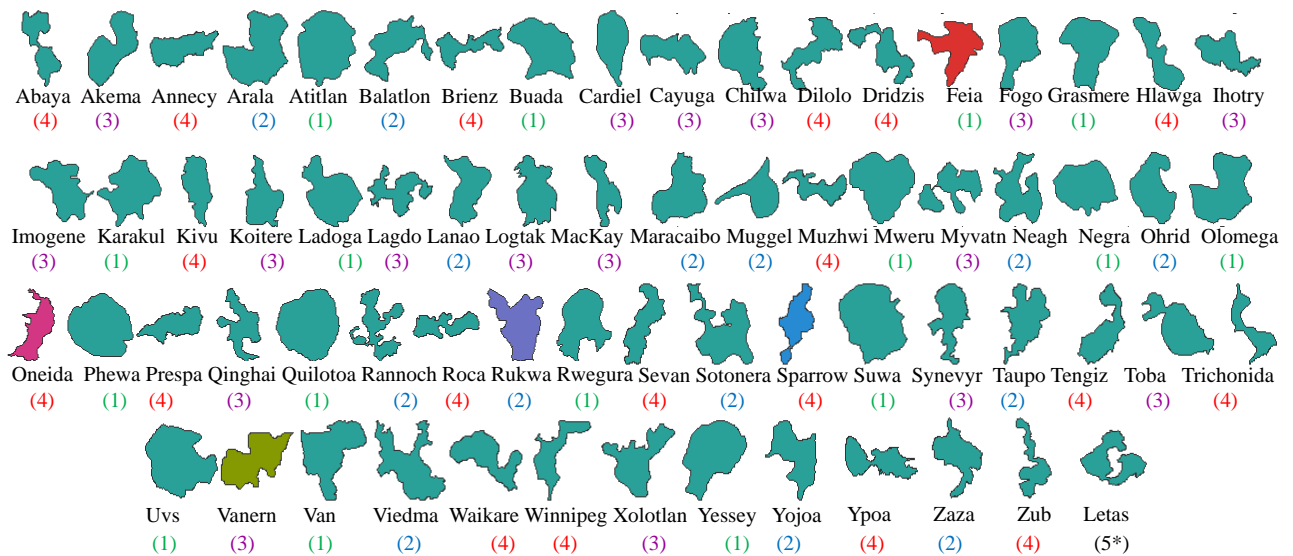


Figure 4.6: Top panel represents the lake shapes with their respective names on the north pole of Titan. The numbers in the brackets indicate the group (using our k-means cluster analysis) that the lake belongs to. Bottom left panel indicates the first two principal component's plot for Titan lakes (from the top panel). We randomly chose five standard lakes (Feia Lacus, Oneida Lacus, Rukwa Lacus, Sparrow Lacus, Vanern Lacus) that we digitized everyday before starting digitization of other lakes. PC1 shows the shape variation from circular to elliptical and explains 30.4% of variation in the shapes of Titan lakes considered in this study. PC2 shows the shape variation from pointy extensions to a curvature in the pointy extensions and explains 15.6% of the variation in data. The ellipse shows the 95% confidence interval so that there is a 95% probability that the Titan lakes lie within the ellipse. Bottom right panel shows the four groups of lakes that we derived from the k-means analysis on the principal component plot.

distance between clusters. We can see that the repeated measurements of our random lakes that we use to determine the approximate errors of digitization are all clustered together lending confidence in the repeatability of our measurements. The clustering tree indicates four major clusters indicating four probable formation or evolution mechanisms.

Treading up the cluster tree, Rannoch, Viedma, and Myvatn Lacus all have high sinuosities in their shorelines and are standalone cases as clusters of their own. Neagh Lacus and Sotonera Lacus in fact look like twin lakes, both having distinctive peninsulas. Overall big picture lake clusters are as expressed by the PCA, circular-ish (**Group 1**) —the upper limb of the cluster tree (Yessey, Uvs, Van, Suwa, Negra, Phewa, Atitlan, Karakul, Quilotoa, Mweru) to elliptical (**Group 4**) —the middle limb of the cluster tree (Sparrow, Ypoa, Waikare, Sevan, Dilolo).

In our k-means analysis, the optimum number of clusters were determined by the elbow method to be four (Figure 8 top panel). Similar to our earlier results Letas Lacus indicates its own cluster. Removing Letas Lacus from the analysis, results in 4 clean clusters as shown in Figure 8. We also show in brackets in Figure 7 (top panel) the group (using our k-means cluster analysis) that the lake belongs to. In the bottom panel of Figure 6 we show in the principal component plot the groups to which the lakes belong in shaded ellipses. Finally, in Figure 9 we plot the geographic location of the four groups of lakes (in their respective colors) on the north polar map of Titan to understand if there is any geographic similarity in groups' locations. Most of the round lakes in Group 1 seem to be in the upper left quadrant ( $180^{\circ}\text{W}$  to  $90^{\circ}\text{W}$ ). The 'long' (Group 4) lakes, might have a preferred orientation (more seem to be up-down (line joining  $0^{\circ}\text{W}$  to  $180^{\circ}\text{W}$ ) than left-right (line joining  $90^{\circ}\text{W}$  to  $270^{\circ}\text{W}$ ))

All the analysis give roughly four groups.

Group 1 : round lakes

Group 2 : moderately long lakes with a strong asymmetry along their long axis

Group 3 : moderately long lakes with a strong asymmetry across their short axis

Group 4 : long lakes

## 4.6 DISCUSSION AND CONCLUSION

We show that the Elliptical Fourier Descriptor Analysis methodology for outline shape analysis is a robust way to decipher differences and similarities in lake outlines. We validate through our synthetic lake example that the size and rotation normalized algorithm helps in clustering similarly shaped outlines together. The Earth lake examples of clustering of Type I and Type II lakes bolsters the algorithm's strength.

Since the algorithm can be used on any shape without a synchronous point, it is very useful for shapes like lakes or other planetary geomorphic landforms which do not necessarily have a synchronous point. ?? used a similar morphometric technique to investigate the paterae on Io.

Our statistical analyses of the fourier coefficients demarcate the Titan lake shapes into four groups. Our methodology determines that the maximum variation of shape on Titan lakes are from circular to elliptical. The second component shows that lake shapes vary from moderately long lakes with a strong

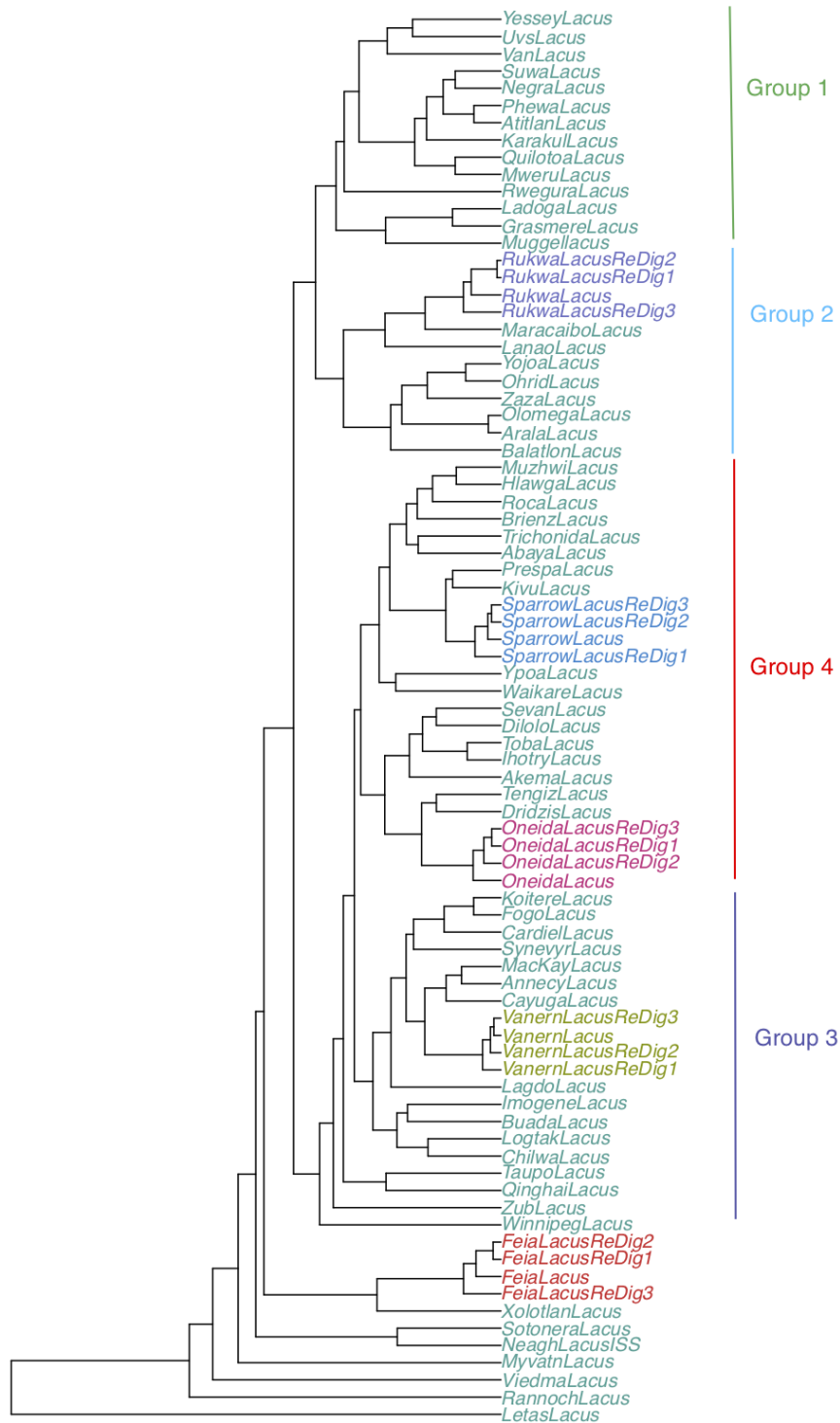


Figure 4.7: Phylogram for the hierarchical clustering of Titan north polar lakes. Letas Lacus exists by itself like in the principal component analysis. Same lakes re-outlined to determine the error are all together in same clusters. Other clusters of lakes when compared with their shapes can be seen clustering well in similar shapes. The hierarchical cluster helps us group similar shapes together thereby indicating similar formation mechanisms.

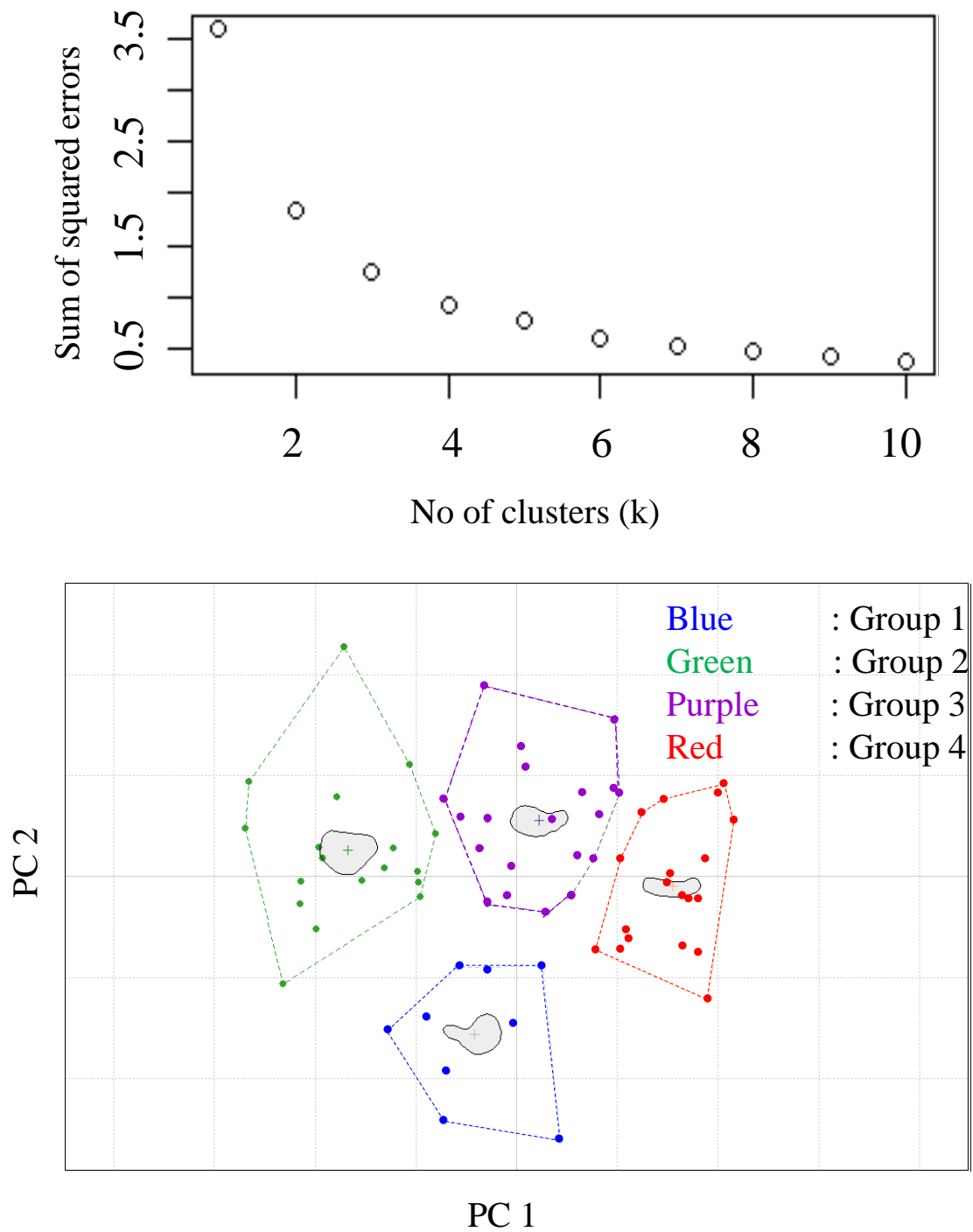


Figure 4.8: Top panel shows the elbow method for the determination of number of clusters in the k-means clustering analysis. Bottom panel shows the four clusters of lake shapes.

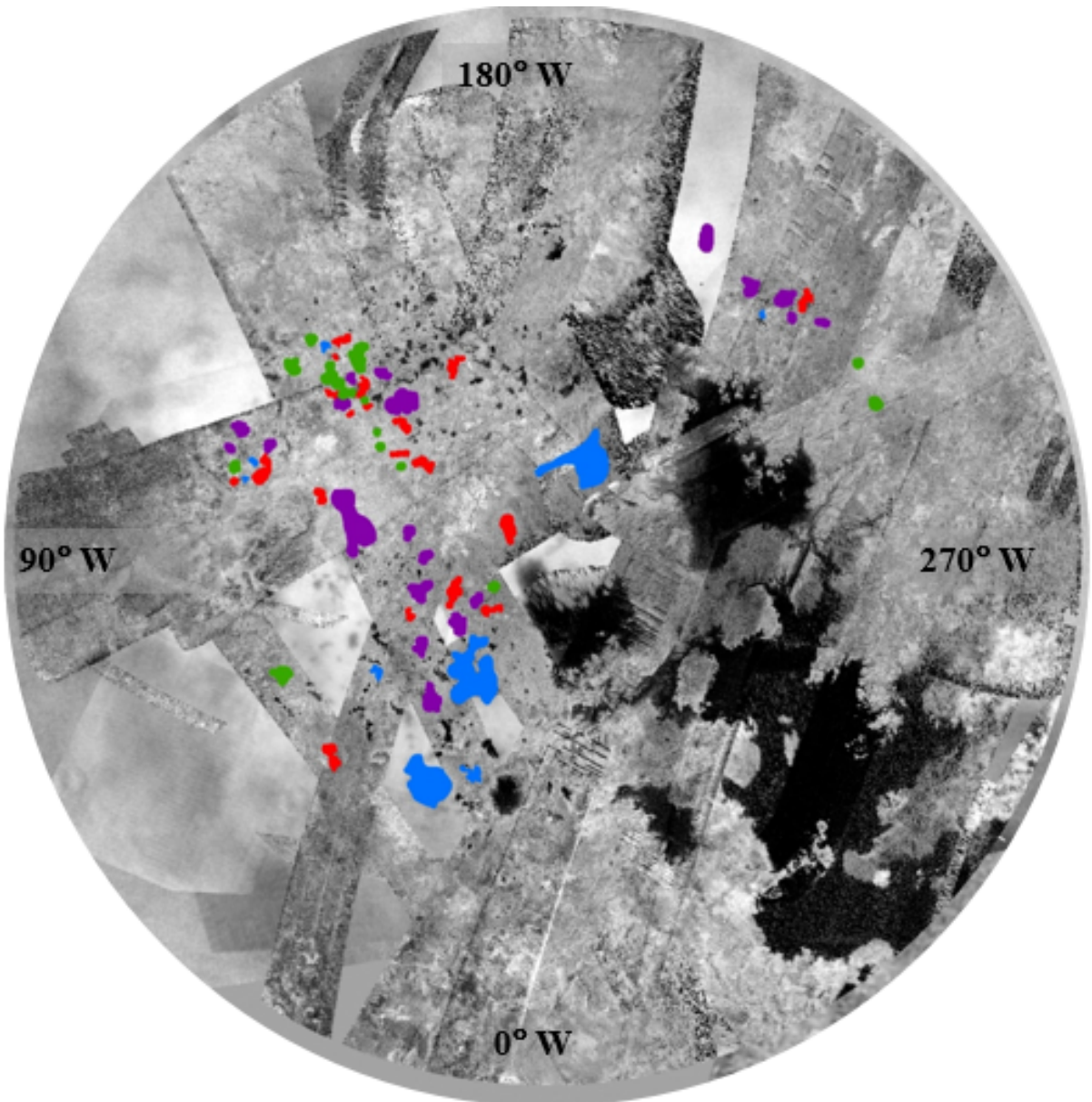


Figure 4.9: Geographic location of the four clusters of lake shapes (derived from k-means clustering) on the north pole of Titan. The base images are ISS and RADAR north polar image of Titan. The colors are **Group 1**: round, e.g :Yessey Lacus), **Group 2**: (long with asymmetries along their long axis, e.g :Rukwa Lacus), **Group 3**: (long with asymmetries along their short axis, e.g :Vanern Lacus), and **Group 4**:long lakes, e.g :Oneida Lacus

asymmetry along their long axis to moderately long lakes with a strong asymmetry across their short axis. We also find that Letas Lacus is a total outlier among the (presently analyzed) Titanian lakes. This brings into focus the lake shapes that are dissimilar from the other lakes on Titan directing us to another challenge of how these outliers were formed or evolved into present day lakes.

Terrestrial lakes show similar formation mechanisms based on their geographic location. The Siberian lake packets are formed by thermokarst processes and lakes in Minnesota are formed due to glacial recession. Similarly the lakes in the East African Rift are mostly tectonic (?). In our analysis we see that the round and elliptical lakes cluster in the upper left quadrant ( $180^\circ\text{W}$  to  $90^\circ\text{W}$ ) of the north pole. We also see that the group 2 and 3 lakes cluster along a line near the borders of the bigger seas/lakes.

According to our size analysis Titan lakes follow lognormality like the terrestrial thermokarst lakes. However, temperature differences to sustain thermokarst mechanisms on Titan are improbable according to our current understanding. Thermokarst can be intriguing as a putative lake formation hypothesis but posits the weak thermal insolation on Titan's north pole as an issue. ? in their model assume that the terrestrial thermokarst lakes form over a small interval of time. We can't assume this for Titan's lakes owing to the 30 times slower dissolution rates on Titan. However, a combination of karst and thermokarst processes can not be ruled out wherein the dissolution of a permafrost equivalent with the hydrocarbon combinations raining from the atmosphere, is highly probable (?).

Recently ? propose that the seasonal thawing of permafrost, with a minimum temperature difference of 3K between winter and summer, forms lakes in at least 45 freeze and thaw cycles and a drainage network by the 135th cycle. Yet, *Cassini* surface temperatures from 2004 - 2014 decrease by only 2K for southern hemisphere and increase by 1K in northern hemisphere (?) making an active permafrost thawing an unlikely mechanism. Titan lakes also show a slight preferred orientation for a NE-SW (NorthEast-SouthWest) or ( $45^\circ\text{W}$  -  $225^\circ\text{W}$ ) direction, indicating probable tectonic lake formation mechanisms.

We observe a size relationship between the groups in Figure 9. Group 2 is associated with big lakes as opposed to group 1 which is more roundish. A common feature of Titan's lakes are that the smaller lakes are mostly circular with simple outlines while the larger ones are of myriad shapes with sinuous outlines. This could be telling us that the initial lake formation mechanism could be something simple but as soon the lake starts to grow there must be different processes developing to cause the sinuosities and growth.

A permafrost thawing lake formation mechanism may only work on Titan if the temperature of hydrocarbons that make up the permafrost is below the mean surface temperature under the consideration that the freezing point is depressed by dissolved nitrogen. Also, the seasonal temperature variation range must be sufficient for thawing of the permafrost.

An alternative theory of surface-ice cracking where smaller evaporation puddles formed from seasonal precipitation likely leave a bottom ice layer that sublimates after the liquid puddle evaporates (evidenced by the equatorial brightening events) (Barnes et al., 2013) is plausible. Such a process of seasonal yet cyclic evaporation-sublimation over millions of years will likely have an erosional impact on the immediate water-ice bedrock that could carve out and deepen a surface depression.

Our present study considers the IAU named lakes on Titan. We wish to expand the lake population to consider all the lakes present on Titan's north pole and the south pole. We intend to carry out the

same analysis over the other larger seas to understand how or where they lie in the formation mechanism groups. We also intend to use the equatorial Hotei and Tui Regio apart from the south polar paleo basins to understand how the filled lakes in the north pole contrast the paleo-lakes and basins. Apart from this, we would like to test the tectonic lake formation hypothesis by comparing our orientations with the straight rivers in the region. A statistical size correlation with the geographic location is under consideration once we have the analysis for all the lakes on the north pole.

## CHAPTER 5: CONCLUSIONS

The presence of standing bodies of liquids, nitrogen rich atmosphere and active surface-atmosphere hydrological interactions arguably makes Titan the most Earth-like planetary body in the solar system. Understanding Titan's hydrologic system will teach us about the history of volatile components across the solar system and the development and evolution of Earth-like planets both in our own solar system and around other stars. The research presented in this thesis has investigated the hydrological flow paths, precipitative hydrology and constrains probable lake formation mechanisms, addressing some key questions in Titan research:

The key questions addressed include

- How do hydrological flow paths affect the catchment areas on Titan?
- The report of the first rainfall observation on the north pole and how does rainfall affect the surface?
- What are the differences and similarities between Titan and Earth's lake formation/evolution mechanisms?

This chapter will both review and expand upon the foundations of the research presented in preceding chapters and describe future work.

We found out that the hydrological flow paths affect the catchment areas on Titan, in similar ways as they do on Earth. The reason that Ontario Lacus is the only filled lake on Titan's south pole is strongly influenced by its enormous catchment area that extend upto southern mid-latitudes. This is consistent with cloud observations at similar latitudes which suggests that if the clouds are precipitative in nature, all the fluid will drain into Ontario Lacus.

We reported the first rainfall on Titan's north pole. This was a valuable observation for the following reasons : First, this discovery observation heralded the much awaited arrival of the north polar summer rains on Titan. This atmospheric phenomenon has been delayed compared to the theoretical predictions and was perplexing Titan researchers and climate modelers especially because the north pole hosts most of Titan's lakes and seas. Second, it is extremely difficult to detect rainfall events on Titan due to its thick atmospheric haze and very limited opportunities to view the surface (and its changes). We have used a novel phenomenon —the smoothening of a previously dry, rough surface by a thin layer of fluid after rainfall, similar to a wet sidewalk —as evidence for rainfall events on the surface of Titan.

We also used a new methodology for exploring the probable mechanisms of origin for the depressions hosting the fluid inventory on Titan. We adapted the technique called EFDA (Elliptical Fourier Descriptor Analysis) to quantify closed shapes and group them w.r.t their similar parameters. These groups of similar shapes could indicate similar formation or evolution mechanism. The strength of this methodology is it could be applied to virtually any shape, even the ones that fold amongst themselves. The big picture application of this new method that has not been previously used in planetary science is that it can be

used on any kind of landform across planetary bodies. In our study of using this method on Titan’s lakes, we found that the major variation in Titan’s lake shape is from circular to elliptical. Overall we did cluster the lakes into four groups with circular, elliptical, long lakes with asymmetry along their long axis and long lakes with asymmetry along their short axis.

Apart from my first project – determining the catchment area of Ontario Lacus, I wish to expand both my other projects. Motivated by the T120 observation (Chapter 2) we sifted through other VIMS north polar observations to detect more such transient features. We find additional such transient features—bright areas that appear, disappear, and shift from flyby to flyby. I intend to document the temporal and spatial evolution of these bright areas that we termed —Bright Ephemeral Feature in our discovery paper of T120 observation.

The significance of this documentation will be that we might be able to determine when and where it has rained on the north pole of Titan without having to actually observe the rainfall event. Only a few rainfall observations have been documented in thirteen years of *Cassini* mission. The difficulty of observing rainfall on Titan is incremented by observation geometry, position of the spacecraft, evaporation rate and the atmosphere. Active rainfall could even be obscured by the presence of clouds.

One outstanding question after the T120 analysis was if the transient feature was on surface or near-surface. In our analysis, we could not rule out the possibility that the Bright Ephemeral Feature (BEF) could be a near-surface fog. SRTC++ (Barnes et al., 2018) is a new radiative transfer code that works well for the polar regions of Titan. We would like to hash out this possibility of the transient feature being a near surface fog.

I wish to extend my analysis on Titan’s other lakes and come up with a clean clustering of lake groups. I also wish to compare the larger seas amongst themselves and with the paleoseas on the south pole and the probable paleoseas, Tui and Hotei in the equatorial region. I think an exhaustive analysis of all the filled surface features and unfilled surface features on Titan would help us nail the question of lake formation mechanism on Titan.

I have contributed to the New Horizons team’s exploration of the distant cold classical KBO (Kuiper Belt Object) as a member of the GGI (Geology, Geophysics and Imaging) team. I am a co-author on various manuscripts from the team and intend to keep contributing to the team and science.

After I graduate, I am joining the Jet Propulsion Laboratory (JPL), NASA to work with Dr. Bonnie Buratti on Europa’s photometry.

## REFERENCES

- Ádámkóvics, M., Wong, M. H., Laver, C., de Pater, I., 2007. Widespread morning drizzle on titan. *Science* 318 (5852), 962–965.
- Aharonson, O., Hayes, A. G., Lunine, J. I., Lorenz, R. D., Allison, M. D., Elachi, C., Dec. 2009. An asymmetric distribution of lakes on Titan as a possible consequence of orbital forcing. *Nature Geoscience* 2, 851–854.
- Baines, K. H., Drossart, P., Momary, T. W., Formisano, V., Griffith, C., Bellucci, G., Bibring, J. P., Brown, R. H., Buratti, B. J., Capaccioni, F., Cerroni, P., Clark, R. N., Coradini, A., Combes, M., Cruikshank, D. P., Jaumann, R., Langevin, Y., Matson, D. L., McCord, T. B., Mennella, V., Nelson, R. M., Nicholson, P. D., Sicardy, B., Sotin, C., Jun. 2005. The Atmospheres of Saturn and Titan in the Near-Infrared First Results of Cassini/vims. *Earth Moon and Planets* 96, 119–147.
- Barnes, J. W., Bow, J., Schwartz, J., Brown, R. H., Soderblom, J. M., Hayes, A. G., Vixie, G., Le Mouélic, S., Rodriguez, S., Sotin, C., et al., 2011. Organic sedimentary deposits in titanâs dry lakebeds: Probable evaporite. *Icarus* 216 (1), 136–140.
- Barnes, J. W., Brown, R. H., Soderblom, J. M., Soderblom, L. A., Jaumann, R., Jackson, B., Le Mouélic, S., Sotin, C., Buratti, B. J., Pitman, K. M., Baines, K. H., Clark, R. N., Nicholson, P. D., Turtle, E. P., Perry, J., May 2009. Shoreline features of Titan’s Ontario Lacus from Cassini/VIMS observations. *Icarus* 201, 217–225.
- Barnes, J. W., Brown, R. H., Soderblom, L., Buratti, B. J., Sotin, C., Rodriguez, S., Le Mouélic, S., Baines, K. H., Clark, R., Nicholson, P., 2007. Global-scale surface spectral variations on titan seen from cassini/vims. *Icarus* 186 (1), 242–258.
- Barnes, J. W., Buratti, B. J., Turtle, E. P., Bow, J., Dalba, P. A., Perry, J. E., Brown, R. H., Rodriguez, S., Le Mouélic, S., Baines, K. H., Sotin, C., Lorenz, R. D., Malaska, M. J., McCord, T. B., Clark, R. N., Jaumann, R., Hayne, P. O., Nicholson, P. D., Soderblom, J. M., Soderblom, L. A., 2013. Precipitation-Induced Surface Brightenings Seen on Titan by Cassini VIMS and ISS. *Planetary Science* 2:1.
- Barnes, J. W., MacKenzie, S. M., Young, E. F., Trouille, L. E., Rodriguez, S., Cornet, T., Jackson, B. K., Ádámkóvics, M., Sotin, C., Soderblom, J. M., 2018. Spherical radiative transfer in c++ (srte++): A parallel monte carlo radiative transfer model for titan. *The Astronomical Journal* 155 (6), 264.
- Barnes, J. W., Radebaugh, J., Brown, R. H., Wall, S., Soderblom, L., Lunine, J., Burr, D., Sotin, C., Le Mouélic, S., Rodriguez, S., Buratti, B. J., Clark, R., Baines, K. H., Jaumann, R., Nicholson, P. D., Kirk, R. L., Lopes, R., Lorenz, R. D., Mitchell, K., Wood, C. A., Nov. 2007. Near-infrared spectral mapping of Titan’s mountains and channels. *Journal of Geophysical Research (Planets)* 112, E11006.
- Barnes, J. W., Sotin, C., Soderblom, J. M., Brown, R. H., Hayes, A. G., Donelan, M., Rodriguez, S., Le Mouélic, S., Baines, K. H., McCord, T. B., 2014. Cassini/vims observes rough surfaces on titanâs punga mare in specular reflection. *Planetary science* 3 (1), 3.

- Brown, M., Smith, A., Chen, C., Ádámkóvics, M., 2009. Discovery of fog at the south pole of titan. *The Astrophysical Journal Letters* 706 (1), L110.
- Brown, M. E., Smith, A. L., Chen, C., Ádámkóvics, M., Nov. 2009. Discovery of Fog at the South Pole of Titan. 706, L110–L113.
- Brown, R. H., Baines, K. H., Bellucci, G., Bibring, J.-P., Buratti, B. J., Capaccioni, F., Cerroni, P., Clark, R. N., Coradini, A., Cruikshank, D. P., Drossart, P., Formisano, V., Jaumann, R., Langevin, Y., Matson, D. L., McCord, T. B., Mennella, V., Miller, E., Nelson, R. M., Nicholson, P. D., Sicardy, B., Sotin, C., Dec. 2004. The Cassini Visual And Infrared Mapping Spectrometer (Vims) Investigation. *Space Science Reviews* 115, 111–168.
- Brown, R. H., Soderblom, L. A., Soderblom, J. M., Clark, R. N., Jaumann, R., Barnes, J. W., Sotin, C., Buratti, B., Baines, K. H., Nicholson, P. D., Jul. 2008. The identification of liquid ethane in Titan's Ontario Lacus. *Nature* 454, 607–610.
- Burr, D. M., Drummond, S. A., Cartwright, R., Black, B. A., Perron, J. T., 2013. Morphology of fluvial networks on titan: Evidence for structural control. *Icarus* 226 (1), 742 – 759.
- Burr, D. M., Jacobsen, R. E., Roth, D. L., Phillips, C. B., Mitchell, K. L., Viola, D., Nov. 2009. Fluvial network analysis on Titan: Evidence for subsurface structures and west-to-east wind flow, southwestern Xanadu. 36, L22203.
- Burr, D. M., Perron, J. T., Lamb, M. P., Irwin, R. P., Collins, G. C., Howard, A. D., Sklar, L. S., Moore, J. M., Ádámkóvics, M., Baker, V. R., et al., 2013. Fluvial features on titan: Insights from morphology and modeling. *Geological Society of America Bulletin* 125 (3-4), 299–321.
- Cartwright, R., Clayton, J. A., Kirk, R. L., 2011. Channel morphometry, sediment transport, and implications for tectonic activity and surficial ages of titan basins. *Icarus* 214 (2), 561–570.
- Clark, R. N., Curchin, J. M., Barnes, J. W., Jaumann, R., Soderblom, L., Cruikshank, D. P., Brown, R. H., Rodriguez, S., Lunine, J., Stephan, K., Hoefen, T. M., Le Mouélic, S., Sotin, C., Baines, K. H., Buratti, B. J., Nicholson, P. D., Oct. 2010. Detection and mapping of hydrocarbon deposits on Titan. *Journal of Geophysical Research (Planets)* 115 (E14), 10005.
- Comas Sola, J., 1908. Observations des satellites principaux de jupiter et de titan. *Astronomische Nachrichten* 179, 289.
- Cook-Hallett, C., Barnes, J. W., Kattenhorn, S. A., Hurford, T., Radebaugh, J., Stiles, B., Beuthe, M., 2015. Global contraction/expansion and polar lithospheric thinning on titan from patterns of tectonism. *Journal of Geophysical Research: Planets* 120 (6), 1220–1236.
- Cordier, D., Mousis, O., Lunine, J. I., Lavvas, P., Vuitton, V., Dec. 2009. An Estimate of the Chemical Composition of Titan's Lakes. 707, L128–L131.

- Cornet, T., Bourgeois, O., Le Mouélic, S., Rodriguez, S., Lopez Gonzalez, T., Sotin, C., Tobie, G., Fleurant, C., Barnes, J. W., Brown, R. H., Baines, K. H., Buratti, B. J., Clark, R. N., Nicholson, P. D., Apr. 2012a. Geomorphological significance of Ontario Lacus on Titan: Integrated interpretation of Cassini VIMS, ISS and RADAR data and comparison with the Etosha Pan (Namibia). 218, 788–806.
- Cornet, T., Bourgeois, O., Le Mouélic, S., Rodriguez, S., Sotin, C., Barnes, J. W., Brown, R. H., Baines, K. H., Buratti, B. J., Clark, R. N., Nicholson, P. D., Jul. 2012b. Edge detection applied to Cassini images reveals no measurable displacement of Ontario Lacus' margin between 2005 and 2010. *Journal of Geophysical Research (Planets)* 117, 7005.
- Cottini, V., Nixon, C. A., Jennings, D. E., de Kok, R., Teanby, N. A., Irwin, P. G. J., Flasar, F. M., Jan. 2012. Spatial and temporal variations in Titan's surface temperatures from Cassini CIRS observations. 60, 62–71.
- Coustenis, A., Achterberg, R. K., Conrath, B. J., Jennings, D. E., Marten, A., Gautier, D., Nixon, C. A., Flasar, F. M., Teanby, N. A., Bézard, B., et al., 2007. The composition of titan's stratosphere from cassini/cirs mid-infrared spectra. *Icarus* 189 (1), 35–62.
- Davis, W. M., 1899. The geographical cycle. *The Geographical Journal* 14 (5), 481–504.  
URL <http://www.jstor.org/stable/1774538>
- Dhingra, R. D., Barnes, J. W., Brown, R. H., Burrati, B. J., Sotin, C., Nicholson, P. D., Baines, K. H., Clark, R. N., Soderblom, J. M., Jauman, R., Rodriguez, S., Mouélic, S. L., Turtle, E. P., Perry, J. E., Cottini, V., Jennings, D. E., Feb. 2019. Observational Evidence for Summer Rainfall at Titan's North Pole. 46, 1205–1212.
- Dhingra, R. D., Barnes, J. W., Yanites, B. J., Kirk, R. L., 2018. Large catchment area recharges titan's ontario lacus. *Icarus* 299, 331–338.
- Elachi, C., Allison, M., Borgarelli, L., Encrenaz, P., Im, E., Janssen, M., Johnson, W., Kirk, R. L., Lorenz, R., Lunine, J., et al., 2004. Radar: the cassini titan radar mapper. In: *The Cassini-Huygens Mission*. Springer, pp. 71–110.
- Elachi, C., Wall, S., Allison, M., Anderson, Y., Boehmer, R., Callahan, P., Encrenaz, P., Flamini, E., Franceschetti, G., Gim, Y., Hamilton, G., Hensley, S., Janssen, M., Johnson, W., Kelleher, K., Kirk, R., Lopes, R., Lorenz, R., Lunine, J., Muhleman, D., Ostro, S., Paganelli, F., Picardi, G., Posa, F., Roth, L., Seu, R., Shaffer, S., Soderblom, L., Stiles, B., Stofan, E., Vetrella, S., West, R., Wood, C., Wye, L., Zebker, H., 2005. Cassini Radar Views the Surface of Titan. *Science* 308 (5724), 970–974.  
URL <http://www.sciencemag.org/cgi/content/abstract/308/5724/970>
- Elachi, C., Wall, S., Janssen, M., Stofan, E., Lopes, R., Kirk, R., Lorenz, R., Lunine, J., Paganelli, F., Soderblom, L., Wood, C., Wye, L., Zebker, H., Anderson, Y., Ostro, S., Allison, M., Boehmer, R., Callahan, P., Encrenaz, P., Flamini, E., Franceschetti, G., Gim, Y., Hamilton, G., Hensley, S., Johnson, W., Kelleher, K., Muhleman, D., Picardi, G., Posa, F., Roth, L., Seu, R., Shaffer, S., Stiles, B., Vetrella, S., West, R., Jun. 2006. Titan Radar Mapper observations from Cassini's T3 fly-by. 441, 709–713.

- Fulchignoni, M., Ferri, F., Angrilli, F., Ball, A. J., Bar-Nun, A., Barucci, M. A., Bettanini, C., Bianchini, G., Borucki, W., Colombatti, G., Coradini, M., Coustenis, A., Debei, S., Falkner, P., Fanti, G., Flamini, E., Gaborit, V., Grard, R., Hamelin, M., Harri, A. M., Hathi, B., Jernej, I., Leese, M. R., Lehto, A., Lion Stoppato, P. F., López-Moreno, J. J., Mäkinen, T., McDonnell, J. A. M., McKay, C. P., Molina-Cuberos, G., Neubauer, F. M., Pirronello, V., Rodrigo, R., Saggin, B., Schwingenschuh, K., Seiff, A., Simões, F., Svedhem, H., Tokano, T., Towner, M. C., Trautner, R., Withers, P., Zarnecki, J. C., Dec. 2005. In situ measurements of the physical characteristics of Titan's environment. 438, 785–791.
- Griffith, C. A., 2009. Storms, polar deposits and the methane cycle in Titan's atmosphere. *Philosophical Transactions of the Royal Society A: Mathematical, Physical and Engineering Sciences* 367 (1889), 713–728.  
URL <http://rsta.royalsocietypublishing.org/content/367/1889/713.abstract>
- Griffith, C. A., Penteado, P., Rodriguez, S., Le Mouélic, S., Baines, K. H., Buratti, B., Clark, R., Nicholson, P., Jaumann, R., Sotin, C., 2009. Characterization of clouds in Titan's tropical atmosphere. *The Astrophysical Journal Letters* 702 (2), L105.
- Hanel, R., Conrath, B., Flasar, F., Kunde, V., Maguire, W., Pearl, J., Pirraglia, J., Samuelson, R., Herath, L., Allison, M., et al., 1981. Infrared observations of the saturnian system from voyager 1. *Science* 212 (4491), 192–200.
- Hayes, A., Aharonson, O., Callahan, P., Elachi, C., Gim, Y., Kirk, R., Lewis, K., Lopes, R., Lorenz, R., Lunine, J., Mitchell, K., Mitri, G., Stofan, E., Wall, S., May 2008. Hydrocarbon lakes on Titan: Distribution and interaction with a porous regolith. *Geophysical Research Letters* 35, L9204.
- Hayes, A. G., Wolf, A. S., Aharonson, O., Zebker, H., Lorenz, R., Kirk, R. L., Paillou, P., Lunine, J., Wye, L., Callahan, P., Wall, S., Elachi, C., Sep. 2010. Bathymetry and absorptivity of Titan's Ontario Lacus. *Journal of Geophysical Research (Planets)* 115, E09009.
- Hofgartner, J., Hayes, A. G., Lunine, J., Zebker, H., Stiles, B., Sotin, C., Barnes, J., Turtle, E., Baines, K., Brown, R., et al., 2014a. Transient features in a Titan sea. *Nature geoscience*.
- Hofgartner, J. D., Hayes, A. G., Lunine, J. I., Zebker, H., Stiles, B. W., Sotin, C., Barnes, J. W., Brown, R. H., Encrenaz, P., Kirk, R. D., Le Gall, A., Lopes, R. M., Lorenz, R. D., Malaska, M., Mitchell, K. L., Paillou, P., Radebauch, J., Turtle, E., Wall, S., Wood, C., The Cassini RADAR Team, 2014b. The Discovery of Transient Features in a Titan Sea. *Nature Geoscience*, in revision.
- Huygens, C., 1999. 1659. *Systema Saturnium*.
- Jaumann, R., Brown, R. H., Stephan, K., Barnes, J. W., Soderblom, L. A., Sotin, C., Le Mouélic, S., Clark, R. N., Soderblom, J., Buratti, B. J., Wagner, R., McCord, T. B., Rodriguez, S., Baines, K. H., Cruikshank, D. P., Nicholson, P. D., Griffith, C. A., Langhans, M., Lorenz, R. D., Oct. 2008. Fluvial erosion and post-erosional processes on Titan. *Icarus* 197, 526–538.
- Kirk, R., Howington-Kraus, E., 2008. Radargrammetry on three planets. *The International Archives of the Photogrammetry, Remote Sensing and Spatial Information Sciences* 37 (B4), 973–980.

- Kuiper, G. P., 1944. Titan: a satellite with an atmosphere. *The Astrophysical Journal* 100, 378.
- Le Gall, A., Malaska, M. J., Lorenz, R. D., Janssen, M. A., Tokano, T., Hayes, A. G., Mastrogiuseppe, M., Lunine, J. I., Veyssière, G., Encrenaz, P., Karatekin, O., Feb. 2016. Composition, seasonal change, and bathymetry of Ligeia Mare, Titan, derived from its microwave thermal emission. *Journal of Geophysical Research (Planets)* 121, 233–251.
- Leberl, F. W., Thomas, J. K., Maurice, K. E., 1992. Initial results from the magellan stereo experiment. *Journal of Geophysical Research: Planets* 97 (E8), 13675–13689.  
URL <http://dx.doi.org/10.1029/92JE00885>
- Lindal, G. F., Wood, G., Hotz, H., Sweetnam, D., Eshleman, V., Tyler, G., 1983. The atmosphere of titan: An analysis of the voyager 1 radio occultation measurements. *Icarus* 53 (2), 348–363.
- Lopes, R. M. C., Mitchell, K. L., Stofan, E. R., Lunine, J. I., Lorenz, R., Paganelli, F., Kirk, R. L., Wood, C. A., Wall, S. D., Robshaw, L. E., Fortes, A. D., Neish, C. D., Radebaugh, J., Reffet, E., Ostro, S. J., Elachi, C., Allison, M. D., Anderson, Y., Boehmer, R., Boubin, G., Callahan, P., Encrenaz, P., Flamini, E., Francescetti, G., Gim, Y., Hamilton, G., Hensley, S., Janssen, M. A., Johnson, W. T. K., Kelleher, K., Muhleman, D. O., Ori, G., Orosei, R., Picardi, G., Posa, F., Roth, L. E., Seu, R., Shaffer, S., Soderblom, L. A., Stiles, B., Vetrella, S., West, R. D., Wye, L., Zebker, H. A., Feb. 2007. Cryovolcanic features on Titan's surface as revealed by the Cassini Titan Radar Mapper. *Icarus* 186, 395–412.
- Lora, J. M., Mitchell, J. L., Aug. 2015. Titan's asymmetric lake distribution mediated by methane transport due to atmospheric eddies. 42, 6213–6220.
- Lorenz, R. D., Aug. 2014. The flushing of Ligeia: Composition variations across Titan's seas in a simple hydrological model. 41, 5764–5770.
- Lorenz, R. D., Lopes, R. M., Paganelli, F., Lunine, J. I., Kirk, R. L., Mitchell, K. L., Soderblom, L. A., Stofan, E. R., Ori, G., Myers, M., Miyamoto, H., Radebaugh, J., Stiles, B., Wall, S. D., Wood, C. A., Jun. 2008. Fluvial channels on Titan: Initial Cassini RADAR observations. 56, 1132–1144.
- Lorenz, R. D., Stiles, B. W., Aharonson, O., Lucas, A., Hayes, A. G., Kirk, R. L., Zebker, H. A., Turtle, E. P., Neish, C. D., Stofan, E. R., Barnes, J. W., Jul. 2013. A global topographic map of Titan. 225, 367–377.
- Lunine, J. I., Stevenson, D. J., Yung, Y. L., Dec. 1983. Ethane ocean on Titan. *Science* 222, 1229–1230.
- MacKenzie, S. M., Barnes, J. W., Apr. 2016. Compositional Similarities and Distinctions between Titans Evaporitic Terrains. 821, 17.
- MacKenzie, S. M., Barnes, J. W., Sotin, C., Soderblom, J. M., Mouélic, S. L., Rodriguez, S., Baines, K. H., Buratti, B. J., Clark, R. N., Nicholson, P. D., McCord, T. B., 2014. Evidence of titan's climate history from evaporite distribution. *Icarus* 243 (0), 191 – 207.  
URL <http://www.sciencedirect.com/science/article/pii/S0019103514004370>

- Malaska, M. J., Hodyss, R., Lunine, J. I., Hayes, A. G., Hofgartner, J. D., Hollyday, G., Lorenz, R. D., 2017. Laboratory measurements of nitrogen dissolution in titan lake fluids. *Icarus* 289, 94–105.
- Mastrogiuseppe, M., Hayes, A., Poggiali, V., Lunine, J., Seu, R., Hofgartner, J., Le Gall, A., Lorenz, R., Apr. 2016. Bathymetry and Composition of Titan's Hydrocarbon Seas from the Cassini RADAR Altimeter. In: EGU General Assembly Conference Abstracts. Vol. 18 of EGU General Assembly Conference Abstracts. p. 13172.
- Mastrogiuseppe, M., Poggiali, V., Hayes, A., Lorenz, R., Lunine, J., Picardi, G., Seu, R., Flamini, E., Mitri, G., Notarnicola, C., Paillou, P., Zebker, H., Mar. 2014. The bathymetry of a Titan sea. 41, 1432–1437.
- McCord, T., Hansen, G., Buratti, B., Clark, R., Cruikshank, D., DâAversa, E., Griffith, C., Baines, E., Brown, R. H., Dalle Ore, C., et al., 2006. Composition of titan's surface from cassini vims. *Planetary and Space Science* 54 (15), 1524–1539.
- Miller, S., Walker, A., 1993. Further developments of leica digital photogrammetric systems by helava. In: ACSM ASPRS ANNUAL CONVENTION. Vol. 3. AMERICAN SOC PHOTOGRAMMETRY & REMOTE SENSING+ AMER CONG ON, pp. 256–256.
- Miller, S., Walker, A., 1995. Die entwicklung der digitalen photogrammetrischen systeme von leica und helava. *Z. Photogramm. Fernerkundung* 63 (1), 4–16.
- Mitchell, J. L., Sep. 2012. Titan's Transport-driven Methane Cycle. 756, L26.
- Mitchell, K. L., Barmatz, M. B., Jamieson, C. S., Lorenz, R. D., Lunine, J. I., Mar. 2015. Laboratory measurements of cryogenic liquid alkane microwave absorptivity and implications for the composition of Ligeia Mare, Titan. 42, 1340–1345.
- Mitchell, K. L., Malaska, M. J., Horvath, D. G., Andrews-Hanna, J. C., Mar. 2014. Karstic Processes on Earth and Titan. In: Lunar and Planetary Science Conference. Vol. 45 of Lunar and Planetary Inst. Technical Report. p. 2371.
- Mitri, G., Showman, A. P., Lunine, J. I., Lorenz, R. D., Feb. 2007. Hydrocarbon lakes on Titan. *Icarus* 186, 385–394.
- Niemann, H. B., Atreya, S. K., Bauer, S. J., Carignan, G. R., Demick, J. E., Frost, R. L., Gautier, D., Haberman, J. A., Harpold, D. N., Hunten, D. M., Israel, G., Lunine, J. I., Kasprzak, W. T., Owen, T. C., Paulkovich, M., Raulin, F., Raaen, E., Way, S. H., Dec. 2005. The abundances of constituents of Titan's atmosphere from the GCMS instrument on the Huygens probe. *Nature* 438, 779–784.
- Perron, J. T., Lamb, M. P., Koven, C. D., Fung, I. Y., Yager, E., Ádámkóvics, M., Nov. 2006. Valley formation and methane precipitation rates on Titan. *Journal of Geophysical Research (Planets)* 111, 11001.

- Porco, C. C., Baker, E., Barbara, J., Beurle, K., Brahic, A., Burns, J. A., Charnoz, S., Cooper, N., Dawson, D. D., Del Genio, A. D., Denk, T., Dones, L., Dyudina, U., Evans, M. W., Fussner, S., Giese, B., Grazier, K., Helfenstein, P., Ingersoll, A. P., Jacobson, R. A., Johnson, T. V., McEwen, A., Murray, C. D., Neukum, G., Owen, W. M., Perry, J., Roatsch, T., Spitale, J., Squyres, S., Thomas, P., Tiscareno, M., Turtle, E. P., Vasavada, A. R., Veverka, J., Wagner, R., West, R., Mar. 2005. Imaging of Titan from the Cassini spacecraft. *434*, 159–168.
- Porco, C. C., West, R. A., Squyres, S., McEwen, A., Thomas, P., Murray, C. D., Delgenio, A., Ingersoll, A. P., Johnson, T. V., Neukum, G., Veverka, J., Dones, L., Brahic, A., Burns, J. A., Haemmerle, V., Knowles, B., Dawson, D., Roatsch, T., Beurle, K., Owen, W., Jan. 2004. Cassini Imaging Science: Instrument Characteristics And Anticipated Scientific Investigations At Saturn. *Space Science Reviews* 115, 363–497.
- Rannou, P., Montmessin, F., Hourdin, F., Lebonnois, S., Jan. 2006. The Latitudinal Distribution of Clouds on Titan. *Science* 311, 201–205.
- Rodriguez, S., Le Mouélic, S., Rannou, P., Sotin, C., Brown, R. H., Barnes, J., Griffith, C., Buralat, J., Baines, K., Buratti, B., et al., 2011. Titan’s cloud seasonal activity from winter to spring with cassini/vims. *Icarus* 216 (1), 89–110.
- Rodriguez, S., Le Mouélic, S., Rannou, P., Sotin, C., Brown, R. H., Barnes, J. W., Griffith, C. A., Buralat, J., Baines, K. H., Buratti, B. J., Clark, R. N., Nicholson, P. D., Nov. 2011. Titan’s cloud seasonal activity from winter to spring with Cassini/VIMS. 216, 89–110.
- Rodriguez, S., Le Mouélic, S., Rannou, P., Tobie, G., Baines, K. H., Barnes, J. W., Griffith, C. A., Hirtzig, M., Pitman, K. M., Sotin, C., et al., 2009. Global circulation as the main source of cloud activity on titan. *Nature* 459 (7247), 678.
- Rodriguez, S., Le Mouélic, S., Sotin, C., Clénet, H., Clark, R., Buratti, B., Brown, R. H., McCord, T., Nicholson, P., Baines, K., et al., 2006. Cassini/vims hyperspectral observations of the huygens landing site on titan. *Planetary and Space Science* 54 (15), 1510–1523.
- Roe, H., De Pater, I., Macintosh, B., McKay, C., 2002. Titan’s clouds from gemini\* and keck\*\* adaptive optics imaging. *The Astrophysical Journal* 581 (2), 1399.
- Sagan, C., Dermott, S. F., Dec. 1982. The tide in the seas of Titan. *Nature* 300, 731–733.
- Schaller, E. L., Brown, M. E., Roe, H. G., Bouchez, A. H., Trujillo, C. A., 2006. Dissipation of titan’s south polar clouds. *Icarus* 184 (2), 517–523.
- Schneider, T., Graves, S., Schaller, E., Brown, M., 2012. Polar methane accumulation and rainstorms on titan from simulations of the methane cycle. *Nature* 481 (7379), 58.
- Sharma, P., Byrne, S., Dec. 2009. Constraints on Titan’s topography through fractal analysis of shorelines and comparison with terrestrial analogues. *AGU Fall Meeting Abstracts*, G1186+.

- Soderblom, J. M., Barnes, J. W., Soderblom, L. A., Brown, R. H., Griffith, C. A., Nicholson, P. D., Stephan, K., Jaumann, R., Sotin, C., Baines, K. H., et al., 2012. Modeling specular reflections from hydrocarbon lakes on titan. *Icarus* 220 (2), 744–751.
- Sotin, C., Lawrence, K., Reinhardt, B., Barnes, J., Brown, R. H., Hayes, A., Le Mouélic, S., Rodriguez, S., Soderblom, J., Soderblom, L., et al., 2012. Observations of titanâs northern lakes at 5  $\mu\text{m}$ : Implications for the organic cycle and geology. *Icarus* 221 (2), 768–786.
- Suyres, S. W., Thompson, W. R., Sagan, C., Jun. 1984. Voyager Imaging Observations of Titan's Atmosphere: I. Disk-Resolved Photometric Properties. In: *Bulletin of the American Astronomical Society*. Vol. 16 of *Bulletin of the American Astronomical Society*. p. 664.
- Stephan, K., Jaumann, R., Brown, R. H., Soderblom, J. M., Soderblom, L. A., Barnes, J. W., Sotin, C., Griffith, C. A., Kirk, R. L., Baines, K. H., et al., 2010. Specular reflection on titan: liquids in kraken mare. *Geophysical Research Letters* 37 (7).
- Stiles, B. W., Hensley, S., Gim, Y., Bates, D. M., Kirk, R. L., Hayes, A., Radebaugh, J., Lorenz, R. D., Mitchell, K. L., Callahan, P. S., et al., 2009. Determining titan surface topography from cassini sar data. *Icarus* 202 (2), 584–598.
- Stofan, E. R., Elachi, C., Lunine, J. I., Lorenz, R. D., Stiles, B., Mitchell, K. L., Ostro, S., Soderblom, L., Wood, C., Zebker, H., Wall, S., Janssen, M., Kirk, R., Lopes, R., Paganelli, F., Radebaugh, J., Wye, L., Anderson, Y., Allison, M., Boehmer, R., Callahan, P., Encrenaz, P., Flamini, E., Francescetti, G., Gim, Y., Hamilton, G., Hensley, S., Johnson, W. T. K., Kelleher, K., Muhleman, D., Paillou, P., Picardi, G., Posa, F., Roth, L., Seu, R., Shaffer, S., Vetrella, S., West, R., Jan. 2007. The lakes of Titan. *Nature* 445, 61–64.
- Tarboton, D. G., 1997. A new method for the determination of flow directions and upslope areas in grid digital elevation models. *Water Resources Research* 33 (2), 309–319.  
URL <http://dx.doi.org/10.1029/96WR03137>
- Tokano, T., Lorenz, R. D., 2006. Gcm simulation of balloon trajectories on titan. *Planetary and Space Science* 54 (7), 685–694.
- Tokano, T., McKay, C. P., Neubauer, F. M., Atreya, S. K., Ferri, F., Fulchignoni, M., Niemann, H. B., 2006. Methane drizzle on titan. *Nature* 442 (7101), 432.
- Tomasko, M. G., Archinal, B., Becker, T., Bézard, B., Bushroee, M., Combes, M., Cook, D., Coustenis, A., de Bergh, C., Dafoe, L. E., Doose, L., Douté, S., Eibl, A., Engel, S., Gliem, F., Grieger, B., Holso, K., Howington-Kraus, E., Karkoschka, E., Keller, H. U., Kirk, R., Kramm, R., Küppers, M., Lanagan, P., Lellouch, E., Lemmon, M., Lunine, J., McFarlane, E., Moores, J., Prout, G. M., Rizk, B., Rosiek, M., Rueffer, P., Schröder, S. E., Schmitt, B., See, C., Smith, P., Soderblom, L., Thomas, N., West, R., Dec. 2005. Rain, winds and haze during the Huygens probe's descent to Titan's surface. 438, 765–778.
- Turtle, E. P., Del Genio, A. D., Barbara, J. M., Perry, J. E., Schaller, E. L., McEwen, A. S., West, R. A., Ray, T. L., Feb. 2011a. Seasonal changes in Titan's meteorology. 38, 3203.

- Turtle, E. P., Perry, J. E., Hayes, A. G., Lorenz, R. D., Barnes, J. W., McEwen, A. S., West, R. A., Del Genio, A. D., Barbara, J. M., Lunine, J. I., Schaller, E. L., Ray, T. L., Lopes, R. M. C., Stofan, E. R., Mar. 2011b. Rapid and Extensive Surface Changes Near Titan's Equator: Evidence of April Showers. *Science* 331, 1414–1417.
- Turtle, E. P., Perry, J. E., Hayes, A. G., McEwen, A. S., Apr. 2011c. Shoreline retreat at Titan's Ontario Lacus and Arrakis Planitia from Cassini Imaging Science Subsystem observations. 212, 957–959.
- Turtle, E. P., Perry, J. E., McEwen, A. S., Del Genio, A. D., Barbara, J., West, R. A., Dawson, D. D., Porco, C. C., Jan. 2009. Cassini imaging of Titan's high-latitude lakes, clouds, and south-polar surface changes. *Geophysical Research Letters* 36, L2204.
- Wall, S., Hayes, A., Bristow, C., Lorenz, R., Stofan, E., Lunine, J., Le Gall, A., Janssen, M., Lopes, R., Wye, L., Soderblom, L., Paillou, P., Aharonson, O., Zebker, H., Farr, T., Mitri, G., Kirk, R., Mitchell, K., Notarnicola, C., Casarano, D., Ventura, B., Mar. 2010. Active shoreline of Ontario Lacus, Titan: A morphological study of the lake and its surroundings. 37, L5202.
- Willemin, J. H., Nov. 2000. Hack's Law: Sinuosity, convexity, elongation. *Water Resources Research* 36, 3365–3374.
- Wobus, C., Whipple, K. X., Kirby, E., Snyder, N., Johnson, J., Spyropolou, K., Crosby, B., Sheehan, D., 2006. Tectonics from topography: Procedures, promise, and pitfalls. *Geological Society of America Special Papers* 398, 55–74.
- Wood, C. A., Stofan, E. R., Hayes, A. G., Kirk, R. K., Lunine, J. I., Radebaugh, J., Malaska, M., Mar. 2013. Morphological Evidence for Former Seas Near Titan's South Pole. In: *Lunar and Planetary Science Conference*. Vol. 44 of *Lunar and Planetary Inst. Technical Report*. p. 1764.
- Wye, L. C., Zebker, H. A., Lorenz, R. D., Aug. 2009. Smoothness of Titan's Ontario Lacus: Constraints from Cassini RADAR specular reflection data. 36, L16201.